Reconstruction of the 01 February 1814 Eruption of Mayon Volcano, Philippines

by

Maria Hannah Terbio Mirabueno

A thesis
submitted in partial fulfillment
of the requirements for the degree
of

Master of Science in Geology

2001

Abstract

Mayon Volcano's eruption on 01 February 1814 is considered as the volcano's most violent eruption episode, devastating five towns in the southern slopes of the volcano and killing at least 1,200 people.

The deposits of the 1814 eruption are mainly distributed on the southern slopes of the volcano. The primary volcanic succession consists of, from bottom to top, tephra fall deposit, lower ignimbrite, pyroclastic surge deposit and upper ignimbrite. Two post-eruption lahar units were also recognized in the field area. The tephra fall unit, although not observed in direct contact with any of the other primary deposits, was distinguished based on petrologic and geochemical similarities with the lower ignimbrite and pyroclastic surge deposit. The lower ignimbrite and the overlying pyroclastic surge deposit are both scoriaceous, and are similarly bombs-rich; the surge deposit is distinguished by its characteristically good sorting. In contrast, the upper ignimbrite contains abundant angular altered clasts derived from pre-eruption deposits.

All the primary deposits are interpreted to have been derived from an eruption column that was generated by multiple explosive eruptions occurring in close succession. This column initially generated the tephra fall. Discrete phases of column collapse produced the succession of lower ignimbrite, pyroclastic surge deposit and upper ignimbrite. The wide dispersal, composition and textural characteristics of the pyroclastic surge indicate that it was generated by a discrete phase of an eruption column collapse. The upper ignimbrite is the deposit from a density current produced during the cessation of the eruption that was accompanied by partial collapse of the crater wall.

The 1814 deposits are predominantly composed of basaltic andesite, with minor more acidic andesite. Petrographic texture and contact relationships, bimodal distribution of plagioclase, and variation in glass composition indicate mixing of two magmas. A geologic model for the 1814 eruption is proposed in which an intermediate andesite magma residing in a small, shallow chamber beneath Mayon was intruded by a comparably larger magma of basaltic andesite composition. The resulting magma mixing may have triggered the explosive eruption of 1814.

Table of Contents

List of Figures

List of Tables

Acknowledgment

I am most grateful to my supervisors: Prof. Jim Cole, for the great opportunity for postgraduate study and for the helpful suggestions; Dr. Kari Bassett for the critical review of my thesis; and Prof. Steve Weaver for the help in geochemistry. Very special thanks to Dr. Christopher Newhall for generously imparting his knowledge on Mayon, for sponsoring the carbon dating, and for the fruitful discussions in the field – including non-volcanology topics. I am very thankful to Assoc. Prof. Dave Shelly for his patience in helping me analyze my thin sections. I am also grateful for the help of the Department's technicians – John, Rob, Cathy, Jane, Steve and Arthur.

I thank PHIVOLCS, through Dr. Raymundo S. Punongbayan, for giving me invaluable support during my postgraduate studies. I am especially grateful to Mariton Bornas and Maricar Arpa for providing technical assistance as well as light relief during boring field days! Thanks also to the Lignon Hill Observatory people for the fieldwork support.

Thanks to Dave Milner for the numerous volcanological consultation. To Kim Baxter for editing my thesis and for her encouraging words. And to Jamie and Steve, for the early morning rides after all-night work. Thanks, too, to my classmates, Philippa, Greg Cook, Greg Martin and Jo for the companionship. To Gus, Scott, Alex, Beatriz, Julie and Natalia for the fun times.

Thanks to Károly Németh for the help during probe analyses and for the use of some geochemistry programs, for the encouragement, and for the wonderful time in Dunedin. *Te biztatsz engem.*

To my chums: Deepani, Sue, Yvonne and Ricky for the company, and for supplying dinner during crucial times. To Felisa for keeping my sanity intact...

Thanks to the Filipinos who have helped me and my family so much during our stay in New Zealand: the Tuñgols, the Alcanzares, the Lopezes, the Hernandezes, the Laroyas, the Trenuelas, the Batallers, Gerry Nartea, and my flatmate, Karl Fernandez.

To Norman, for the friendship and help in countless ways (too long to mention!), and Peejay – I wouldn't have met the deadline without you, guys! I can never repay you for the help you have given during the thesis preparation.

To my family which has stood by me all these years – my father, Jaime; my mother Presentacion, who unselfishly devoted time for me and Tsing; and my siblings, Jim Conrad, Jaime Jr., Jemmah Maria, Floranie and James Jude.

Maraming salamat sa inyong lahat!!!

To my little girl, Jhan Mary Adrianne: this is for you...

CHAPTER 1

Introduction

The 01 February 1814 eruption is generally considered the largest and most devastating eruption of Mayon Volcano in recorded history. A recurrence of an eruption akin to this event is potentially far more deadly if it happens today, considering that the population around the volcano has considerably increased since 1814. In order to mitigate potential catastrophic impact of an explosive eruption similar in magnitude to that of the 1814 eruption, there is a need for a more detailed understanding of the volcano's eruptive behavior. This is particularly true in cases where historical eruptions are concerned because there is a paucity of available geologic information.

1.1. Objectives

The aim of this study is to reconstruct the 1814 eruption of Mayon Volcano, which many believe is the only plinian event of the volcano, and determine the eruptive mechanisms involved through the study of historical accounts, geological mapping, and laboratory analyses. By establishing the chronology of events and areal extent of the resultant deposits of the 1814 event, we may have a better understanding of Mayon Volcano's eruptive behavior. This study is further aimed at determining the processes involved in magma ascent and extrusion, and the mechanisms of emplacement of the eruptive products. These may serve as bases for eruption prediction and volcanic hazards assessment. The following are the specific objectives of this study:

- Determine the distribution and stratigraphy of the 1814 deposits;
- Reconstruct the events of the 1814 eruption based on stratigraphic data and historical accounts;
- Characterize the 1814 deposits in terms of granulometry, geochemistry and petrography;

- Discuss the mechanisms of emplacement of the different eruptive deposits; and

- Discuss possible triggers of the explosive basaltic andesite eruption.

1.2. Previous works

In order to have a general understanding of the eruptive history of Mayon Volcano, a review of previous works was done. Literature on Mayon Volcano's eruptive history consisted mostly of accounts written in Spanish but which have subsequently been translated to English. Geologic publications include surveillance and monitoring reports by the Philippine Institute of Volcanology and Seismology (PHIVOLCS), contemporary hazard assessments and maps, and studies on Mayon's most recent eruptions (i.e. 1984 and 1993 events).

Recent eruptive events however have been documented and studied in detail. Deposits from the 1968 vulcanian eruption have been described and documented by Moore and Melson (1970). Stratigraphic and petrologic analyses of the 1984 eruptive products were performed by Corpuz (1985), Ramos-Villarta *et al.* (1985), and Magalit *et al.* (1985). The 1993 deposit was described by Catane *et al.* (1995),. Investigations were conducted on the 1984 lahar deposits by Umbal and Ruelo (1985), Arguden and Rodolfo (1986), Umbal (1986), and Rodolfo *et al* (1989). Knittel-Weber and Knittel (1990) discussed the petrology and geochemistry of neighboring Malinao volcano with reference to the magmatic history and plumbing of Mayon Volcano.

Other studies on Mayon included statistical analysis of Mayon's eruptive events (Lizardo, 1986) and seismic evaluations and tidal effects (Ramos, 1985). Chemistry of Mayon Volcano was analyzed by Arcilla (1998) and he classified the Mayon rocks as mostly basaltic andesite. He combined geochemistry and studies on tomography to locate the possible depth at which magmatism occurred below the Bicol Volcanic Chain.

Of more significance to this study were the historical references to the 1814 eruption of Mayon Volcano. However, considering the timing of the explosive eruptive event, the bulk of the literature on the 1814 eruption were generally on Spanish, written by friars. One of the most detailed descriptions of the 1814 eruption was written by a Spanish priest, Fr. Aragoneses (1814). Aragoneses' account has been mostly quoted in reviews pertaining to Mayon's eruptive history (Maso, 1904,1911; Foreman, 1906; Perry, 1860). Fr. Mata (1814), also a Spanish priest, provided detailed post-eruption observations. Other helpful documents included references made to the 1814 eruption as part of the compilations on Mayon's historic eruptions by Abella (1882), Martinez (1859), Huerta (1865), Maso (1911), Packard (1900), Selga (1902) and Faustino (1929). The 1814 event also appears in more literary-type stories or poems such as Calleja-Reyes (1988) and Loquez (unpublished).

Geological descriptions of eruptions of Mayon Volcano, specifically the 1814 eruption, were rare. The first detailed eruption chronology of the 1814 event was first presented by Newhall (1977) and was subsequently followed by Villarta-Ramos *et al.* (1985) and PHIVOLCS (1990). One of the basaltic periods coincided with the occurrence of the 1814 eruption. The chemistry of the 1814 tephra yields the lowest SiO_2 among Mayon's deposits, hence the most basaltic signature. An attempt to reconstruct the 1814 eruption was also made by Rodolfo et al. (Unpublished report) based on a trenching study at Budiao Ruins. The most comprehensive and detailed study is a master's thesis by Newhall (1977) followed by a publication on the petrology of Mayon Volcano (Newhall, 1979). Based on petrologic and stratigraphic studies, he postulated that a cyclical variation in the erupted lavas occurs in Mayon's lavas as a result of the periodic influx of basaltic magma into a shallow andesite magma chamber.

1.3. Methodology

Stratigraphic studies, supported by geochemical and other geological laboratory techniques, have been employed in reconstructing historical eruptions (Cas and Wright, 1987). Similar studies have been conducted for archaeological sites in volcanic areas like at Popocatépetl Volcano in Mexico (Panfil *et al.*, 1999). Other reconstruction of

eruptive history include the 1538 Monto Nuovo eruption (Di Vito *et al.*, 1987), the 1835 Cosigüina eruption (Self *et al.*, 1989), the A.D. 472 "Pollena" eruption of Vesuvius (Rosi and Santacroce, 1983), and the 1641 Vesuvius eruption (Rosi *et al.*, 1993). This research had been patterned after such studies where stratigraphic studies are combined with eyewitness accounts.

The study consisted of a thorough review of historical accounts on the 1814 eruption and related publications. Two phases of field surveys were conducted along the major gullies of Mayon Volcano in order to identify, map the extent, and sample the deposits of the 1814 event. Detailed stratigraphic study was made on 1814 outcrops in order to correlate units along various gullies and document facies changes. Trenching was also conducted outside Budiao Church, one of the churches destroyed during the 1814 eruption. Grain size analyses were conducted on selected 1814 samples from four major gullies, Anuling, Miisi, Budiao and Mabinit.

Samples were sieved at half phi intervals in the Sedimentology Laboratory at the Department of Geology, University of Canterbury and at the Philippine Institute of Volcanology. Petrographic descriptions were done for representative samples. Major and trace element chemistry of the representative samples were determined by X-Ray Spectrometry analysis. The thin sections were prepared at the University of Canterbury while some rock slices were prepared at the Philippine Institute of Volcanology and Seismology (PHIVOLCS). In order to further understand the eruptive mechanism/s involved in the 1814 eruption, microprobe analyses were also conducted on representative samples of the juvenile scoria at University of Otago, Dunedin.

1.4. Mayon Volcano

Mayon Volcano is the most active volcano in the Philippine Archipelago. It is an andesitic stratovolcano with a near-perfect symmetry located in the province of Albay, Bicol Peninsula, in southeastern Luzon (Figure 1.1). Mayon Volcano rises to an elevation of 2462 m above sea level and has a basal circumference of 63 km. Mayon's lower slopes are gentle. The top 100 meters, however, is marked by steep upper slopes

with about 30-45° angle. The crater rim is currently breached on the southeastern sector. Thus, during the volcano's most recent eruptions in 1993, 2000 and 2001, flows and some pyroclastic flows were funneled towards this sector of the volcano (Figure 1.2). Several towns and a city (Legaspi City) are sited on Mayon's lower slopes. The city of Legaspi alone has population of 141, 657 (NCSO, 2001).

Two permanent volcano observatories are currently being maintained by the Philippine Institute of Volcanology and Seismology (PHIVOLCS) in the vicinity of Mayon Volcano: the Lignon Hill Observatory, 11.5 km southeast of the summit, and the Mayon Resthouse Observatory (MRHO), 3.8 km northwest of the summit. Both are manned on a 24-hour basis and equipped with analogue seismographs to monitor the volcano's activity. Telemetered seismic stations were also established on strategic locations around the slopes of the volcano.

About 40 major tributaries and gullies are draining from Mayon Volcano that had been crucial in the delivery process of eruptive products during each eruption. Since its first historically documented eruption in 1616, Mayon had a total of 47 eruptions, the most recent of which was the June 2001 eruption (Table 1.1). Mayon's eruptions are generally central and were predominantly of mild to moderate intensity. None of these historical eruptions were explosive enough to cause sector collapse.

Most historical and recent eruptions of Mayon have a Volcanic Explosivity Index (VEI) value about 2 (Catane *et al.*, 1995). However, the 01 February 1814 eruption has been classified as a plinian eruption, probably with a higher VEI, because of the violence described in historical documents (Newhall, 1977; Ramos-Villarta *et al.*, 1985; PHIVOLCS, 1990). The 1814 event caused the death of 1,200 people and devastated five towns sited on the southern slopes of the volcano.

Figure 1.1. The near-perfect symmetry of Mayon Volcano is blighted by a notch in the southeastern rim where lava and pyroclastic flows were funneled during the volcano's recent eruptions (*Source: DV Javier, PHIVOLCS*).

Figure 1.2. Mayon Volcano as viewed from the west. Incised gullies are prevalent from upslope to the lower reaches of the volcano. Steaming from newly deposited lava flow is noticeable in the southeast. Brown patches are deposits from the 2000 eruption. (*Source: PHIVOLCS*)

Table 1.1. Mayon Volcano's documented eruptions (PHIVOLCS, 1990).

Year	Duration	Description
1616	19 - 23 February	Earliest recorded eruption
1766	20-25 July	Vulcanian, generated major lahar, 49 deaths
1800	30-31 October	Vulcanian
1811	5-6 October	Vulcanian
1814	1 February	Plinian, generated major lahar, 1,200 deaths
1827-1828	June 1827 - February 1828	Vulcanian
1834	Up to May 1835 (?)	Vulcanian
1839		Minor ash eruption, phreatic eruption (?)
1845	21 January	Vulcanian
1846	11 May	Vulcanian
1851	26 May - June	Two minor ash eruptions, phreatic eruptions
1853	13 July - 26 August	Vulcanian
1855	22 March	Minor eruption
1857		Minor ash eruption
1858	January - 1 December	Strombolian
1861		Minor ash eruption
1862		Minor ash eruption
1868	17 December	Vulcanian
1871-1872	8 December 1871 - January 1872	Vulcanian
1872	5 September - 9 October	Ash emission and "lava"
1873	20 June - 22 July	Minor eruption w/ sudden 30 cm subsidence in Malinao
1876	April - 26 November	Minor ash eruption
1881-1882	6 July 1881 - August 1882	Strombolian
1885	21 November - 2 December	Minor overflow of "lava"
1886-1887	July 1886 - 10 March 1887	Strombolian
1888	15 December	Two minor ash eruptions
1890	10-30 September	Vulcanian & strombolian
1891	3 October - 3 December	Minor explosions & lava flows
1892	3 - 29 February	Vulcanian, cone lowered by 100 meters
1893	4 - 31 October	Minor ash, lapilli & bomb eruption, generated lava flows
1895	20 July - 26 November	Minor eruption & lahar, emission of lava flow
1896	31 August - 27 September	Minor ash & lava eruption
1897	4 June - 23 July	Strong vulcanian, 350 deaths
1900	1 - 6 March	
1902		Minor ash eruptions
1928	January (?) - August	Vulcanian
1938	5 June	Vulcanian
1939	21 Aug.	Minor explosion
1941	13 Sept.	Minor emission of ash & steam, phreatic eruption (?)
1943		Minor emission of ash & steam, phreatic eruption (?)
1947	8 Jan.- Feb.	Vulcanian
1968	20 Apr - 20 May	Vulcanian
1978	3 May - 4 Jul.	Strombolian
1984	9 Sept. - 6 Oct.	Vulcanian
1993	2 Feb. - 3 Apr.	Strombolian-vulcanian
2000	Feb. - Mar.	Vulcanian & strombolian but predominantly strombolian
2001	June - July	Vulcanian & strombolian but predominantly strombolian

The recorded eruption history of Mayon Volcano, which dates back to 1616, shows that since 1984, the bulk of the eruptive products have been emplaced towards the southern slopes (Ramos-Villarta *et al.*, 1985). Although the 1766 eruption mainly affected the eastern sector of the volcano, the towns of Cagsawa, Budiao, Guinobatan, Albay and Ligao were severely affected by the vulcanian event (PHIVOLCS, 1990). Damages incurred during the 1766 event were mainly from lahars due to passage of a typhoon and occurrences of intense monsoonal rains. Tephra and density flows were generated during the vulcanian eruption in 1800 that impacted the settlements of Budiao and Cagsawa. Another vulcanian eruption occurred in 1811, which involved forceful injection of a column of ash and rocks and lava flow described as a "big river of fire". However, no damage was reported during this event.

Several eruptions occurred after the explosive eruption in 1814 and prior to 1853, but these eruptions were described as minor (Coronas, 1898). Vulcanian eruptions followed intermittently until 1897. The 1897 eruption is considered as the second most destructive eruption after the 1814 eruption in terms of damages and casualties. This eruption generated density flows, lava flows and tephra fall that affected most of the towns in the eastern and northern sectors of Mayon Volcano.

1.5. Regional, Tectonic and Geologic Setting

Mayon Volcano is located in the Bicol Peninsula in southern Luzon, Philippines (13°15.4'N, 123°41.1'E) (Figure 1.3). It forms part of the northwest-trending predominantly basaltic andesite-andesite Bicol Volcanic Chain (Figure 1.4).

The Bicol Peninsula consists largely of Upper Tertiary and Pleistocene sedimentary and volcanic rocks (Newhall, 1977). Pre-tertiary metamorphic rocks are exposed in the mountains comprising the western part of southern Luzon. The immediate vicinity of Mayon Volcano is also underlain by metamorphic rocks, as evidenced by plagioclase-rich granulite xenoliths in some of Mayon tephra deposits (Newhall, 1977). Aside from Mayon Volcano, Iriga and the Bulusan Volcanic Complex (BVC) are two other active

centers found within the volcanic belt. Other major volcanic cones are Mounts Bacacay, Labo, Colasi, Isarog, Malinao, Masaraga, Juban, Pocdol and Gate complexes.

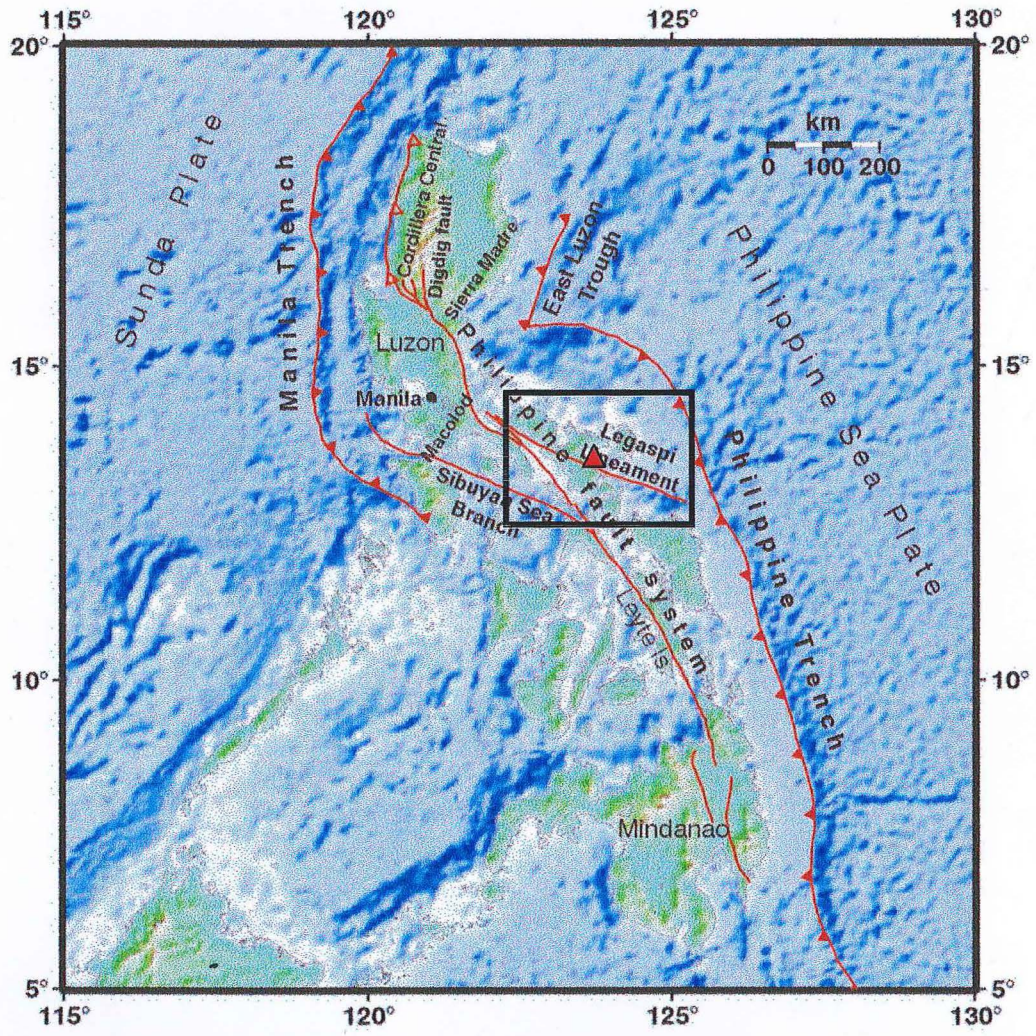

Figure 1.3. Map of the Philippines showing the Bicol Peninsula and the major tectonic features relevant to the Bicol Volcanic Arc (shown by box). Bathymetry is lit from the southeast. Sunda Plate comprised by southeast Asia and the South China Sea (*modified from Beavan et al., 2000*). Mayon Volcano (shown by red triangle) lies along a pull-apart basin formed by the left-lateral Legaspi Lineament and the predominantly left-lateral Philippine Fault (*Aurelio et al. 1997*).

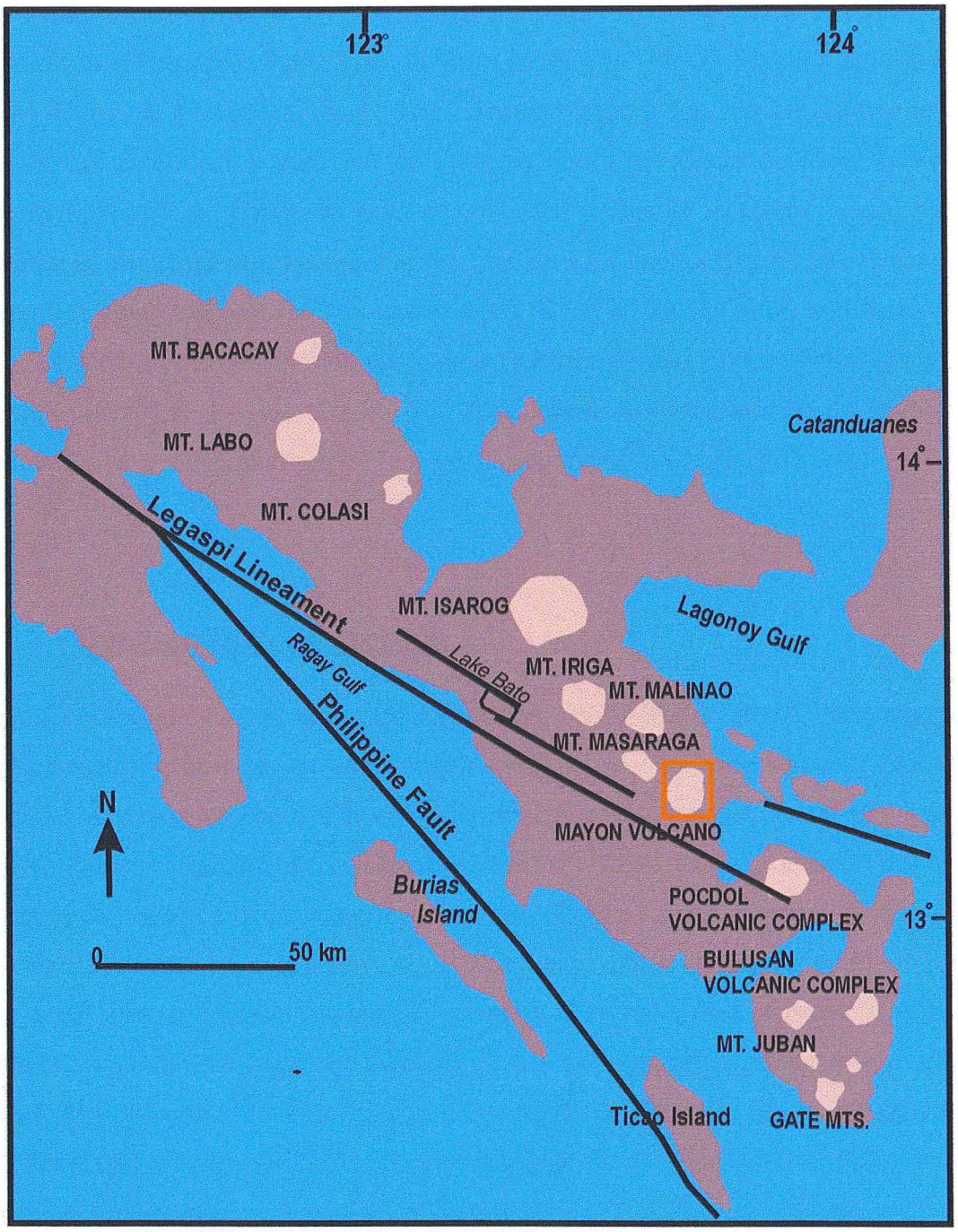

Figure 1.4. The Bicol Peninsula and the major volcanic centers (*after Newhall, 1977*). Area of study is shown by box. Black solid lines denote approximate locations of the Philippine Fault and the Legaspi Lineament (*from Aurelio, 1997*).

The Bicol Peninsula lies between the Philippine Trench and the Philippine Fault (Figure 1.3). Magmatism along the Bicol Volcanic chain is attributed to the west-subducting Philippine Sea Plate. As such, subduction-related processes greatly influenced petrology and geochemistry of the Bicol volcanoes.

The northern part of the Bicol Peninsula is transected by a segment of the left lateral, 1200 km-long Philippine Fault Zone (PFZ) (Aurelio *et al.*, 1997) (Figure 1.3). From the Ragay Gulf, the Philippine Fault Zone extends offshore for 300 km and continues onshore at the Masbate Island. No fault directly transects volcano's edifice. However, Mayon Volcano lies within the narrow, elongated pull-apart structure formed by the presence of the strike slip zone along the Legaspi Lineament. The identified sense of movement along the Legaspi Lineament is left-lateral strike slip fault, with Lake Bato being formed as a result of this movement (Aurelio, *et al.*, 1997). The trace of the Legaspi Lineament extends offshore and stops where it meets up with the Philippine Fault to the east. Several unnamed faults exist southwest of Mayon Volcano.

1.6. Eruption style and deposits

Mayon's eruptions vary in style and magnitude. PHIVOLCS (1990) cited magmatic physico-chemical changes as the probable cause of the differing styles of eruptions observed at Mayon Volcano. The eruptions are concentrated at the central vent and are predominantly vulcanian but combination of strombolian and vulcanian styles were observed during some of the historical eruptions (Figure 1.5). It is common for Mayon Volcano to change from explosive to non-explosive phase during an eruptive event. Two sequences of eruptive phases are generally observed. One phase starts with an explosive episode involving the ejection of ash and generation of pyroclastic flows followed by effusion of lava flows (*e.g.* 1968 eruption). The other phase may start with lava flows followed by pyroclastic flow events (*e.g.* 1984) (PHIVOLCS, 1990). Purely strombolian eruptions are characterized by minor ash ejections, and culminate with lava effusion. Dome building occurred during Mayon Volcano's most recent eruptions in 1993, 2000 and 2001 eruptions (Figure 1.6). During these recent eruptions, growth of lava dome was accompanied by phreatic explosions and ash ejections.

Figure 1.5. Density currents are generated by a column collapse during a vulcanian eruption in 1993. (*Source: PHIVOLCS*)

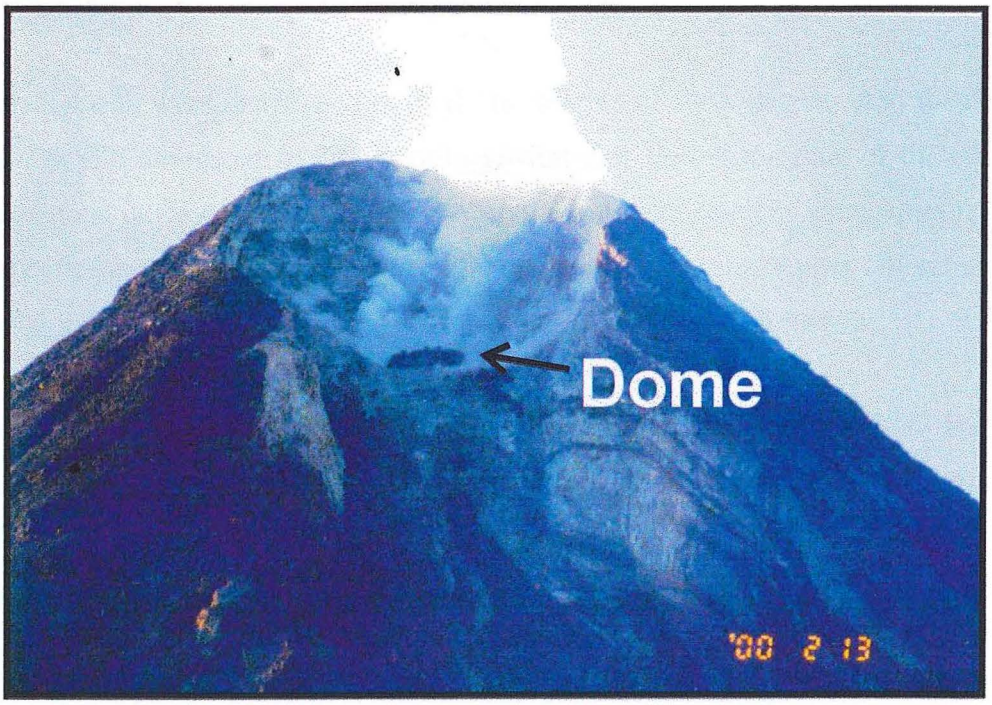

Figure 1.6. Dome formation prior to the onset of explosive eruption in February 2000. View is from the southeast. (*Source: PHIVOLCS*)

The combination of strombolian and vulcanian eruptions generated pyroclastic flows and surges, tephra fall and lava flows that were deposited mostly on the flanks of the volcano. Tephra fall resulting from these eruptions, commonly reached as far as 12 km from the crater. Density currents were generated from the collapse of eruption columns and sometimes as a result of boil-over type flows (Umbal, 1984). Collapse of an unstable dome and newly emplaced lava fronts generated Merapi-type pyroclastic flows (Catane *et al.*, 1995). Phreatic explosions generally occur prior to more explosive eruptions. These phreatic explosions generate ash and steam, and like the 1993 eruption, they may generate lithic-rich block- and- ash flow deposits (Catane *et al.*, 1995, unpublished paper).

Among the volcano's documented eruptions, it was observed that vulcanian eruptions generated 'St. Vincent type' pyroclastic flows such as those ejected during the 1968 (Moore and Melson, 1969) and 2000 (Bornas, pers. comm., 2000) eruptions. Ground surges were also produced from vulcanian eruptions, as documented during the 1968 eruption (Moore and Melson, 1969). Strombolian eruptions, on the other hand, generated intermittent explosions of bombs and incandescent coarse pyroclasts and lava flows. Lava flows frequently preceded the explosive phase or signaled the waning stage of an eruption.

Ashfall deposits were distributed over all the sectors of the volcano. Ash distribution was lobate and elongated in the prevailing wind direction at the time of the eruption. Where tephra fall events coincided with prevailing northeasterly wind, dispersal was mostly concentrated to the west and southwest. However, some tephra fall mantled the topography of the northeastern sector of the volcano (PHIVOLCS, 1990).

Remobilization of old and newly emplaced volcanic deposits generated syn- and post-eruption lahars that were transported along incised gullies around the volcano. Non-eruption related lahars also occurred in historic times (*e.g.* 1886) and in recent years (*e.g.* 1995), which resulted in casualties and considerable damage to properties.

1.7. Petrology, geochemistry and petrogenesis of Mayon Volcano

Mayon Volcano's deposits consisted mostly of basaltic andesite to andesitic rocks. These deposits were predominantly augite-hypersthene andesite rocks, with subordinate (olivine)-augite hypersthene basalt (Newhall, 1977). These rocks, including the more evolved dacitic and rhyolitic volcanics in the Bicol Volcanic Chain, had medium to high-K calc- alkaline signatures, typical of the volcanic products in the Bicol arc (Knittel-Weber and Knittel, 1990).

Recent studies using seismic tomography show that a high attenuation zone exists under the Bicol area (Besana, 1997). The high attenuation zone is interpreted to be the site of active slab dehydration associated with current magmatism in the Bicol arc (Arcilla, 1998). Using petrologic transects coupled with results from seismic tomography studies, Arcilla (1998) placed Mayon Volcano and most of Bicol volcanoes almost directly above the amphibole breakdown curve at about 90-km depth (Figure 1.7).

Newhall (1977, 1979) ascribed the observed cyclic variations in historical lavas of Mayon Volcano to the periodic influx of less differentiated basaltic melt into the magma reservoir and subsequent fractional differentiation. Newhall (1977) further postulated that the mixing of the basaltic melt and more differentiated magma in the volcano's feeder system could have triggered the more violent eruptions.

Knittel-Weber and Knittel (1990) found similarities in the evolution of basaltic and basaltic lavas in Malinao Volcano, a volcano north of Mayon (Figure 1.4) to Mayon lavas. They proposed that the basaltic magma evolved principally by fractional crystallization producing basaltic andesite and andesite.

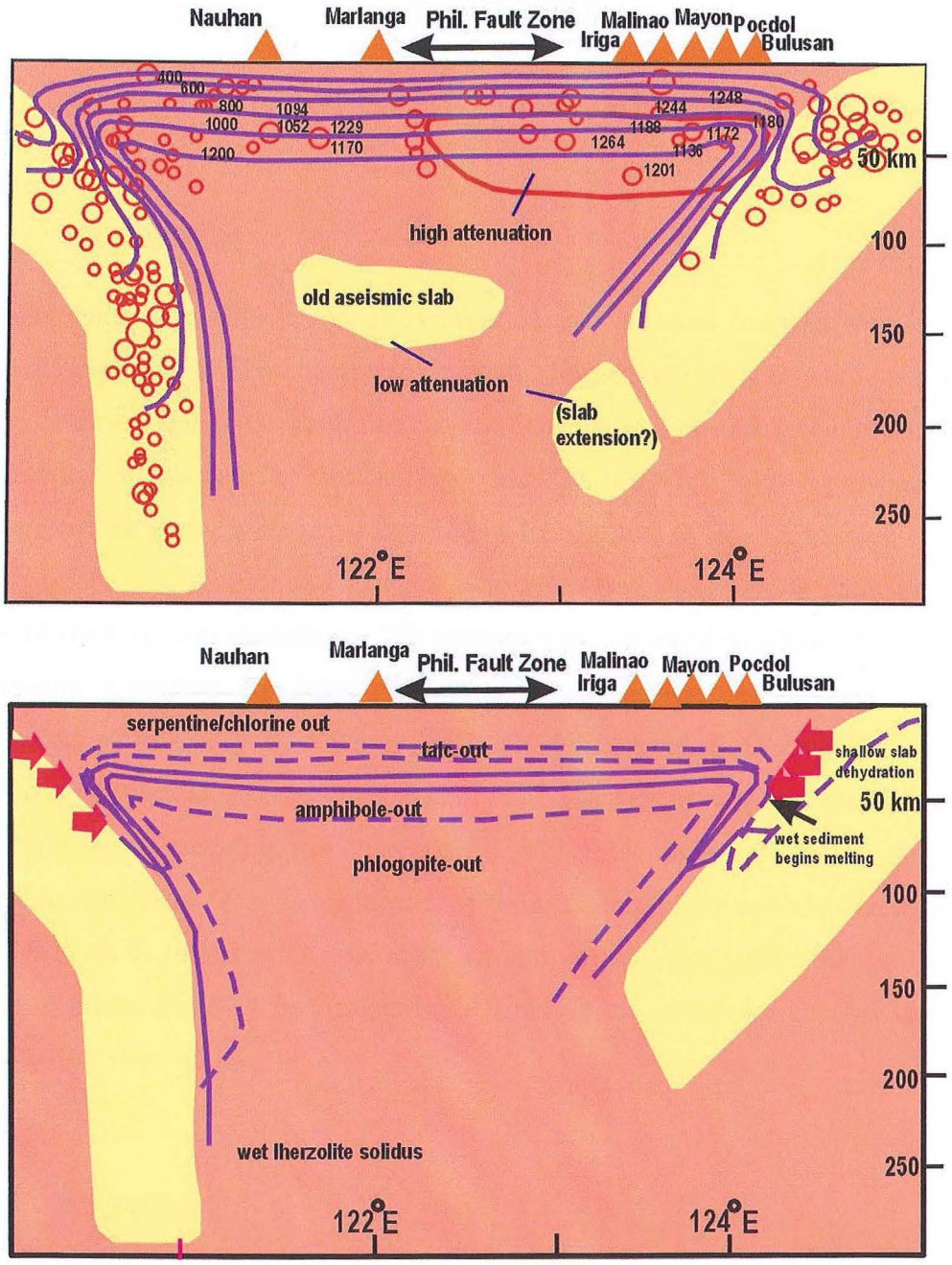

Figure 1.7. Thermo-petrologic transect on the southern volcanic area. Top photo shows tomography beneath the southern Bicol volcanoes as interpreted by Arcilla (1998) from Besana (1997). Magmatism in the Bicol volcanic arc is attributed to subduction processes along the Philippine Trench. Mayon Volcano is located within the zone of amphibole breakdown (bottom photo) (*Source: Arcilla, 1998*).

CHAPTER 2

Chronology of Events: Historical Perspective

2.1. Introduction

The sequence of events in the 1814 eruption was inferred from existing eyewitness accounts that were written mainly in Spanish. English translations were done for most of the historical accounts. Both English and Spanish versions are found at the library of the Philippine Institute of Volcanology and Seismology. Among these historical accounts, none gives more vivid detail than the account of Fr. Aragoneses (1814), the parish priest of Cagsawa and Budiao, who witnessed the eruption from the vantage point of the Cagsawa settlement. His account was contained in a letter to the residents in Manila appealing for help. Fr. Aragoneses' account is substantiated by six documents published in 1814 pertaining to the 01 February 1814 eruption. One of the supporting historical accounts was that of Fr. Mata (1814) which contained details of the eruption and post-eruption observations. Other accounts were mostly quoted from the original account of Fr. Aragoneses. Although some of the accounts were unable to add descriptions of the eruptions, each account corroborated each other and validated the descriptions made by Fr. Aragoneses. However, discrepancies in dates and number of casualties were noted.

2.2. Precursors

The only identified precursor for the 1814 eruption was a series of locally felt earthquakes that described as having commenced on 31 January, a day before the eruption. A strong earthquake was felt at 0200h, and 0400h. Forthwith, these earthquakes subsequently persisted with increasing frequency and magnitude until the eruption began at 0600h on 1 February 1814 (Aragoneses, 1814; Martinez, 1859; Selga, 1914).

From the historical records of the 1814 eruption, no significant observations can be interpreted as long-term precursors. There was no increase in steam emission. However, subterranean or precursory lava dome growth was documented.

2.3. Eyewitness accounts

Fr. Aragoneses (1814) wrote a detailed description of the 6-hour 1814 eruption. His point of observation was at Cagsawa, a flourishing town situated on the southern slopes of the volcano (Figure 2.1). This town now exists as part of Daraga. Aragoneses (1814) narrated that it was a fine day when the villagers were awaken by rumbling sounds. At 630h, a light ash fall occurred while the subterranean noise persisted. This was subsequently followed by two hours of powerful ejection of ash, lapilli and bombs from 0800h-1000h of 01 February 1814. At 1000h, the ejection of lapilli stopped but the rain of ash and smaller lapilli continued until 1330h. The following are portions of Aragoneses' description of the main eruptive phase:

> *Eight o'clock that fatal morning rang, at which time the volcano suddenly started to throw out a dense column of rocks, stones, sand, and ashes with such a great velocity that in a moment it reached into the upper levels of the atmosphere, at which sight we were taken by surprise and fear and more so when we noticed the volcano sides were also being covered.*
>
> *...and then we perceived a great river of fire which was coming towards us to consume us. The speed at which that horrible flood was coming towards us did not give us time to think much less hold long discussions. The frightful noise emitted by the volcano caused great terror even in the hearts of brave men. The horizon and the skies started to get dark and our anguish was redoubled. Incessantly, the terrible roar of the volcano increased, and so with the darkness, we continued our flight unalterably to save our lives by putting a greater distance between us and the terrifying object. But no matter how fast we were running we were caught in our misadventurous flight by a great rain of stones to which violence many unfortunate ones lost*

their lives instantly. These unforeseen and cruel circumstances, make us pause in our race and take refuge under the houses but from the skies fall flames and glowing stones that in a short time the houses were reduced to ashes.

In the house we no longer found refuge. To go out in the open was to expose one's self to another danger, because the rocks and stones that were falling were of huge sizes and they fell like a real rain. Those who were able to defend themselves in some ways stayed alive, but those who were caught in the open with nothing at hand to cover themselves, almost all died or were gravely injured.

The horrible and fearsome roar of the volcano increased further, more rains of stone and coarse sand falls, rocks and flaming comets continued.

At 1000h of the morning, the rain of stones stopped and everyone stayed in his place for the rains of sand to stop too. We remained thus up to 1300h in the afternoon at which time the volcano abated and the skies cleared a little.

2.4. Interpretation of volcanic processes

From Aragoneses' narration, light ash fall signaled the beginning of the eruption. The initial tephra fall was derived from the eruption column that was observed to have developed at 0800h of 01 February 1814. Concomitantly, density flows were observed hugging and covering the southern slopes of the volcano and traveling at a very high speed. From Fr. Aragoneses' description, the observance of density flows and occurrence of tephra fall appear to have been experienced simultaneously, but tephra fall persisted until 1330h.

From the vantage point of Guinobatan in the south-southwest, the eruption column and formation of density flows were observed at the same time. A Franciscan friar, Fr.

Tubina described the column as having a "black foot due to the shade above (referring to the top of the eruption column) (Huerta, 1865).

The historical accounts indicate that a column collapse had already occurred as early as witnesses observed the formation of an eruptive column at approximately 0800h. The collapse of some portions of the eruption column generated pyroclastic flows and surges that reached the settlements of Budiao, Cagsawa, Guinobatan and Albay (Figure 2.1). Several eruptive episodes were described with eruption columns billowing into the sky. One observer noted that after the development of the eruption column, a violent earthquake occurred followed by "violent vomiting of lava" (Huerta, 1865). This would imply that another explosion occurred that resulted in the development of a new eruption column. As narrated by Huerta (1865), the same observer further noted that "the cloud then spread, obscured the ground and set the atmosphere on fire". Several documents narrate of tephra fall that burned buildings and houses (Aragoneses, 1814; Huerta, 1865).

Very large bombs and blocks were seen rolling near the crater. Airfall as big as "jars" reached Bublusan, a municipality of Guinobatan, 10km from the crater, and "as big as chicken's egg" in San Miguel Island, 18 km from the crater. The lapilli and ash fell on Camalig, Cagsawa and Legaspi (formerly known as Albay), Sto. Domingo, Tabaco and Tiwi (Espinas, 1968) (Figure 2.1). Due to the prevailing northeast monsoon wind, tephra fell mostly on the southern and southwestern sectors of the volcano. The towns of Camalig, Cagsawa, Legaspi, Budiao and Guinobatan were the most affected by heavy tephra fall. However, substantial tephra fall was also deposited in the east and southeast affecting the towns of Sto. Domingo and Tabaco in the eastern sector, and Tiwi in the northern part of Mayon Volcano. Ash fall was described to have reached Manila that is 325 km northwest of the volcano and some towns in Northern Luzon (Peralta, 1814; Huerta, 1865; Maso, 1904, 1911). Peralta (1814) performed chemical analysis on the ash that fell in Manila. There were also reports that ashfall reached China and the South China Sea (Huerta, 1865) but this might be confused with the ash from the 1815 eruption of Tambora.

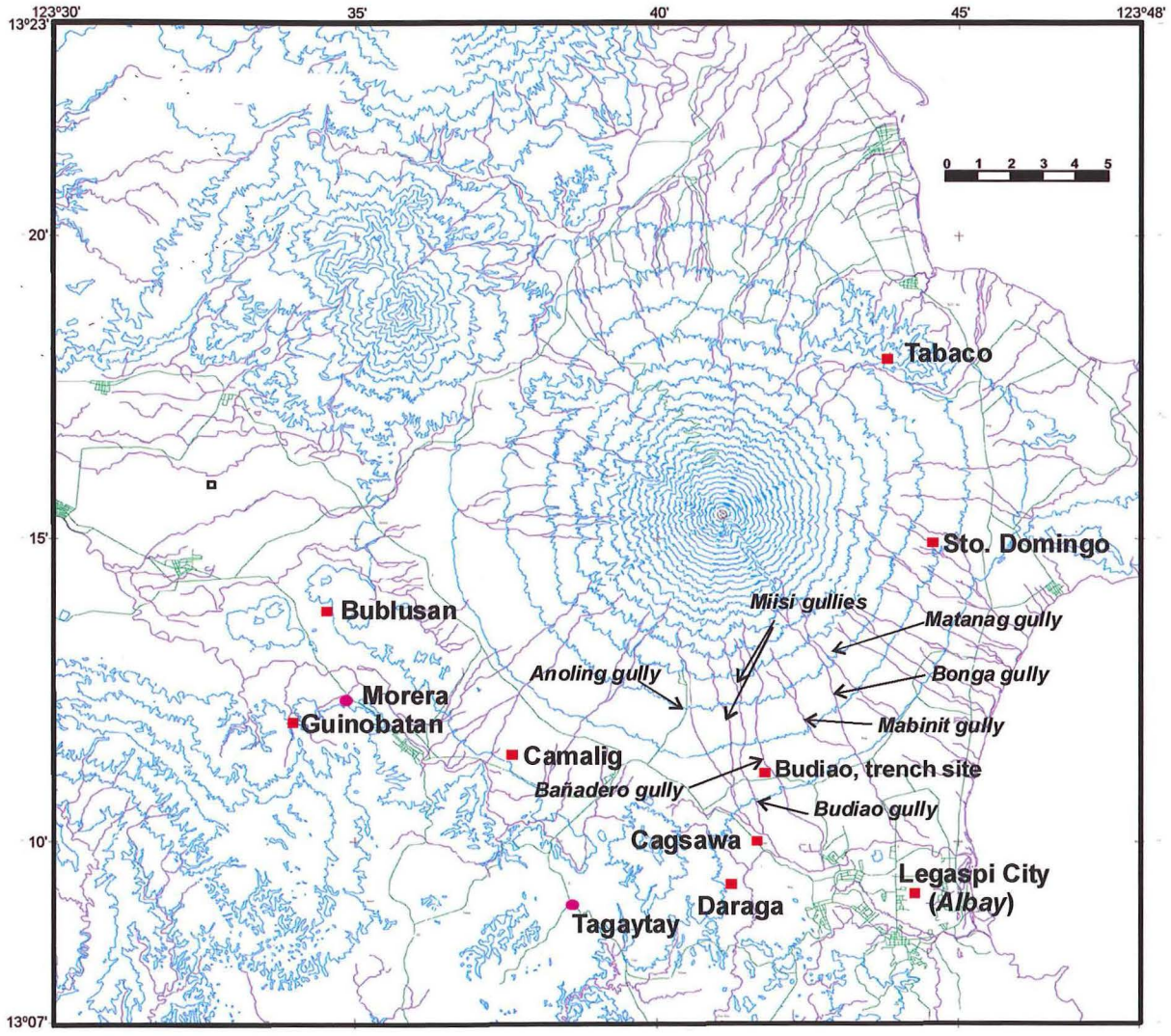

Fig. 2.1 Map showing the locations of towns that were affected by the 1814 eruption. Present locations approximate the 18th century town locations. Old names are italicized.

The documents described wide areas covered by black sandy material (Aragoneses, 1814). Deposits in some areas reached as much as 1 meter in thickness (Aragoneses, 1814). Approximately 50 to 100 cm of black tephra was deposited in the towns of Budiao and Cagsawa (Aragoneses, 1814; Calleja, 1937). At 10 km from the crater, the deposit was 0.4m thick (Maso, 1911).

The eruption generated heavy tephra fall that were dense enough to cause darkness in the impacted areas and in the northern parts of Mayon Volcano. There were also reports that darkness was experienced at Laong, Samar (Mata, 1814) and parts of northern Luzon, including Manila, 325 km northwest of the volcano (Abella, 1881; Coronas, 1897, Packard, 1900; Selga, 1914). From these accounts, it can be inferred that a relatively tall eruption column developed to cause heavy fallout in areas hundreds of kilometers from Mayon. Explosions were also heard in Laong, Samar, an island located approximately 200km southeast of Mayon Volcano (Maso, 1911).

The sequence of events from historical documents is summarized as follows and a sketch of the events as interpreted from historical data is shown in (Figure 2.2):

- Earthquakes a day before the eruption with increasing frequency and magnitude until the commencement of tephra falls at 0800h.

- Ash fall at 0630h, probably associated with a phreatic eruption (vent-opening phase of the eruption).

- Main tephra fall at 0800-1000h and within this period, fountain collapse occurred generating pyroclastic flow and surge. A resurgence of activity might have occurred and produced another eruption column.

- Lahars swept through the settlements of Budiao and Cagsawa, two settlements situated near major river channels.

31 January 1814	*Locally-felt earthquakes started in the afternoon which persisted and increased in intensity until the following day.*	
1 February 1814	*0630h* *Ash was felt in the southern sectors of the volcano.*	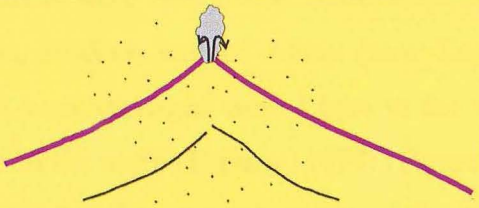
1 February 1814	*0800h-1000h* *Development of a column and formation of a density flow in the southern slopes. Ash and lapilli fall simultaneously experienced.* *Tephra fall was dense enough to cause darkness in the affected areas.*	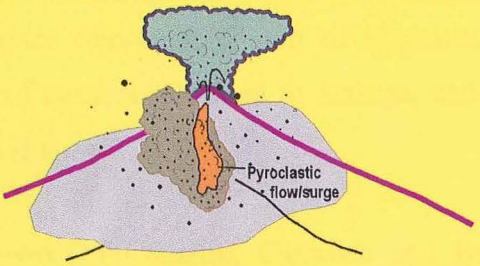
1 February 1814	*1000h-1300h* ***At 1000h, lapilli stopped but ash fall continued until 1330h.***	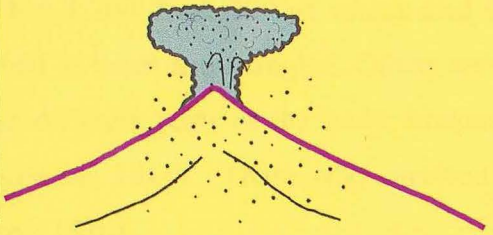
3 Weeks after the eruption	*Steaming at the main crater and from three smaller craters formed during the eruption continued until three weeks after the eruption.*	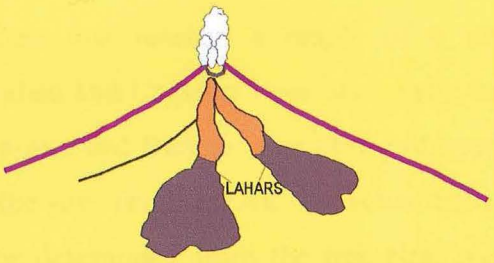

Figure 2.2. Schematic diagram of the eruptive sequence as inferred from narrative accounts.

Damages

At least six towns in the southern portion of Mayon were devastated during the 01 February 1814 eruptive event. The affected areas were established settlements in the province of Albay, namely, Cagsawa, Daraga, Budiao, half of Albay (now Legazpi City) and Guinobatan. Other settlements that were damaged were Ligao in the west, Sto. Domingo in the east, and Tabaco and Tiwi in the north (Espinas, 1978) (Figure2.1). Some of these towns became uninhabitable which led to the relocation of the whole settlement of Daraga (Selga, 1902). The once important church of Cagsawa was abandoned and never rebuilt. Villagers from Cagsawa relocated to Daraga, and later incorporated their town, Cagsawa into Daraga (Figure 2.3).

The 1814 eruption set on fire the entire towns of Camalig, Cagsawa and Budiao (Saderra, 1904). Casualties included more than 1,200 dead, 200 of which died inside the Budiao church. The corpses were described as burnt and mangled. Others survived the eruption but sustained injuries wounds in different parts of the body, broken legs and arms or crushed in various ways (Aragoneses, 1814). Those who survived took refuge in caves and sturdy shelters (Aragoneses, 1814).

Torrential rains were formed initiating lahars that reached a height of 6 meters (Newhall, 1977). The towns of Cagsawa, Budiao and Camalig were also partly buried by these lahars. The Spanish churches at Cagsawa and Budiao were also destroyed but portions of these ruins can still be found on the sites (Figure 2.4). However, the exact timing of the occurrence of lahars cannot be determined from the historical records alone. It is quite certain that there was a significant time before lahars occurred, judging from the fact that the eyewitnesses were able to describe the dead and destroyed houses.

2.5. Post-eruption events and observations

Two weeks after the eruption, smoke and ashes were still observed from the volcano. "Fire" (presumably crater glow) was observed at night in the crater on February 9 and 10 and on February 13, 14 and 16. Smoke and minor ash ejections were witnessed three days after the eruption (Mata, 1814). Three small vents were created near the main crater through which smoke and ashes were emitted ejected several days after the eruption (Aragoneses, 1814; Perry, 1860). The crater was breached in the southern side and lowered by approximately 40 meters as a result of the eruption (Aragoneses, 1814; Huerta, 1865; Packard, 1900).

Figure 2.3 The Daraga Church, built after the destruction of Cagsawa in 1814 (Photo by A. Baloloy, PHIVOLCS).

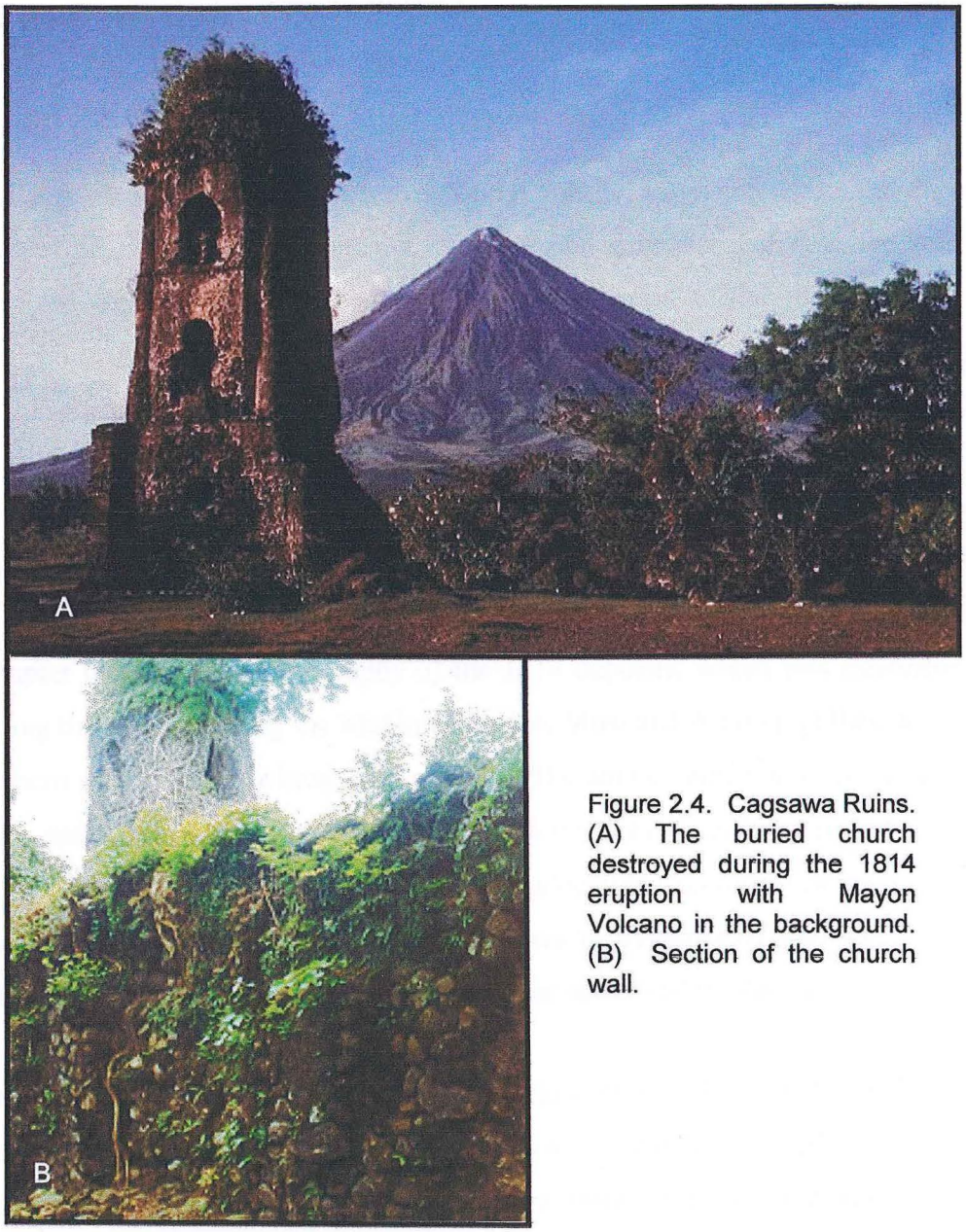

Figure 2.4. Cagsawa Ruins. (A) The buried church destroyed during the 1814 eruption with Mayon Volcano in the background. (B) Section of the church wall.

CHAPTER 3

Stratigraphy

3.1. Introduction

The 01 February 1814 eruption generated two ignimbrite, surge and tephra fall deposits. As inferred from historical documents, the deposits were distributed in the southern slopes of the volcano. The most proximal primary deposit of the 1814 eruption was exposed about 4km from the vent but most of the deposits were preserved and mapped at 5 to 7 km from the crater. Coarse tephra fall deposits were the most distal eruptive products, traced as far as 15 km from the vent. Correlation of the units from four adjacent gullies resulted in the establishment of a composite stratigraphy of the eruptive deposits from the 1814 eruption.

This chapter describes the stratigraphy of the 1814 deposits, which was established by correlating the deposits along the Mabinit, Budiao, Miisi and Anoling gullies, located at the southern sector of the volcano (Figure 3.1). The data gathered were correlated with trenching data and historical accounts. The 1814 deposits were also mapped along the Bonga and Matanag gullies, located in the southeastern sector of Mayon Volcano (Newhall, pers. comm., 1998). However, there was no evidence of emplacement of the 1814 deposits along other major gullies in the other sectors of the volcano.

The stratigraphic study was supported by descriptions of the lithologic, mineralogic, and geochemical compositions, grain size analyses, analyses of thermo-remanent magnetization (TRM) of representative deposits from each eruptive unit, and 14C dating of charred wood. This was done for the purpose of establishing the stratigraphic sequence of the 1814 eruptive products. A fluxgate magnetometer was utilized to determine the TRM data. The ^{14}C dating of charred wood found in the 1814 surge deposit provided an independent source for age and aided in correlating the lithostratigraphic units across the southern gullies.

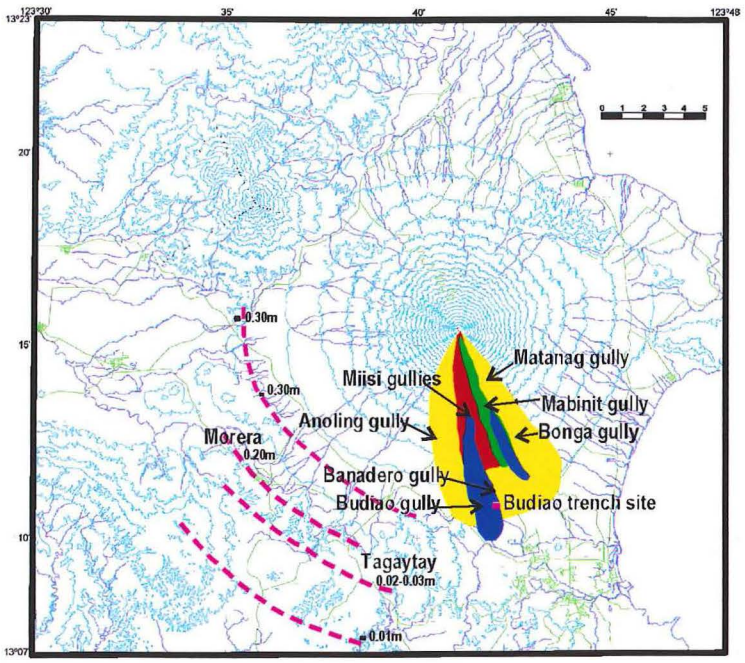

Legend:

- Post-eruption hot lahar deposits
- Upper ignimbrite
- Pyroclastic surge deposit
- Lower ignimbrite
- Thickness of tephra fall deposit

Lh	Hot lahar
Uig	Upper ignimbrite
S	Pyroclastic surge deposit
Lig	Lower ignimbrite

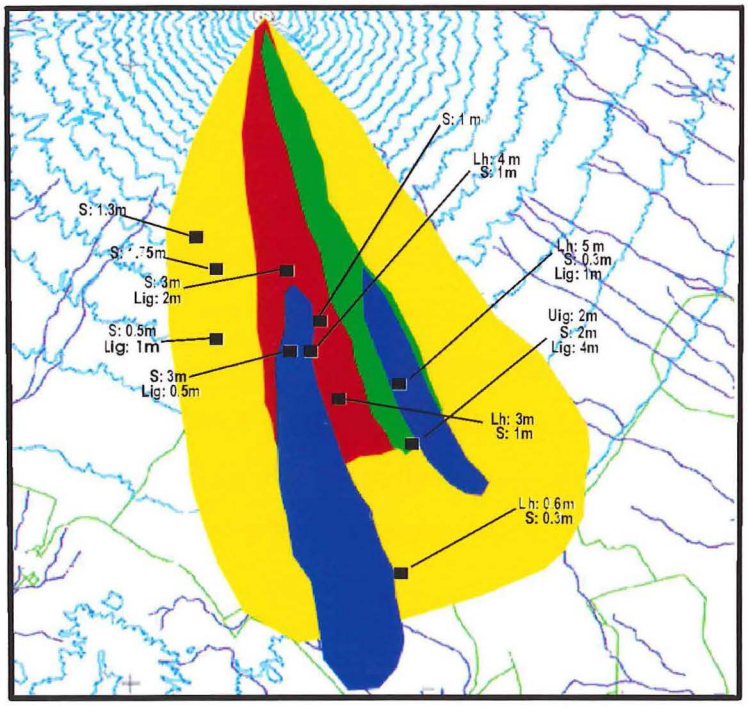

Figure 3.1 Approximate delineation of extent of the 1814 deposits. Delineation is based on field mapping and other geological data. Enlarged figure shows thickness of the deposits measured in the field.

The composite stratigraphy of the 1814 deposits, from bottom to top, is comprised of pre-1814 layer, tephra fall, lower ignimbrite, pyroclastic surge, upper ignimbrite and two major post-eruption lahar units (Figure 3.2A). The composite stratigraphic sequence was drawn from the stratigraphy of the 1814 deposits emplaced along the affected gullies (Figure 3.2B).

3.2. Stratigraphic descriptions

3.2.1. Pre-1814 layers

The 1814 deposit lies on top of older lahar, soil or ignimbrite deposits. The contact between the pre-1814 layers was observed to be commonly erosive except where the overlying 1814 deposit was tephra fall. In some affected gullies, the primary 1814 deposits were underlain by massive, polymictic lahar deposits with gray, sandy matrix. The pre-1814 lahar deposits were noted to be gray in color and had thickness ranging from 0.5 to 2 m. Medial and proximal lahar outcrops showed preponderance of boulder-sized clasts.

In the Budiao gully and the Budiao trench site, the 1814 deposit directly overlies the pre-1814 layer, a brownish-yellow ignimbrite with zones of lapilli concentration (Figure 3.3). The lowermost part of the unit is generally matrix-supported and overlies an older lahar unit. The clasts in the matrix- to clast-supported portions of the ignimbrite consisted of angular to subangular, brown to reddish lapilli of scoria and dense lithics with minor altered clasts. The matrix consisted of brownish-yellow medium-grained ash. The brown ignimbrite was 1.5 m thick at the Budiao gully and was less than 1m at the trench site. The upper contact is highly eroded by an overlying surge unit at Budiao gully but is gradational at the trench site.

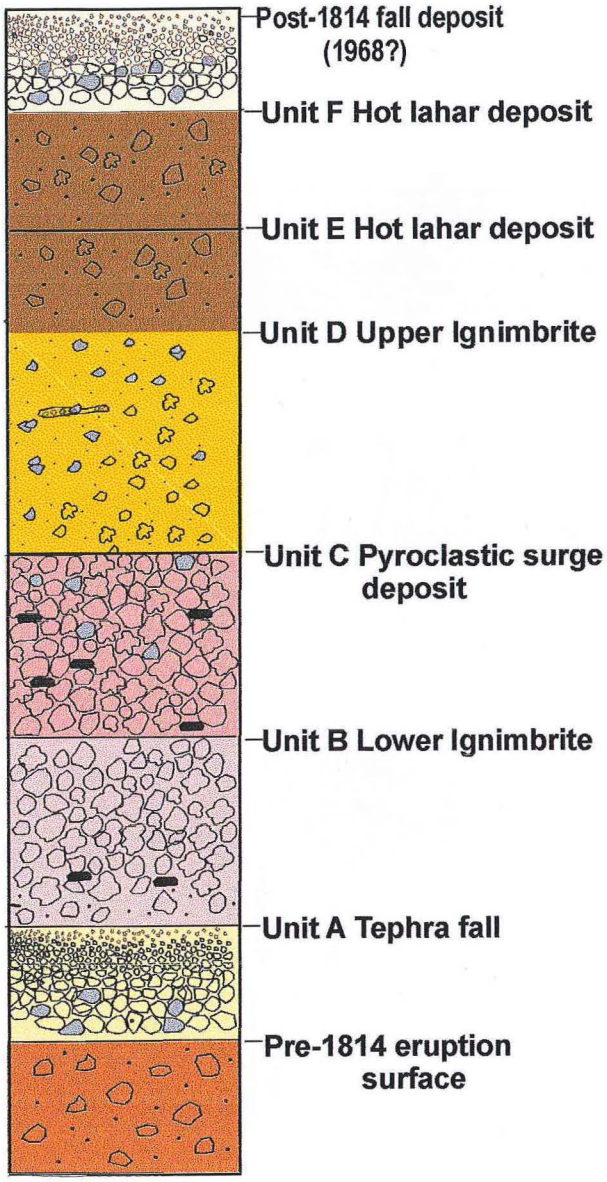

3.2A. *The composite 1814 stratigraphy.*

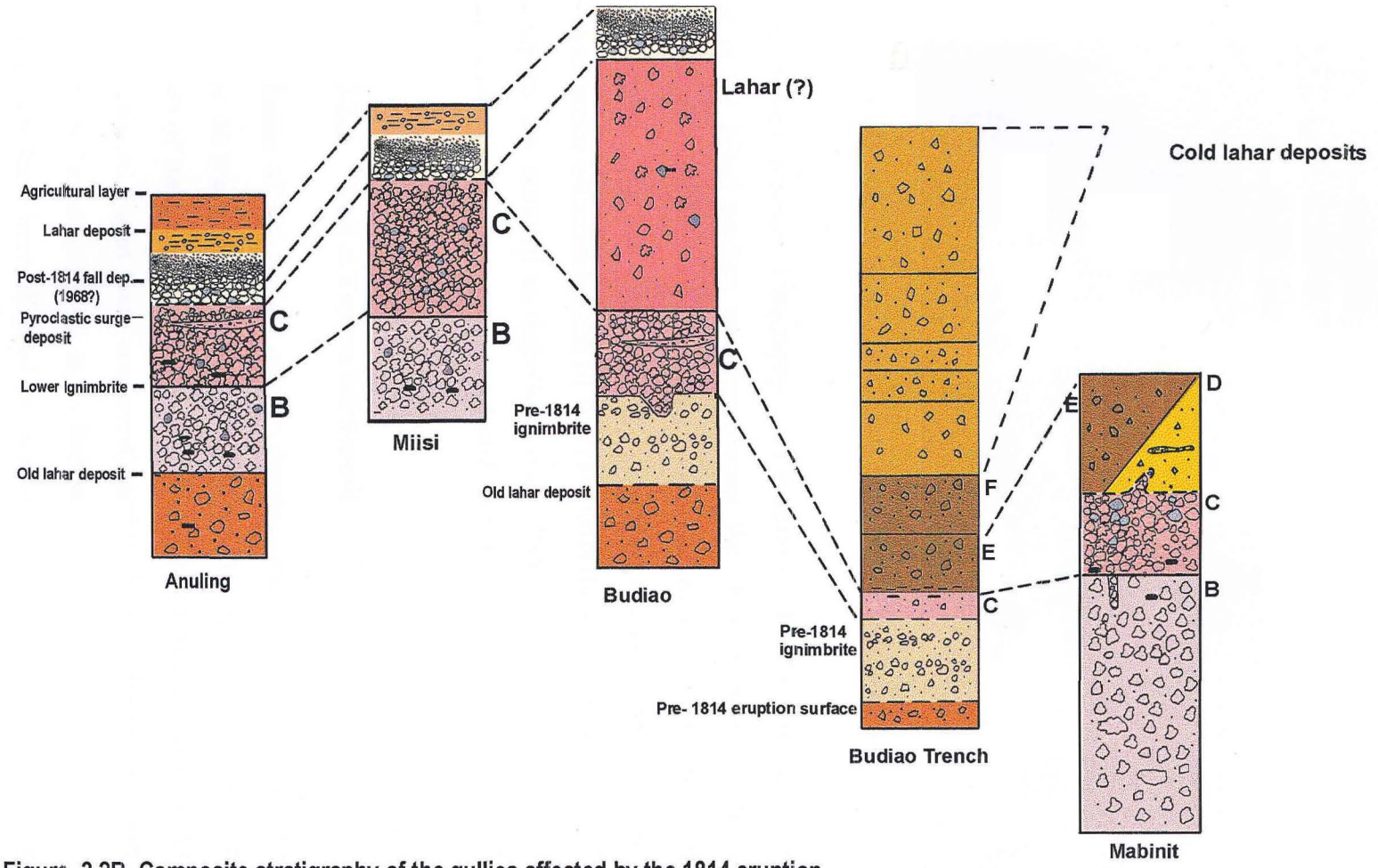

Figure. 3.2B Composite stratigraphy of the gullies affected by the 1814 eruption.

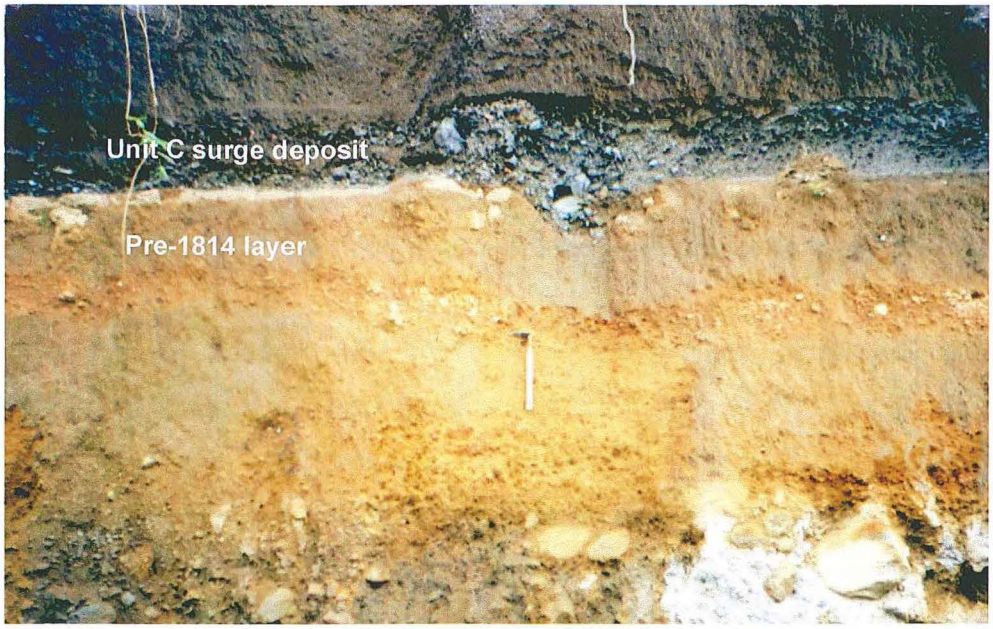

Figure 3.3. Erosive contact of Unit C with a pre-1814 deposit at Budiao gully.

Based on the composite stratigraphy, Unit A consists of tephra fall deposits which form part of the initial product emplaced during the 1814 eruption of Mayon Volcano. Tephra fall occurs in poorly exposed outcrops that were mapped in the southern sector of the volcano. The few preserved units were noted in undisturbed low-lying hills in the southern sector with distal extent of 10-12km from the vent. At distances of 12 to15km, the tephra unit occurred as dispersed clasts. Beyond 15km, the tephra fall unit was sporadically observed in topographic highs such as undisturbed low-lying hills.

3.2.2. Unit A Tephra fall deposit

The thickness of the tephra unit predictably decreased away from the vent and depending on prevailing wind direction during the time of eruption. The measured thicknesses of the tephra fall unit were 0.35 m in Bublusan, Guinobatan (southwest), 0.30 m in Nasisi, Ligao (west-southwest), and 0.25 m in Morrera, Guinobatan (Figure 3.1). The Bublusan (referred to as Bulusan in the account) area was referred to in documents to have been affected by "rains of rocks as big as chicken's egg" (Calleja, 1937).

In another trench study conducted by JICA at the Cagsawa Ruins (Tubianosa *et al.*, 1999, unpublished report), a correlative tephra fall layer may have been part of the 1814 eruptive product but was not utilized as part of the stratigraphic study for this paper. Thickness of the coarse and fine tephra is 0.1 and 0.03 m, respectively. Farther out at 14 to 15 km from the vent, the deposit occurs as dispersed clasts on topographic highs.

Very few tephra fall outcrops were preserved. In places where they are still noted, the fall occurred as unconsolidated, dark gray unit consisting of vesiculated, angular to subangular, gray scoria lapilli, angular greenish-gray andesite and a few angular altered lithics. The unit exhibited normal grading. Outsized clasts of lapilli were mapped with medial facies measuring about 0.35 m. The average clast size of the coarser base is 0.2 m.

Tephra fall was not observed in association with the primary pyroclastic deposits from the 1814 eruption in any of the investigated gullies. The fall deposits were correlated mainly through petrologic and geochemical similarities with the juvenile scoria from dated surge and ignimbrite units. Previous studies in the upper slopes of the volcano showed a possible 1814 tephra fall, which occurred below the 1814 pyroclastic surge at 475m-elevation in the Bonga Gully (Newhall, pers. comm., 1998). The unit consisted of red scoria layer with maximum thickness of 0.13 m. Investigation of the said outcrop was not done due to the ongoing eruptive activity of Mayon Volcano at the time of the field survey.

3.2.3. Unit B lower ignimbrite

Unit B is comprised of black, bomb-rich, coarse ignimbrite exposed in the gullies of Anuling (south-southwest, Miisi (south), and Mabinit (southeast) (Figure 3.4). The unit was also noted in Matanag and Bonga gullies at elevation 350m and 500m, respectively (Newhall pers. comm., 1998). Outcrops of the ignimbrite were sporadically exposed and were often obscured when traced laterally along and across gullies. Most of the ignimbrite outcrops were exposed at 200 to 300m elevations. There was no general lateral trend in the thickness of the unit. Proximal deposits found at elevations from 500

to 350 m have maximum thickness of 4m while outcrops at 200 to 300m were measure to be 2 to 5 m thick.

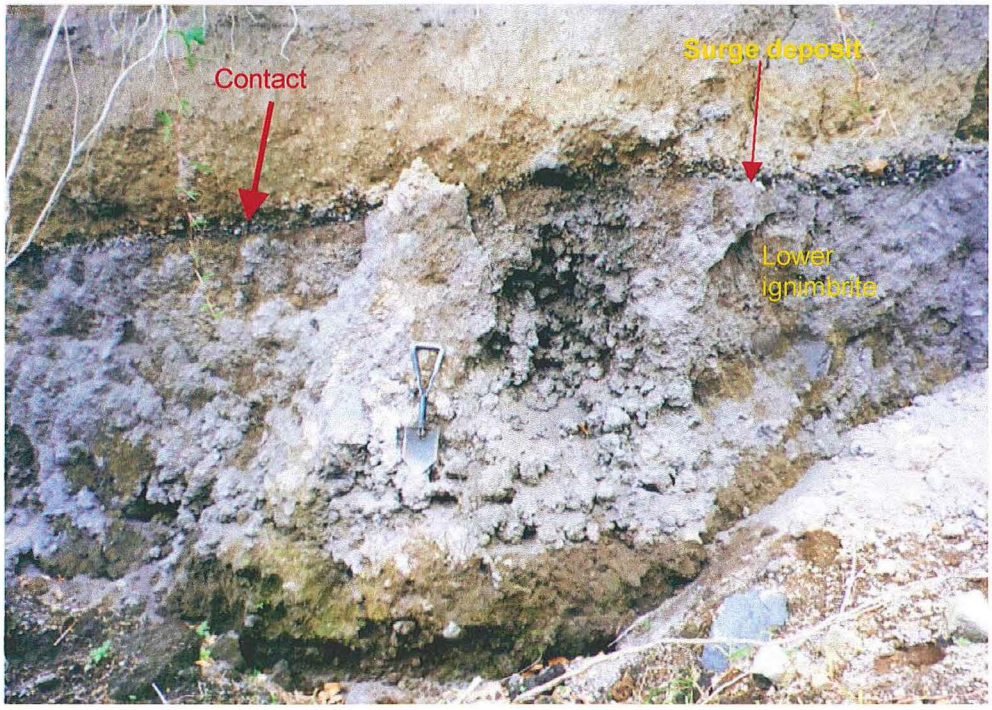

Figure 3.4. A 3m-thick 1814 Unit B lower ignimbrite overlain by a thin Unit C pyroclastic surge at Mabinit gully.

Fines-depleted degassing pipes, as much as 0.5 m in diameter and 0.8 m long, were present and usually occurred in the upper portions of the unit. Smaller degassing pipes branch out while bigger pipes appear to coalesce into the overlying surge layer (Figure 3.5). The unit was also noted to be rich in carbonized wood, which was essentially concentrated at the base of the deposit. Dated charred wood collected from the ignimbrite unit found at the Mabinit gully had an age of AD 1725-1813 (uncalibrated age: 300+/-90 year) (Newhall, pers. comm., 1998).

The base of the flow unit has an erosive contact with the underlying pre-1814 lahar unit, but is often obscure. In places where the 1814 pyroclastic flow and surge units occur successively, the surge unit always overlies the flow deposit with a sharp and erosive contact. If the surge is absent, the flow unit is succeeded by non-1814 lahar and ignimbrites.

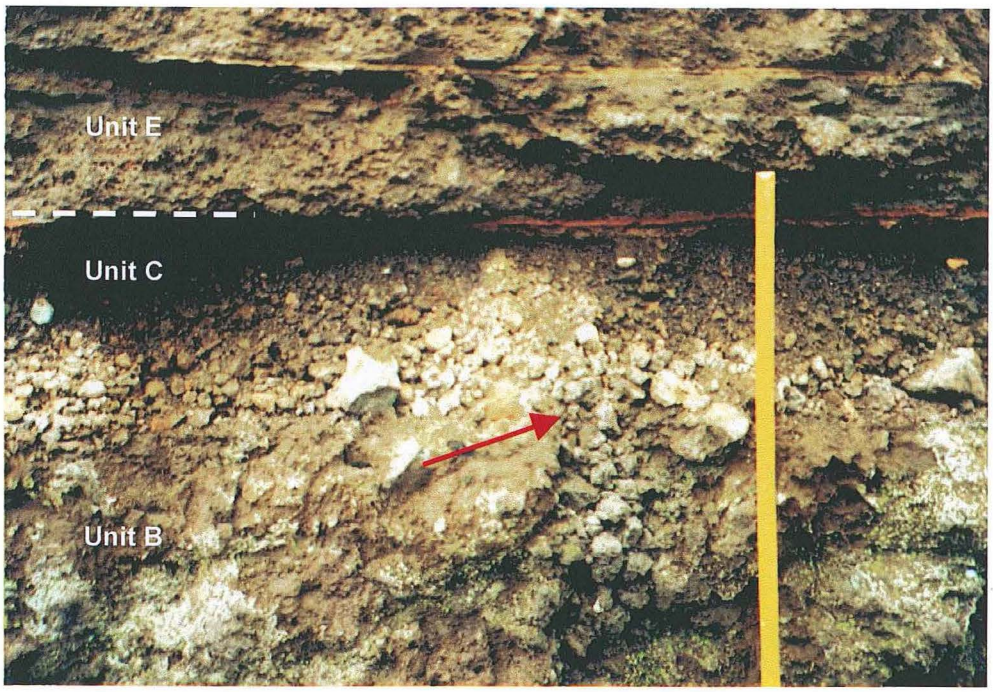

Figure 3.5. Degassing pipe (shown by arrow) observed in Unit B at Mabinit gully. Unit E hot lahar layer overlies the surge unit. The contact between the surge and lahar consists of a red oxidized lamina of clay/silt. Dashed line marks the contact of the surge and lahar deposits.

3.2.4. Unit C surge deposit

Unit C consisted of highly friable, black to dark gray pyroclastic surge deposit, which is equivalent to the unit at Anoling gully previously described by Newhall (1977). Unit D had a wider distribution in the southern slopes of the volcano than the ignimbrite unit. The surge unit is well exposed and can be traced laterally along the gullies of Mabinit, Anoling, Miisi and Bañadero. Surge outcrops of up to 1m were also exposed in the upper reaches of Matanag and Bonga Gullies (Newhall, pers. comm., 1998) but may have been covered or eroded by flows from the recent eruptions of the Mayon Volcano. The surge deposits also occurred in the interfluve between Bañadero and Budiao Gullies. The thickness of the surge ranged from 2.0 to 0.1 m.

The surge unit has a ubiquitous fines-depleted character in all its outcrops. It is composed mostly of black scoria lapilli and bombs (Figure 3.6). Clasts consist of 80% juvenile dark scoria and bombs, 15% greenish-gray, angular to subangular dense andesite lithics and 5% subangular to subrounded yellow and red altered clasts.

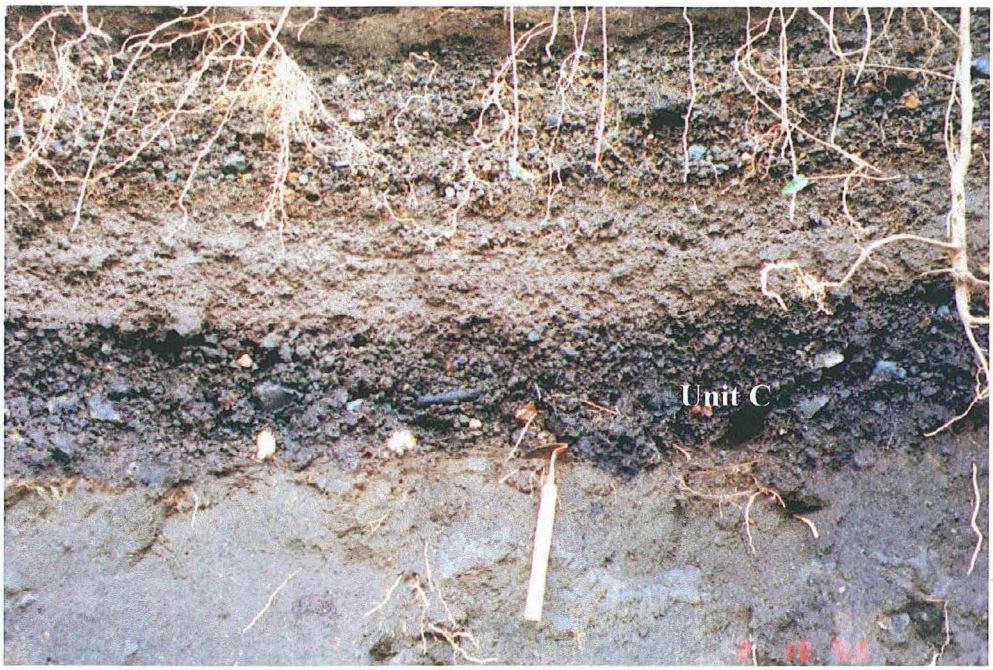

Figure 3.6. The black 1814 Unit C surge can be distinguished by its ubiquitous color and fines-depleted texture as exhibited by the surge outcrop at Anoling gully. The surge is strongly fines-depleted and can maintain thickness laterally. Flow direction is indicated by an arrow.

Scoria clasts were noted to be subangular to subrounded and often had a cauliflower appearance. Altered clasts exhibited cracks, which were probably due to impact during transport by traction. The maximum sizes of juvenile, dense lithic and altered clasts were 0.20 m, 0.15 m and 0.18 m, respectively.

Surge outcrops in the gullies vary from very thin (a few cm) to very thick (2 m). Pinch and swell structures are also common in the deposit. This unit has a sharp, erosive contact with underlying pre-1814 Unit B ignimbrite, as evidenced by truncated fumarolic pipes in the flow deposit. The basal contact is undulating and shows scour features on the underlying lahar and soil units, as well as baking features (Figure 3.7).

The surge unit shows good sorting and grading. It is generally normally graded but may exhibit reverse and symmetric grading (Figure 3.8). Density grading is absent as exhibited by the occurrence of outsized juvenile and dense lithic clasts throughout the surge bed. TRM signature of the surge deposit exhibits uniformly oriented clasts with a strong N and horizontal orientation. The unit maintains its thickness over some distance although it thickens in valleys and thins in topographic highs.

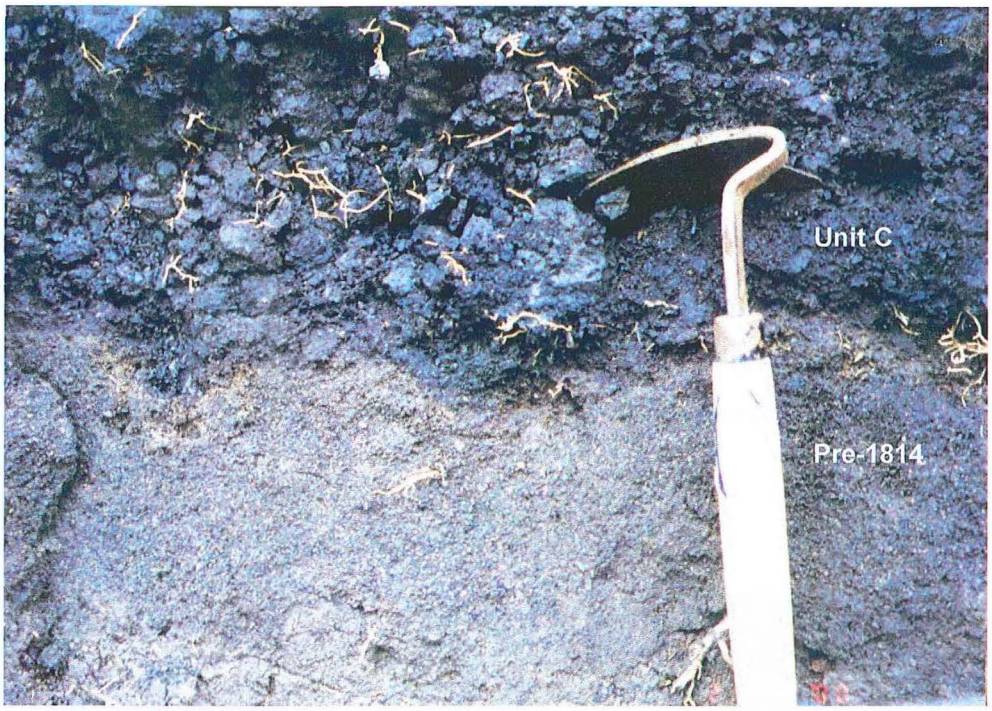

Figure 3.7. The lower boundary of the Unit C surge deposit at Anoling gully exhibits scour and baking features on the underlying pre-1814 lahar unit.

Figure 3.8. The 1814 Unit C pyroclastic surge exhibits good sorting and symmetric reverse to normal grading. Photo taken at Budiao gully.

Charred twigs are prevalent in this unit and are concentrated near the lower boundary but are not uncommon in mid and upper portions. Twigs with diameter greater than 20 mm are aligned parallel to the flow direction (Figure 3.9). Thinner twigs (<2 cm) don't exhibit preferred orientation and tend to be dispersed within the unit. The ^{14}C ages for charred twigs collected from the surge at Anoling are AD 1800-1902 (uncalibrated age: 130+/-50y), AD 1724-1814 (uncalibrated age: 200+/-40), and AD 1728-1811 (uncalibrated age: 350+/-200y) from a surge outcrop at Miisi (Dr. Christopher Newhall, pers. comm., 1998). All of the calibrated ^{14}C ages are consistent with the 1814 eruption date at 2 sigma confidence level.

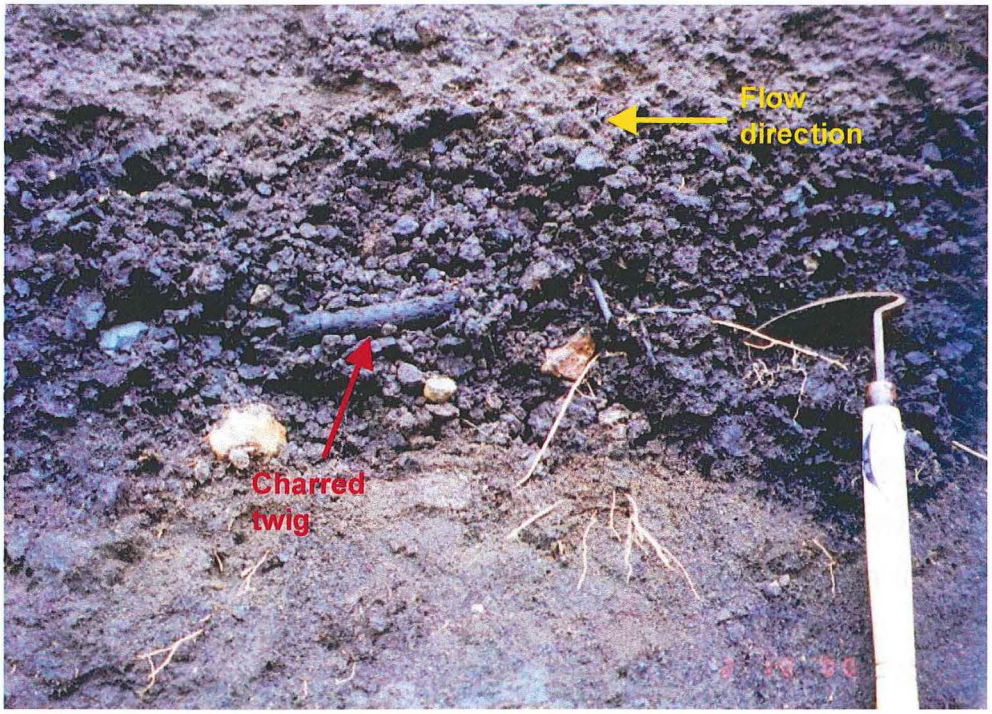

Figure 3.9. Flow oriented charred twig in Unit C surge deposit exposed at Anoling gully. Flow direction and upper boundary indicated by the yellow arrow.

The surge grades laterally into a massive, black, matrix-supported outcrops in the Budiao trench with a thickness of 0.3 m (Figure 3.10). Small charred twigs are dispersed within the unit, which render black stains on the fingers. The distal facies has an indistinct, non-erosive contact with the underlying pre-1814 brown ignimbrite. It has a wavy contact with the overlying lamina of light gray ash.

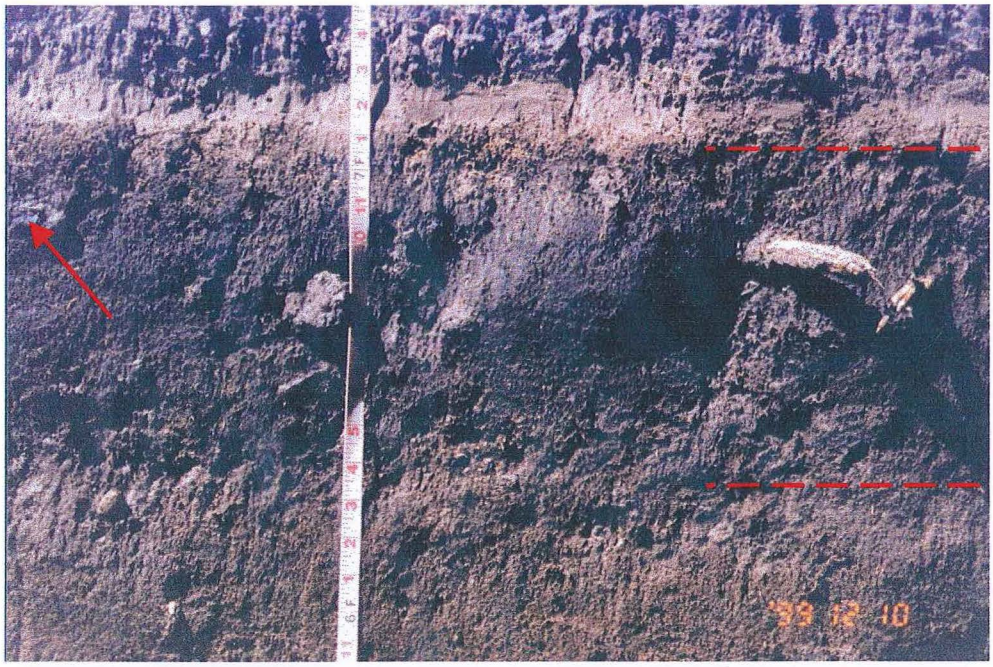

Figure 3.10. Black, massive carbon-rich Unit containing sparse lapilli in Budiao trench. Arrow points to a 0.03m-long charred twig. Dashed lines marked boundaries of the surge boundaries. A diffuse thin lamina of ash overlies the distal surge facies.

3.2.5. Unit D upper ignimbrite

A highly localized ignimbrite overlies the pyroclastic surge in Mabinit gully only. The ignimbrite unit at Mabinit Gully was observed to be yellowish brown, generally massive but contained lenses of clast-supported scoria that were derived from the underlying surge unit (Unit C) (Figure 3.11).

The ignimbrite has a fine, light brown ash matrix is matrix supported. Clasts consist predominantly of altered angular lapilli (80%) with minor dense lapilli. Pieces of charred wood are found within the flow unit. The boundary between the ignimbrite and the underlying surge is sharp and erosive with the lenses and stringers of the surge unit that are observed within the overlying flow deposit.

Figure 3.11. The succession of lower ignimbrite, pyroclastic surge unit and the upper altered-rich deposit at Mabinit. Dashed line outlines eroded portions of the underlying surge unit.

3.2.6. Unit E post-eruption lahar deposit

Overlying the pyroclastic surge deposit is a lahar deposit. The lahar deposit is exposed in the gullies of Budiao, Mabinit and at Budiao trench. The lahar unit is massive, gray to grayish-brown and matrix-supported. It is composed of poorly sorted granule to pebble and subordinate cobble clasts. Clasts are composed of subangular to subrounded scoria, dense basaltic andesite and altered lithics in coarse sand matrix.

The lower lahar layer is 0.2 m in Anuling and 0.6 m at Budiao Trench (Figure 3.12). The base of the unit is vesiculated and highly oxidized while the rest of the layer is strongly indurated. In a separate trenching study conducted near the vicinity of Budiao Church, some portions of the layer are described as containing crusted surfaces (Solidum, unpublished). The clasts show imbrication that is more pronounced in smaller clasts. TRM of the juvenile clasts does not show any coherent magnetization direction (Solidum and Rodolfo, unpublished abstract) implying that the deposits were transported below the Curie temperatures (Arguden and Rodolfo, 1986). The base of

the lahar is in erosional contact with the co-ignimbrite ash in Budiao trench. A lamina of clay/silt layer occurs between the underlying surge and the lower lahar unit.

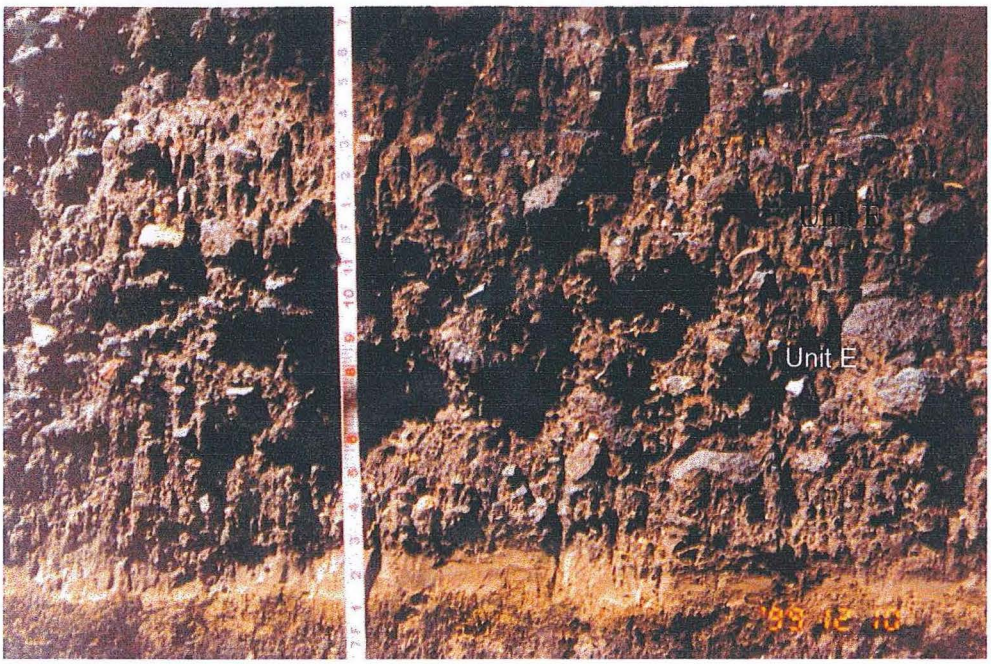

Figure 3.12. Unit E post-eruptive lahar deposit overlying a light gray thin ash layer at Budiao trench.

3.2.7. Unit F post-eruption lahar deposit

The same composition and texture of the second lahar unit is similar to the first lahar unit but it is less indurated. The thickness is approximately 0.7 m at Budiao Trench. The two lahar deposits are separated by a silt/ clay lamina. Overlying the second surge unit in the trench are several layers of cold lahar deposits. The succeeding lahar units consist of polymictic clasts of subrounded to subangular clasts of differing compositions. Matrix consists of gray medium to coarse sand. Crusted surfaces are visibly lacking in the later lahar deposit. The boundary between the lahar deposits is separated by a thin lamina of sand/silt.

3.3. Granulometry

Results of granulometric analyses on representative samples from the 1814 tephra, ignimbrite and surge deposits are presented in this section. Very coarse deposits were not sieved but clast proportions were estimated by measuring the 10 largest clasts for each species (altered, juvenile and dense lithic). The aim of granulometric studies is to further characterize each of the deposits. Analyzed samples were first oven dried at 105 °C overnight. The samples were then sieved using the half-phi interval from -4 to 4 ϕ. Results are presented in graphs (Figure 3.13). Where possible, samples were taken from proximal to medial deposits. Graphs are named according to gullies where samples were taken and marked as medial, distal or proximal.

Histograms of the medial tephra fall show bell-shaped graphs that are skewed to the left with peaks at -2.5 ϕ to 1.5 ϕ. The graphical signatures of the tephra fall signify good sorting commonly observed in tephra fall deposits. The coarseness of the clasts in the upper portion of the 1814 tephra is reflected in the left skewness of the graphs, while presence of outsized is shown by peaks in the two modes.

Matrix and clast portions of the lower and upper ignimbrite were sampled. Graphs are bell-shaped and often polymodal (Figure 3.13), with peaks occurring both in the coarse (-4.0 ϕ) and fine modes (2.5 ϕ). Peaks are interpolated to occur at >-4 if the coarser clasts (<4 ϕ) were included. The bimodality and polymodality of flow deposits reflect poor sorting that is typical in ignimbrites (Cas and Wright, 1988).

Surge deposits were sampled at different parts in an outcrop section whenever there was a relative change in clast size distribution or if the surge contained lenses. The 1814 surge deposits show unimodal graphs which are skewed to the left reflecting the coarseness of the unit. The unimodal graphs suggest good sorting in the pyroclastic surge deposits. Grain size graph of the distal ground surge at Budiao trench shows a graph skewed to the right suggesting relative concentration of finer clasts as compared to the coarse fraction.

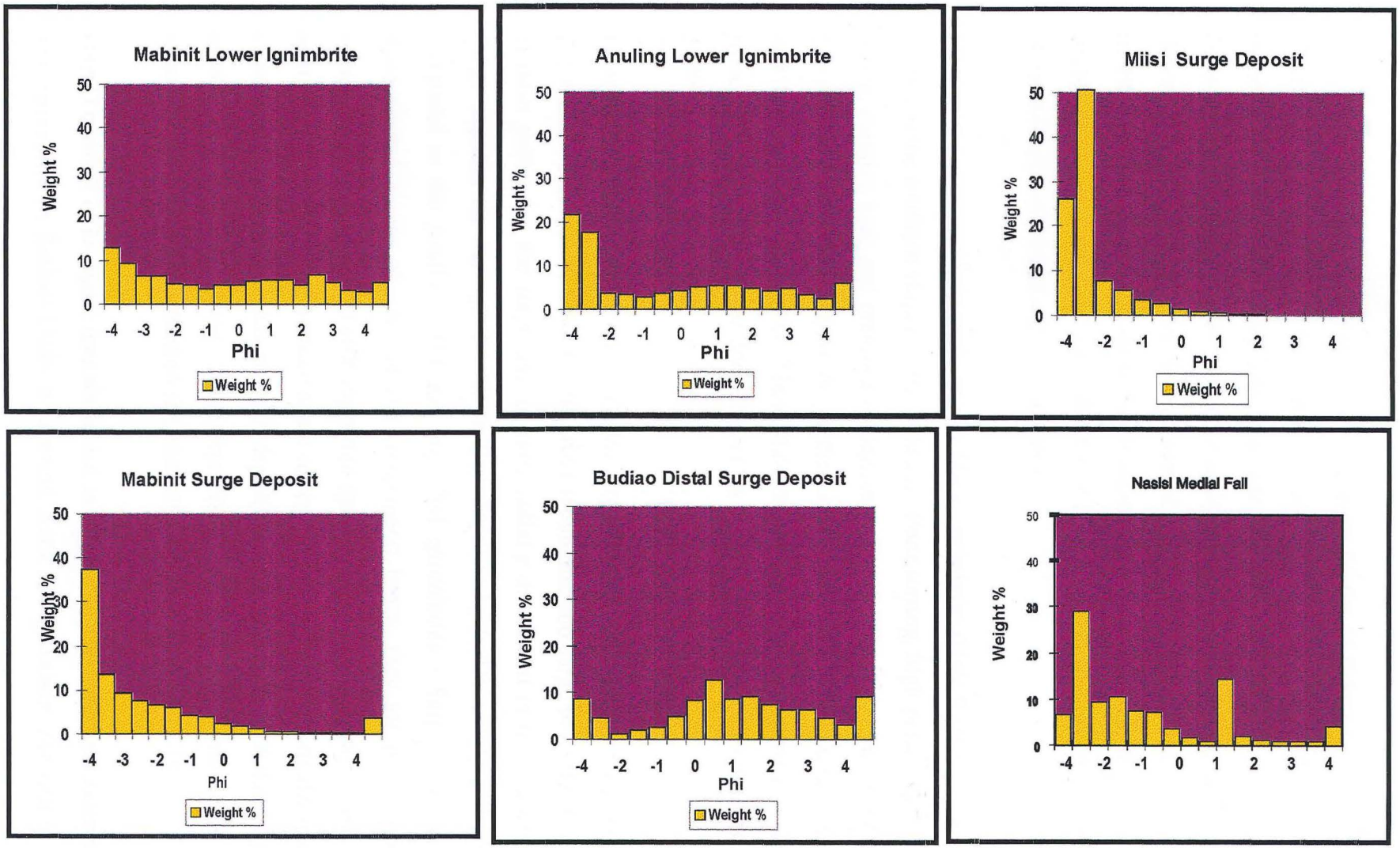

Figure 3.13 Selected histograms of weight % versus phi for the lower ignimbrite, surge and fall deposits.

3.4. Discussion

At the base of the composite stratigraphic column for the 01 February 1814 eruption is a tephra fall unit. Although the fall unit was never observed together with the 1814 pyroclastic flow and surge deposits, it is clear from eyewitnesses' accounts that a lapilli fall signaled the commencement of the eruption. Eyewitnesses described the tephra fall deposit as a rain of ash and lapilli experienced mostly in the southern slopes at 0800h on 01 February 1814. Tephra fall is distinguished from the similarly normally graded and friable 1814 surge deposits by the absence of charred twigs, uniform thickness, absence of cross-stratification and segregation pipes.

Next in the sequence is a dark gray to black ignimbrite (Unit B) that occurs in some gullies in the southern slopes of the volcano. Poor sorting, high percentage of juvenile scoria, massive beds and presence of degassing pipes characterize this deposit. Local topography controls the deposition of this unit as indicated by thicker gully outcrops and thinner overbank deposits. These features, together with the presence of carbonized wood are consistent with the definition of an ignimbrite (Cas and Wright, 1988; Druitt, 1996).

Directly overlying the ignimbrite is a layer of similarly dark gray to black bombs-rich pyroclastic surge layer (Unit C). The lower ignimbrite and surge deposit occur together in most gullies but the surge unit is more radially distributed in the southern slopes. Surge deposits are distinguished from flow deposits by better sorting and grading as compared to the poorly sorted and ungraded ignimbrites. Surge units are further distinguished by the absence of ash component; hence, they are clast-supported as compared to the strongly matrix-supported ignimbrites. The 1814 surge can easily be mistaken for a tephra fall because some of its characteristics (i.e. normally graded and clast-supported) resemble that of a fall deposit. However, the base of the surge unit is usually undulating and erosive. Surge deposits also exhibit uniform orientation of TRM signature in contrast to the random signature of a fall deposit (Table 3.1).

Unit D consists of an upper ignimbrite that is mapped in only two southeastern gullies. The ignimbrite in Budiao Gully is different from the ignimbrite exposed at Mabinit

Unit D consists of an upper ignimbrite that is mapped in only two southeastern gullies. The ignimbrite in Budiao Gully is different from the ignimbrite exposed at Mabinit Gully. The ignimbrite exposures at Mabinit and Budiao Gullies are compositionally and texturally different from the lower ignimbrite Unit B. The absence of a soil, tephra fall or lahar between the upper ignimbrite and the underlying surge unit suggests that its emplacement is contemporaneous with the emplacement of the other 1814 eruptive units.

Table 3.1. TRM of 1814 surge (A) and overlying non-1814 airfall deposit (B) at Anoling Gully. Clasts of the surge deposit show uniform orientation.

A. Surge deposit			**B. Fall deposit**		
Orientation	**Inclination/ Declination**	**Description**	**Orientation**	**Inclination/ Declination**	**Description**
N	Horizontal	Scoria	N	Horizontal	Scoria
N	Horizontal	Scoria	N	30° down	Scoria
N	Horizontal	Scoria	N	10° down	Dense lithic
N	Horizontal	Dense lithic	NE	70° down	Scoria
N	Horizontal	Scoria	NW	10° down	Scoria
NW	Horizontal	Dense lithic	N	Horizontal	Dense lithic
N	Horizontal	Scoria	N	30° down	Dense lithic
N	Horizontal	Scoria	NE	10° up	Scoria

At least two events of lahars occurred successively after the deposition of the primary volcanic deposits. The deposits contain high proportions of primary 1814-derived scoria clasts strongly suggesting the lahar units were emplaced immediately after the deposition of the flow deposits. Hot lahars emplaced the units based on the presence of vesicles, induration and surficial crust.

TRM analyses have been used to classify deposits as lahar or pyroclastic flow in some ambiguous outcrops. Ten juvenile and dense lithic clasts were selected for TRM and checked for their orientation. Ignimbrites have coherent magnetically oriented clasts while lahar deposits show random clasts (Table 3.2). The TRM orientation pattern enabled positive identification of primary vs. secondary flow deposits from the 1814 eruption. Lahar deposits showed random magnetic orientation indicating deposition after the clasts had cooled to close to ambient temperature (Hoblitt and Kellog, 1979; Arguden and Rodolfo, 1990).

Table 3.2. TRM of ignimbrite clasts show uniform orientation while those of lahar deposit are randomly oriented.

A. Ignimbrite			B. Lahar deposit		
Azimuth	**Inclination/ Declination**	**Description**	**Azimuth**	**Inclination/ Declination**	**Description**
N	Horizontal	Scoria	S	Horizontal	Scoria
N	Horizontal	Scoria	N	30° down	Scoria
N	Horizontal	Scoria	N	10° down	Dense lithic
N	Horizontal	Scoria	N	70° down	Scoria
N	Horizontal	Scoria	N	10° down	Scoria
N	Horizontal	Scoria	NW	Horizontal	Dense lithic
N	Horizontal	Scoria	N	30° down	Dense lithic
N	Horizontal	Scoria	S	45° down	Scoria
N	Horizontal	Lithic	S-SW	Horizontal	Scoria

3.5. Summary

The stratigraphy of the 1814 eruptive deposits was established by integrating data from lithologic descriptions, petrographic composition, geochemical composition, TRM, radiocarbon dating and historical documents. Detailed stratigraphic studies on the 1814 outcrops paved the way for across gully correlation of the different volcanic deposits.

Textural criteria and granulometric results are used to distinguish the tripartite pyroclastic deposits and lahars generated from the 1814 eruption. The black surge deposit (Unit C) was the most conspicuous and widespread in gullies, and has been used as a stratigraphic marker.

The stratigraphy and distribution of the 1814 eruption corroborate eyewitnesses' descriptions of the eruption. Historical data were vital to the inclusion of the fall unit in the stratigraphy, as this unit has never been observed in contact with the other 1814 units. Absence of a soil or lahar layer indicate that the different units comprising the 1814 stratigraphy were deposited from a single eruption, and that there was no significant pause in that eruption.

CHAPTER 4

Geochemistry of the 1814 Deposits

4.1. Introduction

This chapter aims at presenting the major and trace element geochemistry of the 1814 deposits. Thirty juvenile scoria from stratigraphically-constrained 1814 outcrops were analyzed for their geochemical properties. Clasts in the 1814 eruptive products are composed predominantly of juvenile dark scoria and bombs, cognate lithics and altered yellow clasts. A light brown scoria is also found as streaks in the dark scoria and as rare clasts. All analyzed samples came from fresh clasts of the dark scoria. None of them came from the minor brown rock due to lack of samples having the necessary volume to allow whole rock analyses.

4.2. Methodology

Major element compositions of the 1814 eruption products are listed in Appendix B. All data are normalized to 100% anhydrous. Locations of sampling sites and descriptions of raw major and trace element data are presented in Appendix C.

All samples were oven-dried overnight before analyses were made. During sample preparation, extreme care was taken to ensure that samples were homogeneous at macroscopic inspection and xenoliths were removed from the samples prior to analyses.

Major and trace element analyses were carried out using a Philips PW 1400 X-ray spectrometer in the X-Ray Spectrometry Laboratory of the Department of Geological Sciences at the University of Canterbury. X-Ray diffraction analyses of altered samples were conducted at the Department of Geological Sciences, University of Canterbury.

4.3. Whole rock major element and glass geochemistry

Classification of the 1814 deposits was determined through the SiO_2 versus total alkali (Na_2O+ K_2O) content of normalized anhydrous representative samples. The range in silica is relatively small, from 53.5 to 55 %, spanning the basaltic andesite field of Le Bas *et al.* (1986). On the other hand, the total alkali content (Na_2O+ K_2O) varies slightly from 4-5 % (Figure 4.1). The 1814 deposits have almost constant K_2O content within a compositional field of medium-K andesite (Gill, 1981) (Figure 4.2).

No sample from the light component had sufficient volume for whole rock analyses. However, the light component was noted to be more silicic than the dark component from the matrix glass chemistry. Matrix glass chemistry of the light component showed SiO_2 range within the andesite field (57-63%) while matrix glass of the dark component has a more basic signature (55-56 %) (Appendix D). The groundmass glasses form a linear array with the whole rock chemistry of the dark component (Figure 4.1).

Variation diagrams of major element oxides display both positive and negative correlations with SiO_2 (Figure 4.3). The major oxides CaO, Al_2O_3, Fe_2O_3 , Na_2O and TiO_2 correlate negatively with SiO_2 while K_2O increases with SiO_2. The enrichment in K_2O with SiO_2 and depletion in other major oxides is consistent with crystallization of plagioclase and fractionation of the mafic minerals.

4.4. Trace element

The multi-element plot of the 1814 samples is normalized according to Sun and McDonnough (1989) (Figure 4.4). The 1814 samples are enriched in Sr, Ba, La and Nd and depleted in the elements Rb, Nb and Y. The erratic signature of La is due to low precision. The enrichment of these elements suggests incompatible behavior of large ion lithophile element (LILE) except for Sr, which may be concentrated in plagioclase (Wilson, 1989). Enrichment of LILE characterizes most of the Bicol volcanoes Arcilla (1998), and is typical of subduction related magmas (Wilson, 1989).

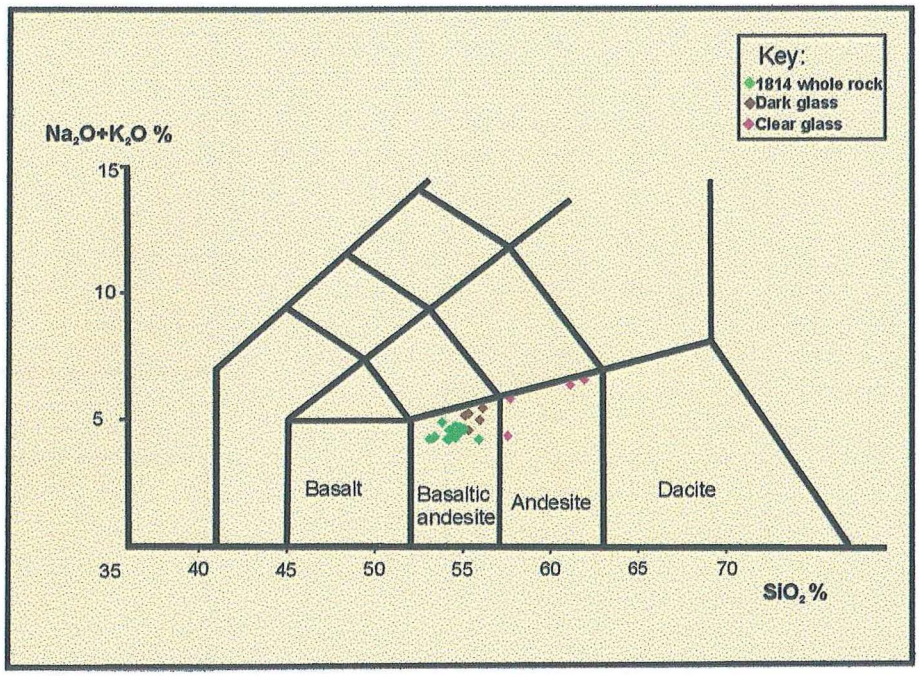

Figure 4.1 TAS diagram of whole rock analyses of the 1814 deposits (*after Le Maitre, 1989*). Matrix glasses from dark component and light component form a linear array with the whole rock chemistry of the dark component.

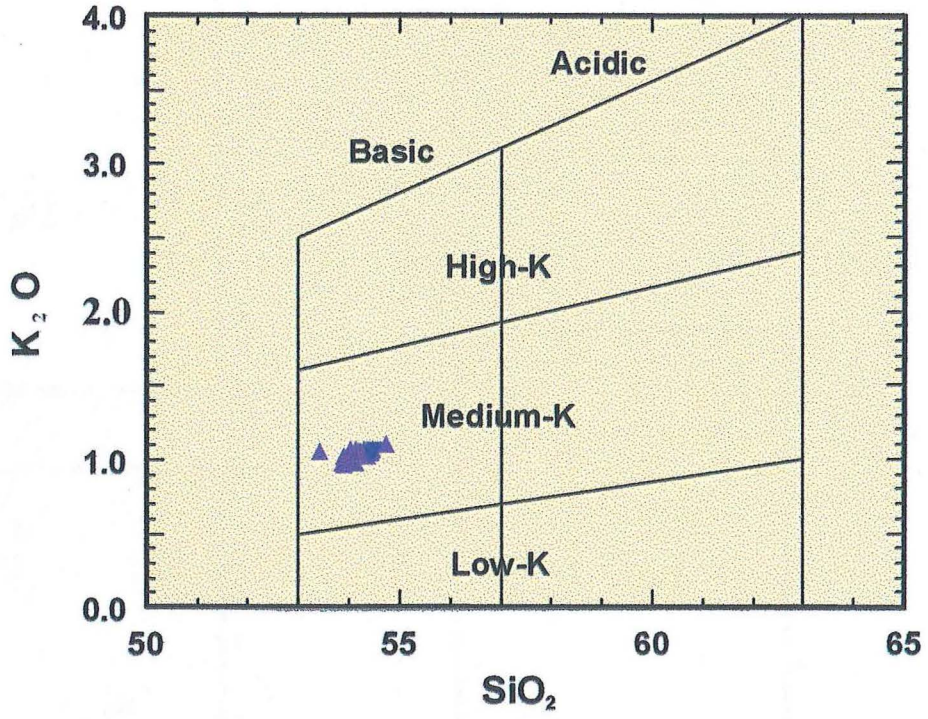

Figure 4.2 The 1814 deposits, together with Mayon's most recent eruptions are of medium-K andesite composition *(after Gill, 1981).*

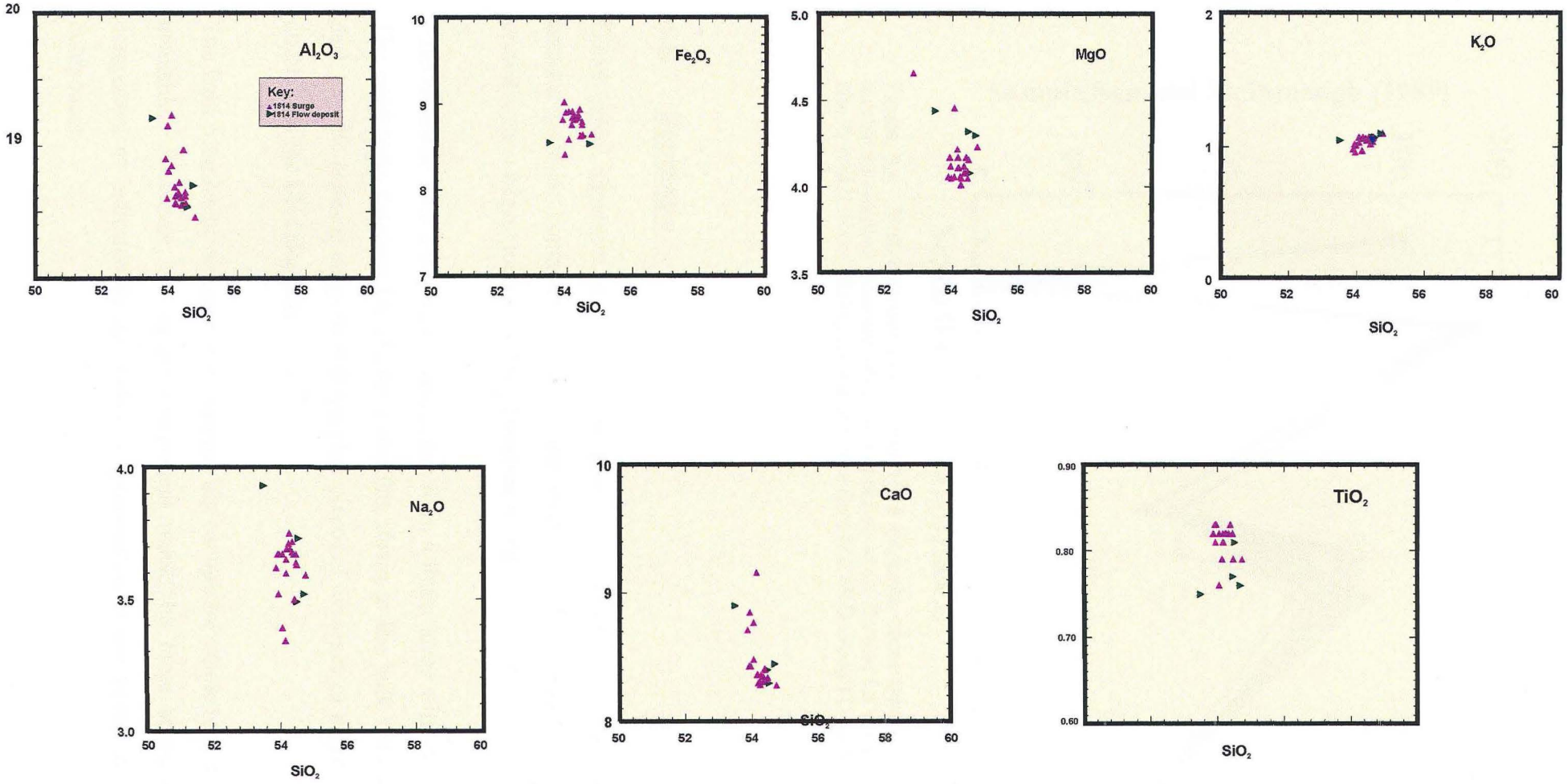

Figure 4.3 Harker diagram for the 1814 dark component clasts.

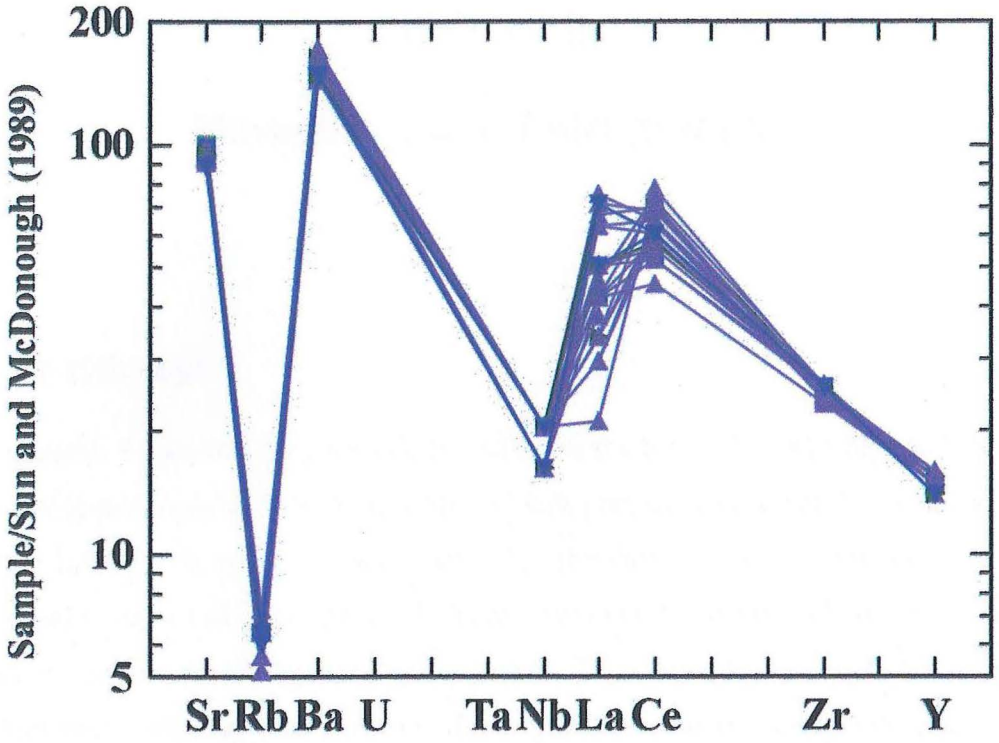

Figure 4.4 Multi-element plot of the 1814 deposits show typical signature of subduction-related magmas which are enriched in Sr, Ba and La while depleted in Nb, Zr and Y. Normalizing values are from Sun and McDonough (1989).

4.5. Synthesis

Geochemical signature of the dark component of the 1814 deposits shows a strong basaltic andesite composition. Variation diagrams of the major elements suggest crystallization of plagioclase and fractionation of mafic minerals.

Plots of whole rock analyses of dark scoria form a linear array with the matrix glasses. The continuum between the glasses extending down to the bulk rock analyses of the dark basaltic andesite supports petrographic pieces of evidence of magma mixing in the eruption of the 1814 deposits.

The light component was rare that a sample big enough for whole rock analyses was not available. However, the lighter component would be more acidic than the dark component as indicated by the andesitic composition of the matrix glass of the light component.

CHAPTER 5

Mineralogy and Petrography

5.1. Introduction

In this chapter, I describe the mineralogy and petrography of the 1814 tephra deposits. The 1814 deposits consisted predominantly of dark gray to black juvenile scoria, bombs and dense lithics with minor altered clasts. The juvenile scoria is composed of minor clasts of light brown vesicular scoria. Petrographic analyses were made on the juvenile dark scoria and bombs of representative samples from each of the 1814 stratigraphic units identified, including three samples of the light brown scoria clasts. For description purposes, the predominant black scoria clasts are referred to as the dark component and the minor brown rocks as the light component. Petrographic descriptions on representative samples are presented in Appendix C.

Electron microprobe analyses of minerals were also performed on eight selected representative samples of the 1814 deposits. The analyses were determined using JEOL JXA-8600 electron microprobe analyzer with cathodoluminescence attachment at Otago University in Dunedin. Measurements were determined on carbon-coated polished sections under a 15-50 μm diameter beam generated with 15 kV acceleration voltage. Results of the analyses for the plagioclase, olivine and pyroxene are presented in Appendix F.

5.2. Mineralogy of the dark component

The 1814 eruptive products predominantly consist of dark, vesicular, cauliflower juvenile scoria and bombs (Figure 5.1). Juvenile dark clasts are of two-pyroxene basaltic andesite composition. In thin section, they are hypocrystalline and porphyritic. Volume percentage of crystals is 15-20%. Phenocrysts are composed of plagioclase

at least three samples, the boundaries of the dark scoria against the coexisting light component display mostly chilled and crenulate margins (Figure 5.3). The mineralogy and petrography of this particular specimen are discussed in a separate section in this chapter.

Figure 5.1. The 1814 deposit consists predominantly of dark-gray to black scoria clasts with cauliflower texture.

The groundmass of the dark component consists of dark glass and microlites of the main phenocryst assemblage. Glass comprises about 30% of the rock and the microlites about 60%. Electron microprobe analyses of the dark glass show it is of basaltic andesite composition with 55-57 SiO_2% content. Quench textures suggesting a degree of undercooling of magma are exhibited by swallow-tailed groundmass plagioclase and presence of the dark glass itself. Small, round to ovoid vesicles mostly measuring <0.05mm are common in the samples (Figure 5.4).

Light gray xenoliths are present in minor amounts (<2%) in the scoria samples and attain a maximum diameter of 1 cm (Figure5.5). The xenoliths have well-defined, sharp boundaries in the dark component clasts. They are composed of light gray, fine-grained

andesite. Under the microscope, the xenoliths are highly porphyritic with a fine-grained groundmass. Phenocrysts consist of plagioclase, augite, and orthopyroxene. The groundmass consists of plagioclase, augite, orthopyroxene, olivine and opaques.

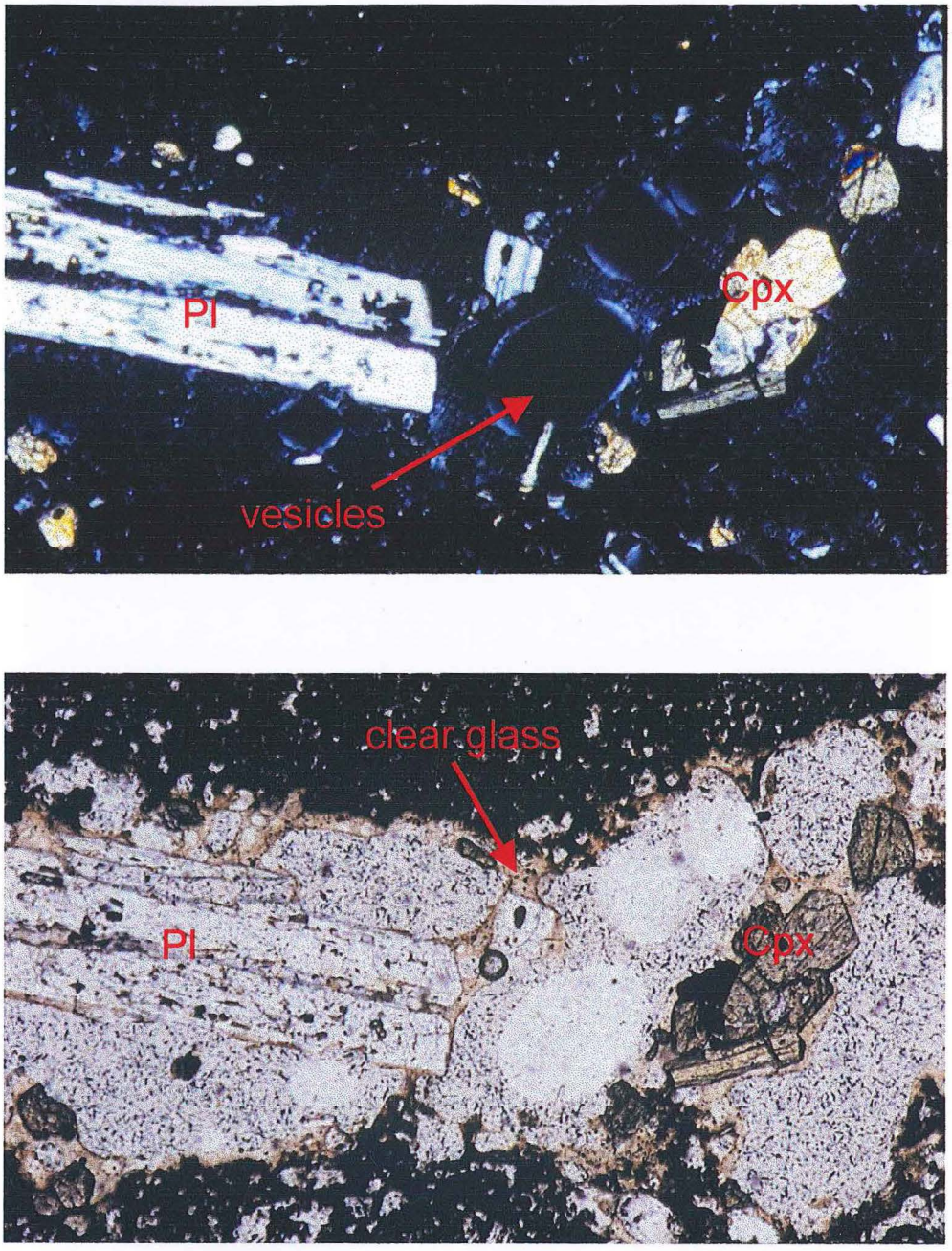

Figure 5.2. Photomicrographs of the streaks of light rock in dark scoria. A, crossed-polars; B, uncrossed polars, view of the same area. Microlitic glass comprises the groundmass in dark scoria. The boundaries of streaky light rock in dark scoria are distinct but crenulate. Field of view = 2.18 mm. Pl = plagioclase; Cpx = clinopyroxene (augite).

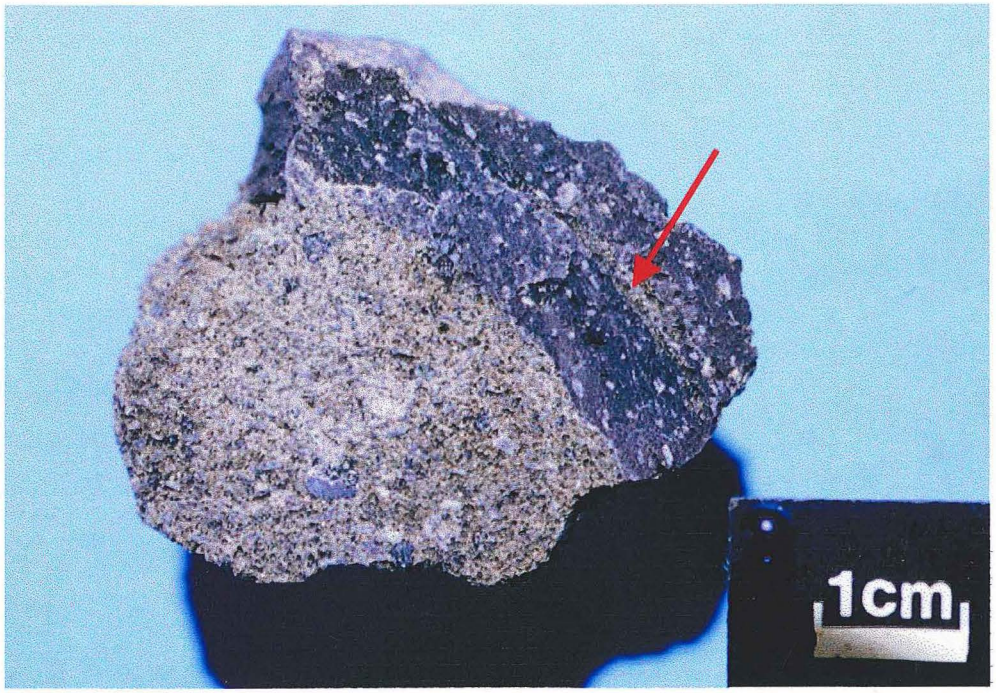

Figure 5.3. A large bleb of the light component coexisting with the dark component in a single clast. A streak of light brown rock in dark scoria is shown by the arrow.

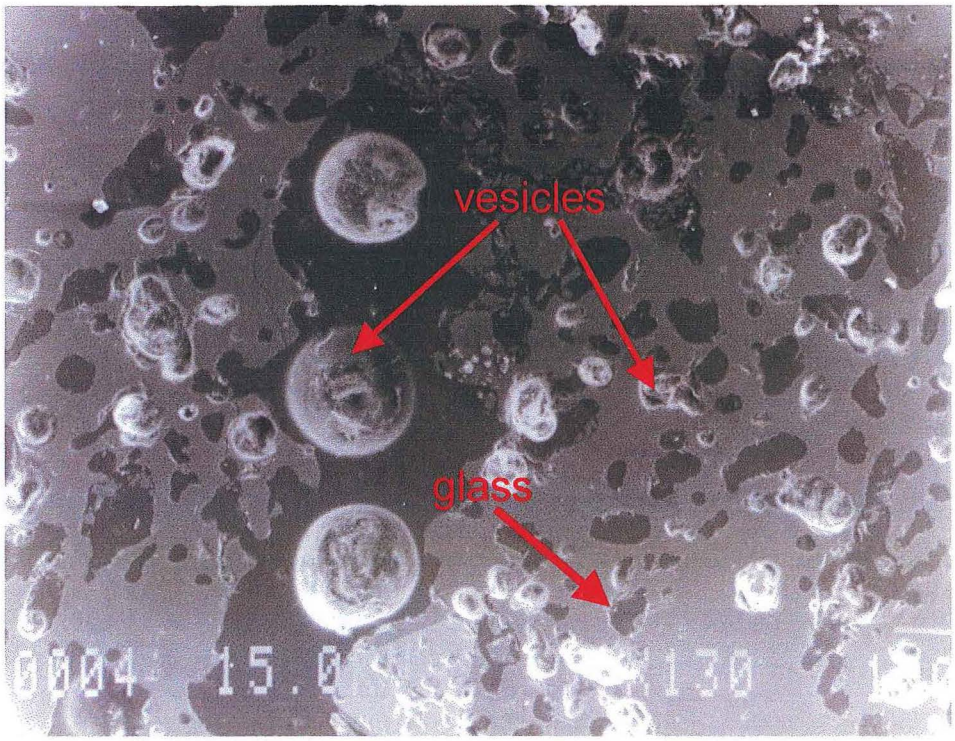

Figure 5.4 SEM image of a typical groundmass of dark scoria consisting of micrometer-size vesicles and glass. Streak of light rock in dark scoria is distinguished by larger open vesicles and clear glass (left corner). Arrows denote positions of matrix glasses.

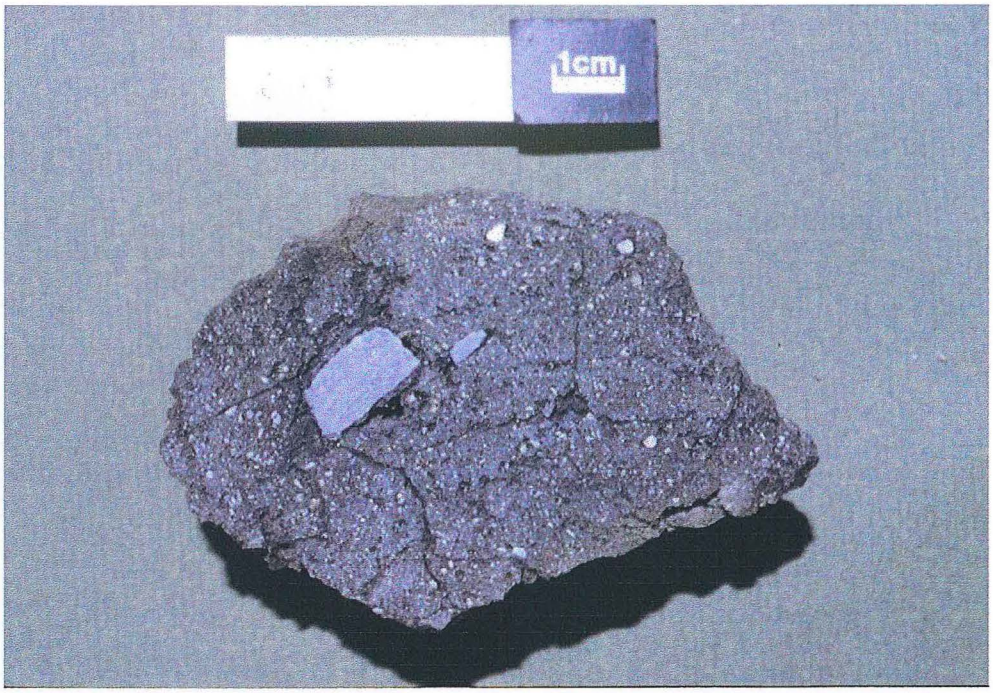

Figure 5.5. Light gray xenoliths in the dark scoria show sharp boundaries.

5.2.1. Plagioclase

Plagioclase accounts for 70% of the phenocryst in the dark scoria and is also the most abundant mineral phase in the groundmass. Plagioclase occurs both as euhedral to subhedral phenocrysts and as small lath-shaped microphenocrysts in the groundmass. Plagioclase ranges from microlitic size to 3mm long. There are two plagioclase size populations recognized in the analyses. The first are relatively small plagioclase crystals measuring less than 1mm. The larger plagioclase group is about 1.5 to 3mm long. Both size populations commonly occur singly or as part of heterogeneous glomeroporphyritic clusters together with augite and orthopyroxene. Some plagioclases have poikilitic texture, enclosing augite and orthopyroxene. Other plagioclase crystals have a spongy cellular appearance surrounded by a clear or inclusion-free rim. Corroded plagioclases are also present. Plagioclase phenocrysts exhibit two habits: euhedral and clear, and inclusion-rich, spongy textured crystals, which are usually large (Figure 5.6). Clear and inclusion free plagioclase are further characterized by sharp, well-defined crystal edges with tabular shape. The dusty plagioclase is commonly associated with clear glass and relatively large vesicles.

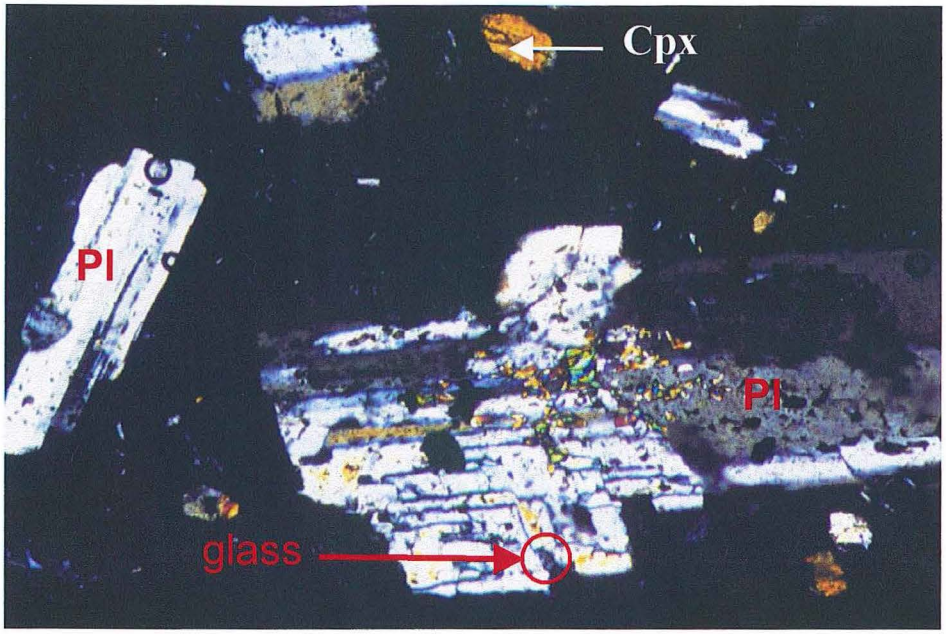

Figure 5.6. Large poikilitic plagioclase in dark rock including mainly augite and clear glass inclusions (near center of field view). Small, inclusion free plagioclase in dark groundmass (left and top right) and small augite (top). Glass occurs in between the prongs of skeletal plagioclase (shown by arrow). Photo taken under crossed polars. Field of view = 2.18mm. Pl = plagioclase; Cpx = clinopyroxene (augite).

Plagioclase range from bytownite (An_{91}-An_{98}) to anorthite (An_{70}-An_{90}) (Figure 5.7). Small unzoned and inclusion-free plagioclase has a very high anorthite content (An_{80}-An_{97}). Compositional zoning is present and is reversed from core to rim from An_{72} to An_{90}) (Figure 5.8). Reversal zoning with a slight increase from An_{70} to An_{80} is also observed Plagioclases exhibiting a sieved-zone texture show increasing anorthite content from rim to the sieved zone. Zoning in other plagioclases is sometimes accentuated by alignment of inclusions of brown glass and augite. Completely sieved plagioclases also occur in the samples (Figure 5.9). Resorbed and sieved plagioclases have pronged skeletal texture with occurrence of glass in between the prongs (Figure 5.6).

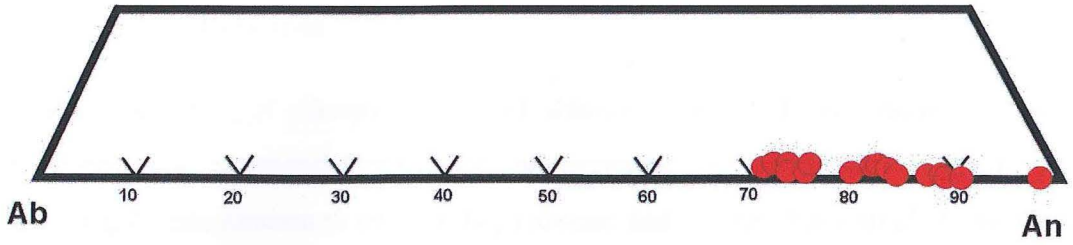

Figure 5.7. Anorthite content of plagioclase in both the light and dark rocks.

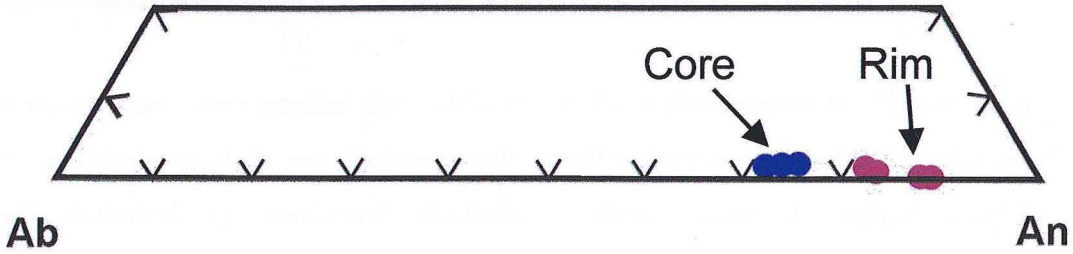

Figure 5.8. Sodic plagioclase shows reverse zoning.

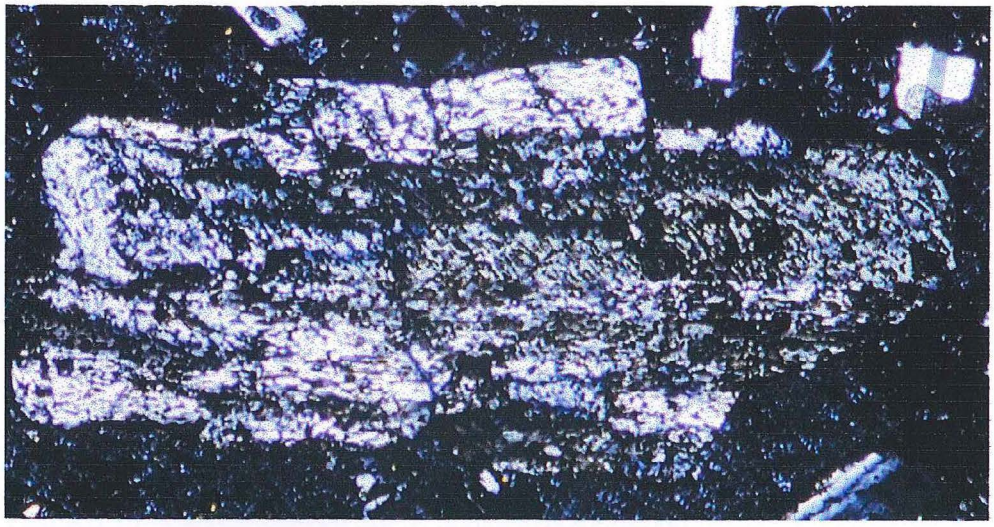

Figure 5.9. Sieved plagioclase in dark scoria. Photo taken under cross polars. Field of view is 2.18mm.

5.2.2. Pyroxene

Pyroxene, consisting of clinopyroxene and orthopyroxene, is the second most abundant mineral occurring as phenocrysts. The clinopyroxenes are all augite (En_{40-47}) (Figure 5.10). Augite predominates over orthopyroxene and ranges from small to very large phenocrysts (2mm). Augite comprises 15 to 20% of the phenocrysts. Similar to plagioclase, it exhibits a bimodal size distribution. Augite phenocrysts are commonly euhedral to subhedral and occur as individual minerals or as part of glomeroporphyritic clots with plagioclase, orthopyroxene and titanomagnetite. Twinning is common and in exceptional cases, optically visible zoning occurs but is very uncommon. Poikilitic texture is also observed in augite, plagioclase and orthopyroxene.

Orthopyroxene forms greater than 10% of the total phenocrysts in all scoria samples. Orthopyroxene crystals are predominantly smaller than augite and frequently occur as small euhedral to subhedral crystals. They occur as single crystals, in glomeroporphyritic clusters, and as inclusions in plagioclase or augite.

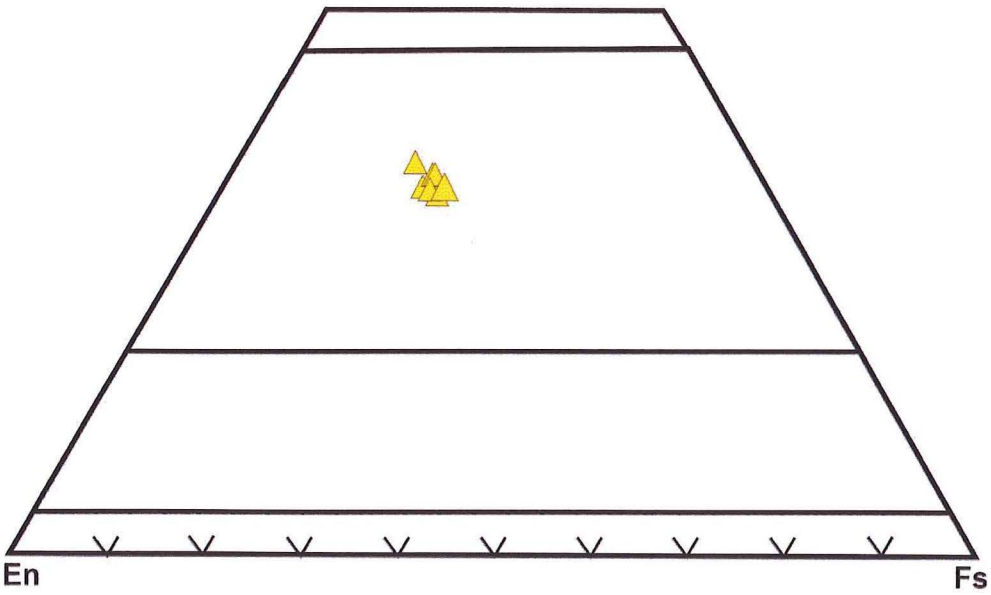

Figure 5.10. Clinopyroxenes are all augite in composition.

5.2.3. Olivine

Olivine is not always present, but when present, it constitutes <1% to 4% of the total percentage of phenocrysts. The olivine is colorless and commonly shows gray to high interference colors. Analyzed olivines are mostly Mg-rich, (Fo_{66}) although one sample has a lower Mg content (Fo_{52}) (Figure 5.11). It occurs as euhedral to anhedral individual crystals (Figure 5.12 and 5.13). Anhedral and corroded olivine shows undulatory extinction and often occurs in mosaics (Figure 5.14). The undulatory extinction and mosaics suggest that these are xenoliths and xenocrysts of mantle peridotite (Shelley, 1993). However, some undeformed euhedral crystals appear to have grown from a magma, and I conclude this is a mixed assemblage of igneous olivine and xenolithic material. It warrants more detailed examination.

5.2.4. Opaque Minerals

Opaque minerals are present and occur as single phenocrysts, as inclusions in poikilitic plagioclase and augite, or in glomeroporphyritic clots together with augite, orthopyroxene and plagioclase. Opaque minerals are most probably titanomagnetite as indicated by its rectangular shape.

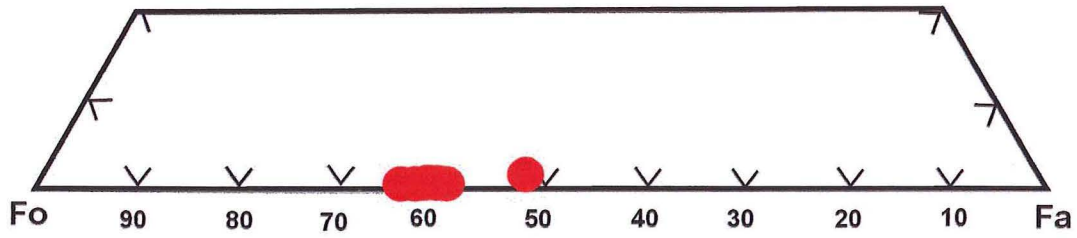

Figure 5.11. Olivine ternary diagram showing mostly magnesian olivine.

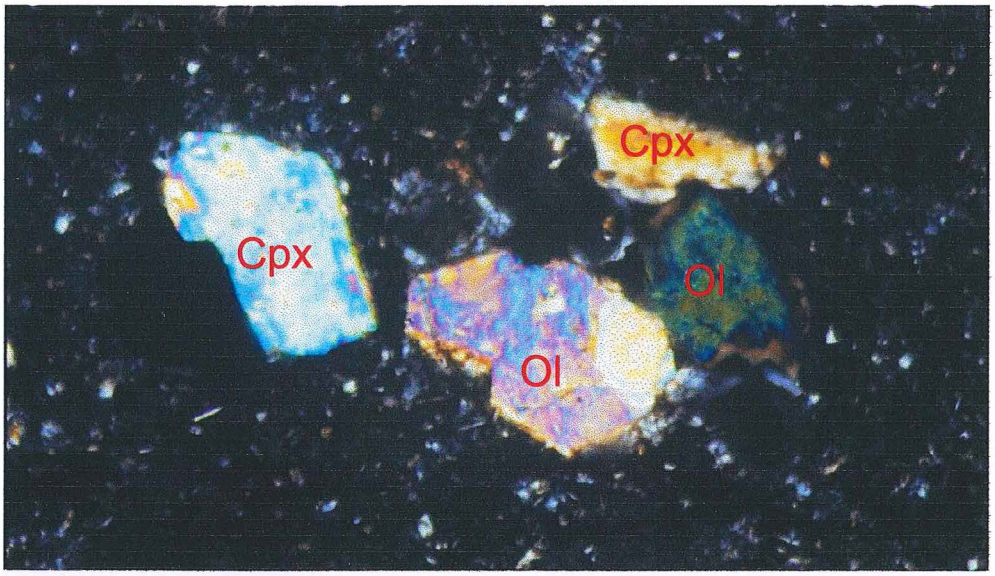

Figure 5.12. Photomicrograph under crossed polars of subhedral olivine grains in dark rock. Leftmost olivine in partial extinction. Field of view is 2.18mm. Ol = Olivene; Cpx = clinopyroxene (augite).

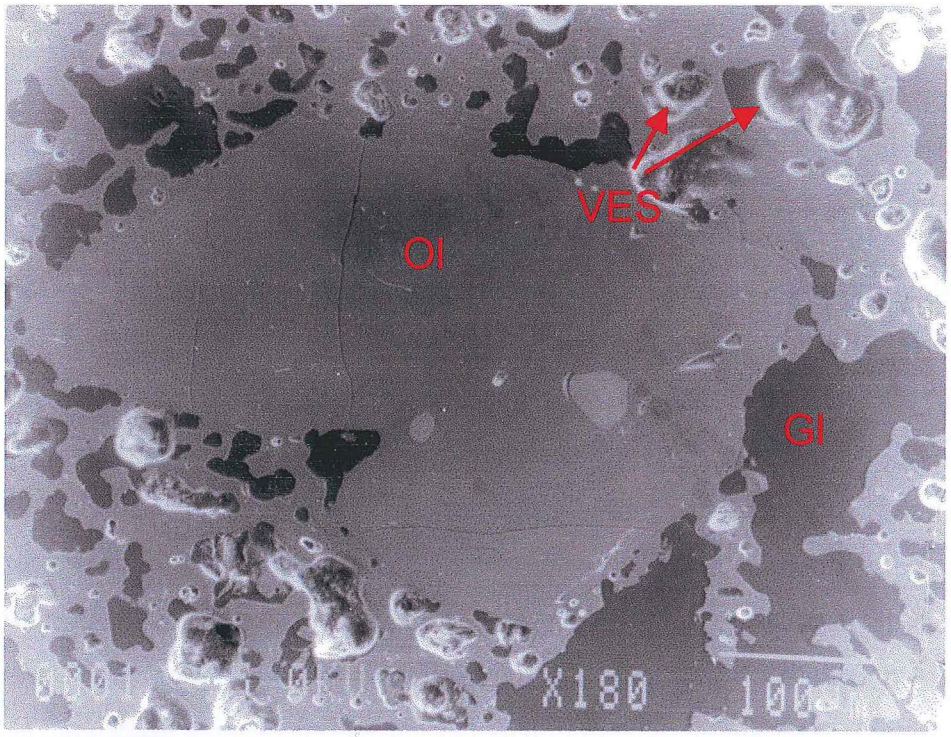

Figure 5.13. SEM image of a euhedral olivine in dark rock. Ol = olivine, Gl = glass, VES = vesicles. Arrows show vesicles in the groundmass.

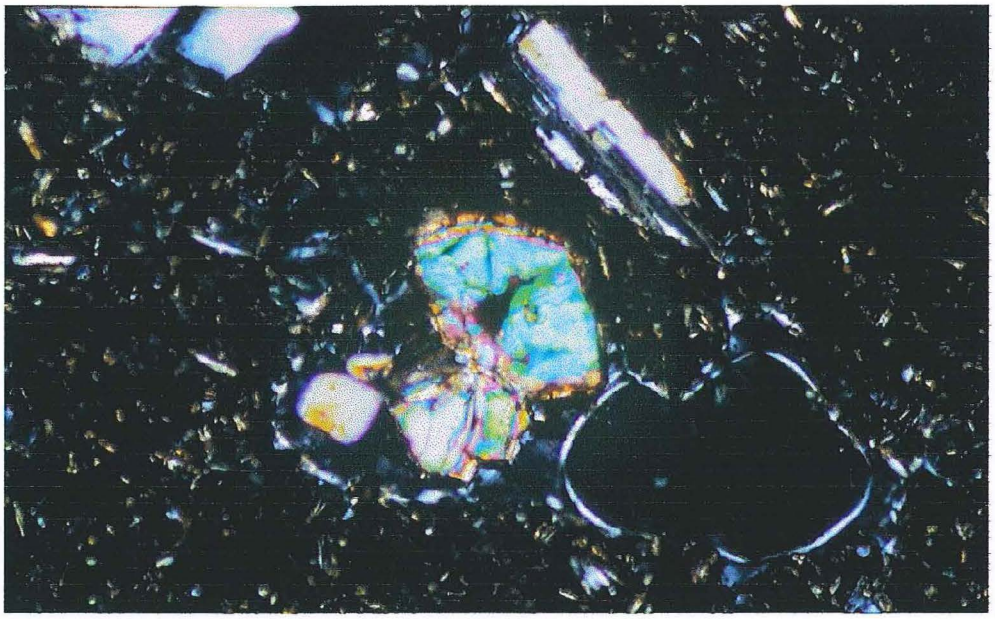

Figure 5.14. Anhedral olivine in dark scoria (center of photo). Olivine shows mosaic texture with all grains simultaneously not in extinction. Note the distinct outline of the growth structure superimposed on the original anhedral crystal. Photo taken under crossed polars with field of view = 1.09 mm.

5.3. Mineralogy of minor light component

The light component was megascopically recognized in only three samples but is highly conspicuous as streaks under the microscope in most samples. Streaks of the light brown rock typically have dimensions up to 3cm long and a few mm thick. Most of the streaks are distinct only under the microscope. The boundaries between the light and dark components are distinct and often crenulated (Figure 5.15). In thin section, the light component is a two-pyroxene basaltic andesite and consists of a similar mineral assemblage to the dark component. It contains the mineral assemblage plagioclase, pyroxene, orthopyroxene and titanomagnetite with rare olivine. In contrast to the host scoria, the light component is highly porphyritic containing 30-40% phenocrysts. Streaks of dark glass with microlites are included in the light component (Figure 5.16).

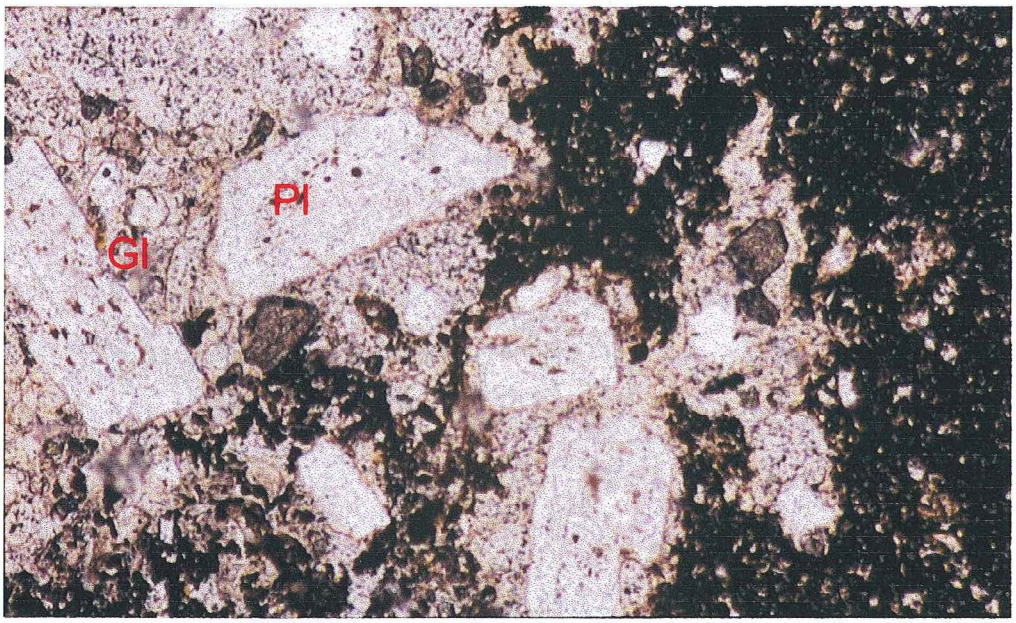

Figure 5.15. Intertonguing texture characterizes the interface between the two rocks under plane-polarized light. Field of view is 2.18 mm. Colorless, microlite-free glass surrounds larger phenocrysts in light scoria rock. Pl = plagioclase, Gl = glass.

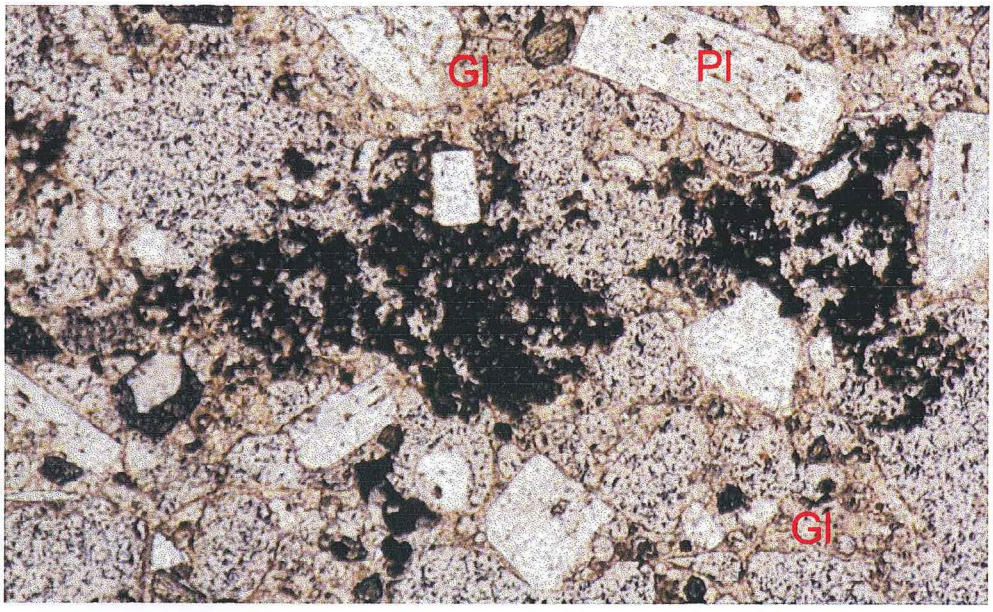

Figure 5.16. Dark glass from the dark component incorporated within the light rock in PPL. Clear brown glass abounds. Field of view is 2.18 mm. Gl = glass and Pl = plagioclase.

The groundmass of the light component consists of clear glass as opposed to the dark microlitic groundmass of the dark component (Figure 5.16). Electron microprobe analyses of the clear, matrix glass in the light component shows a high SiO_2 %, ranging from 57-62 SiO_2 % plotting in the high alumina basaltic-andesite to andesite field (Figure 4.1). This is consistently more SiO_2-rich than the dark component. Vesicles averaged 15% in the analyzed light component. Vesicles were also present in the streaks or patches of the light component in dark scoria, together with the brown glass and large minerals. Vesicles in the lighter component average 1 mm in diameter and are always larger than vesicles in the dark component.

5.3.1. Plagioclase

Plagioclase forms the largest phenocrysts (>2 mm) and constitutes the most abundant mineral (70%) occurring as euhedral to subhedral individual phenocrysts or as part of a glomeroporphyritic clots. The size of plagioclase phenocrysts displays a wide range from greater than 2mm to less than 1mm but predominantly composed of large grains (>2mm). Some cores are sieved and rimmed by clear pristine zones. Twinning is generally present. Plagioclase varies from inclusion-rich to almost clear phenocrysts. Smaller plagioclase crystals commonly contain fewer inclusions or are almost inclusion-free. Completely sieved plagioclases are also present together with the non-sieved plagioclase. Plagioclases are more sodic in composition (An_{70-78}) than those in the dark component (Figure5.8).

5.3.2. Pyroxene

Euhedral and sometimes subhedral orthopyroxene is rare but occurs as very large phenocrysts measuring by as much as 5 mm. This mineral occurs singly or in clots, together with augite and other pyroxene minerals. Orthopyroxene crystals contain glass inclusions. Titanomagnetite are sometimes included in the orthopyroxene.

Augite, like orthopyroxene, is volumetrically low. It is euhedral to subhedral and occurs singly or as part of glomeroporphyritic clots together with orthopyroxene and plagioclase. The size of augite crystals range from 3mm to <1mm.

5.4. Possible evidence of magma mixing and mingling in the 1814 deposits

The petrography of the scoria samples indicates magma mixing and mingling. Mingling is exhibited by the presence of two compositionally different rocks, the dark and light components. The two types coexist with distinct, crenulate boundaries between them. The fluidal character of the two rock types is evidenced by the crenulate boundaries, intertonguing relationship and streaky appearance. The dark component is the more basic and as expected, exhibits chilled margins against the lighter more SiO_2-rich component. Given the number and pervasive nature of the streaks of lighter material it would seem unlikely that no mixing (interchange of material) and mingling took place.

Presence of two compositionally different glass matrix, more sodic and larger plagioclase crystals and vesicles suggest difference in composition. The light component is distinguished from the dark component by the presence of large vesicles, suggesting difference in the style of degassing.

There is evidence of mixing in the resorbed and sieved texture of phenocrysts. Such textures are indications of disequilibrium and are often considered to be pieces of evidence for magma mixing (Hibbard, 1995; Hobden, 1997) which developed as a reaction of phenocrysts to changes in magma composition and temperature caused by magma mixing (Sakuyama, 1984).

Petrographic evidence indicating magma mixing is shown by the coexisting and intermingling of two different materials. A summary of the compositional difference between the dark and light materials is presented in Table 5.1.

Table 5.1. Summary of compositional differences between the dark and light components.

Lighter component	Darker component
57-62% SiO_2	53-57% SiO_2
More sodic plagioclase An_{70-80}	More calcic plagioclase An_{80-97}
Larger phenocrysts	Smaller phenocrysts
Larger vesicles	Smaller vesicles

5.5. Discussion

The aforementioned petrographic evidence presented suggests that the 1814 products underwent the processes of magma mixing and mingling history prior to eruption. The evidence presented includes disequilibrium textures and coexistence of two rock types distinguished by differences in phenocrysts, glass matrix and vesicle size.

It can be argued that the disequilibrium features such as crystal resorption can be initiated by changes in the H2O content and/or pressure in the magma chamber rather than magma mixing. However, the evidence here of magma mixing (presence of streaks of light component in the dark component and distinct compositional differences) provides a setting that strongly suggests at least some of the disequilibrium features result from magma mixing.

The sieved and resorbed textures observed in plagioclase and phenocrysts are interpreted as the result of growths due to undercooling. Such undercooling resulted from changes in temperature as a hotter magma mixes with a magma of lower temperature. The reversals in zoning from sodic to calcic plagioclase in the light component can also be interpreted as possibly being due to crystals from the light component being entrained by mixing in the dark component.

In the 1814 products, one of the end-members of the participating magmas was recognized in both hand specimen and in microscopic analyses. Recognition of mingling suggests that mixing is not complete or very efficient (Donoghue *et al.*, 1990). However, the presence of disequilibrium textures, shows that some degree of mixing occurred between the two magmas.

CHAPTER 6

Geologic Model of the 1814 Eruption

6.1. Introduction

This chapter is primarily aimed at reconstructing the eruptive sequence of the 1814 eruption by integrating stratigraphic and granulometric data with the chronology of events from historical accounts, and discussing the emplacement mechanisms of the eruptive deposits. In addition, a geologic model for the trigger of the explosive eruption is presented based on petrographic and geochemical evidence. Comparison is made on other recent studies in island arc subduction settings in order to establish the model for the eruption.

6.2. Summary of events

The February 1, 1814 eruption occurred in less than 6 hours, commencing with a light ash fall at 0630h. It had two distinct phases: a phreatic, vent-clearing phase, and a climactic phase characterized by pyroclastic flows and surges. Partial collapse of the crater wall accompanied the final stage of the climactic eruptions. The pre-climactic phreatic eruption emplaced the tephra fall deposit (Unit A), while a series of explosive eruptions during the climactic phase resulted in the deposition of the lower ignimbrite (Unit B), the pyroclastic surge deposit (Unit C) and the upper ignimbrite deposit (Unit D) (*Please see Chapter 3*). The collapse of part of the crater wall apparently occurred simultaneous with the emplacement of the upper ignimbrite. A summary of the eruption events is presented in Table 6.1, and discussed in more detail in the succeeding sections.

Table 6.1. Chronology of events as inferred from eyewitnesses' accounts and emplaced deposits.

Time of occurrence	Deposits	Eruptive phase from historical point of view	Remarks
630h	Not observed	Ash fall	Vent-clearing phreatic eruption
0800h-1000h	Tephra fall, lower ignimbrite and pyroclastic surge deposit	Development of an eruption column; generation of pyroclastic flows and surges	Climactic phase with multiple explosive eruptions
1000h-	Upper ignimbrite	Continuation of eruption; lowering of the crater lip	End of climactic phase; partial collapse of the crater wall
1300h	Co-ignimbrite	Cessation of eruption	Deposition of co-ignimbrite ash
Within 3 weeks after the eruption	Lahar deposits	Lahars	Post-eruption lahars

6.3. Vent-clearing phase

The initial ash fall that was experienced at 0630h was most likely from a plume generated by a phreatic eruption related to a vent-opening phase, the deposits of which were not preserved in the stratigraphic record. Phreatic eruptions may develop when overpressurization occurs due to accumulation of volatiles from the exsolving magma. Recent eruptions show that phreatic eruptions are a common pre-climactic activity at Mayon Volcano, occurring months, days or hours prior to the main eruptive phase. (PHIVOLCS, 1990, unpublished reports). Phreatic eruptions preceding the main eruptive phase usually generate ash columns, from which thin ash deposits are derived. Such ash deposits are not usually preserved in the stratigraphy probably due to the thin and highly erodible nature of the deposits.

6.4. The climactic phase

The climactic phase of the 1814 eruption started with the generation of a tall eruption column, closely followed by a sequence of pyroclastic flows and surges, with a late-stage partial collapse of the crater wall. Historical records clearly show that the eruptions were vent-derived and not generated from dome collapse. Dome collapse as eruption mechanism for the 1814 eruption is also ruled out by the predominance of vesicular clasts over dense lithics in all but the uppermost pyroclastic flow unit.

6.4.1. Column-collapse tephra fall

The main eruptive phase commenced with the generation of a tephra fall deposit (Unit A). The timing of emplacement of the tephra fall deposit was constrained by eyewitnesses' observations of an eruption column at 0800h simultaneous with the occurrence of tephra fall. The presence of preserved coarse tephra fall outcrops and concentration of heavy ash fall in the southern slopes indicates a northeasterly wind in the lower atmosphere at the time of the eruption. This is consistent with wind directions that commonly prevail in February (PHIVOLCS, 1990, unpublished reports), assuming that no significant atmospheric variations have occurred since 1814.

Although tephra fall deposits were mapped only as far as 15 km from the vent in the southwestern slope of the volcano, historical accounts report of much wider ash dispersal, with ash reportedly reaching as far as Manila, 325 km from Mayon. Such wide dispersal indicates an eruption column that reached stratospheric heights, which shows the high explosivity of the eruption. The absence of tephra fall deposits is simply due to the low preservation potential of the tephra fall deposit, which owes to the highly erodible nature of the deposit, high erosion rates due to frequent torrential rains, and extensive agricultural and urban activities especially in distal areas.

6.4.2. Pyroclastic flows and surges

Emplacement of the lower ignimbrite

The lower ignimbrite (Unit B) may have been derived from the initial fountain collapse that was observed at the southern slope, which was described as a "black object at the

foot" of the eruption column (Aragoneses, 1814). Outcrops of the lower ignimbrite are valley-confined, poorly sorted, show polymodal histograms, and massive. These characteristics are indicative of a laminar, high-concentration flow (Druitt, 1998). Size grading is present in some outcrops, which suggests that the density current may have been partly fluidized (Cas and Wright, 1988). The emplacement temperature must have been sufficiently high for the ignimbrite to completely char wood.

The lower ignimbrite was found as far as 7 km from the crater, but probably extended farther away, assuming systematic thinning of deposits away from the source. At the farthest point where it was mapped, the deposit had a thickness of 4 m.

Origin of the pyroclastic surge deposit

Pyroclastic surge unit covered a much wider area than the lower ignimbrite, extending as far as 10 km from the vent. Three possible origins of the pyroclastic surge deposit are considered: (1) it's an ash cloud surge deposit associated with the lower ignimbrite, (2) it's a ground surge deposit associated with the upper ignimbrite, or (3) it's a deposit of a discrete phase of the 1814 eruption sequence.

By composition, the surge deposit has a close affinity to the ignimbrite below it. Thus, the unit may be interpreted as a product of an ash cloud surge developing from low-concentration elutriated particles above the pyroclastic flow that emplaced the lower ignimbrite (Fisher, 1995). However, the coarseness of the surge deposit and its clast-supported texture are not consistent with descriptions and models of ash cloud surge deposits, which are characteristically fragment-depleted (Cas and Wright, 1988). The grain size distribution of the surge deposit is essentially similar to that of the lower ignimbrite (>-4ϕ to 1ϕ). The 1814 Mayon surge unit also has an erosive contact with the lower ignimbrite, thus further precluding its ash cloud surge origin.

The pyroclastic surge deposit may also be interpreted as the product of a ground surge, which represents the jetting out of particles from the front of an advancing pyroclastic flow (Cas and Wright, 1988; Valentine and Wohletz, 1989). Because the pyroclastic flow commonly overruns the surge, ground surge deposits are commonly found below the associated ignimbrite in stratigraphic sections. However, the composition and

texture of the 1814 surge unit is markedly different from the overlying ignimbrite. While the surge is composed mostly of black scoria and bombs, the upper ignimbrite is rich in altered clasts. The upper ignimbrite also has an erosive contact with the surge deposit, further attesting to its separate origin.

The 1814 pyroclastic surge deposit is found in all of the studied sites (*Please see Figure 3.1, Chapter 3*). In some sections, it is found directly overlying the lower ignimbrite without the upper ignimbrite; in others, it directly underlies the upper ignimbrite without the lower ignimbrite. The three units are found together in only one section in the Mabinit gully.

This dissociated deposit distribution indicates that the surge was generated from a discrete phase of the eruption, probably from a lower particle concentration density current that closely followed the deposition of the lower ignimbrite. The generation of pyroclastic flows and surges are controlled by turbulence, which relates to the degree of particle concentration (Carey, 1991; Druitt, 1998). Ignimbrites represent the deposit from a less turbulent and higher particle concentration density currents, while surge deposits are derived from the lean phase of the density currents (Druitt, 1998).

Emplacement of the upper ignimbrite and partial crater wall collapse

The upper ignimbrite (Unit D) comprises the last primary volcanic deposit in the 1814 eruptive sequence. This unit extends 7 km down the Mabinit gully, where it has a thickness of 3 m at its farthest exposure. The prevalence of subangular to angular clasts of altered non-juvenile rocks in the upper ignimbrite suggests that the flow that emplaced it incorporated considerable pre-eruption material. Considering historical reports that the southern side of the crater was lowered by approximately 40 m after the 1814 eruption, the altered clasts are interpreted to have been derived from the partial collapse of the crater wall.

6.5. Post-eruption lahars

Torrential rains must have occurred in the vicinity of Mayon and eroded the newly emplaced 1814 primary deposits. Large hot lahars are believed to have been responsible for the damages in Budiao, Cagsawa and Camalig, including the destruction and part burial of the two Spanish churches in Budiao and Cagsawa. Hot emplacement temperature for these lahars is evidenced by the presence of surficial crusts and vesiculation structures that are similar to observed characteristics of hot debris flows from recent eruptions (Rodolfo *et al.*, 1989). Unlike ignimbrites, however, the TRM of the hot lahar deposits show random signatures suggesting that they were sufficiently cooled before being transported (Rodolfo *et al.*, 1989). Subsequent cold lahars that further buried Cagsawa and Budiao Church ruins emplaced deposits that are more polymictic.

6.6. Trigger for the 1814 eruption

6.6.1. Magma mixing and mingling

Magma mixing has been shown to be a common igneous process and has been demonstrated by the studies of plutonic, hypabyssal and volcanic rocks. This process involves the mechanical mixing of two magmas in varying degrees, which may lead to a spectrum of possible results, including: (1) complete mixing, producing a hybrid rock; (2) freezing of one melt, producing enclaves; (3) partial mixing, generating disequilibrium features; and (4) intermingling without mixing, forming heterogeneous deposits on an outcrop scale (*e.g.*, Sakuyama, 1982; Gourgaud and Thouret, 1990; Donoghue *et al.*, 1995).

The petrography of the 1814 products shows evidence for magma mixing and mingling. Although juvenile clasts are compositionally predominated by dark basaltic andesite scoria, there is also a lighter-colored andesite, which occurs rarely in clasts and as streaks in the dark scoria. The streak boundaries are often crenulate, indicating that the two components were in a fluidal state when they interacted. Further evidence for mixing is suggested by the presence of bimodal plagioclase composition, bimodal phenocryts size and differing size of vesicles. Geochemical support for the mixing

comes from the presence of two contrasting groundmass glasses of basaltic andesite (55-57% SiO_2) and intermediate andesite (60-62% SiO_2), which are slightly more silicic than the bulk rock chemistry of the dark basaltic andesite scoria (53-55% SiO_2). The bulk SiO_2 composition of the dark scoria and those of the two groundmass glasses plot linearly in a TAS diagram (*Please see Figure 4.1, Chapter 4*). Although the limited number of glass samples analyzed and the uncertainties involved in the chemical analyses preclude categorical conclusion, the data suggests the possibility that the basaltic andesite glass is the product of mixing of a more basic magma and an intermediate andesite magma. The basic magma is represented by the dark basaltic andesite scoria, while the more acidic magma is represented by the intermediate andesite, which appears as clasts, streaks or groundmass glass. The predominance of basaltic andesite in the 1814 deposits suggests the relative abundance of the basic magma.

6.6.2. Magma mixing as trigger of eruption

It has been shown that magma mixing has influence on triggering eruptions (Sparks *et al.*, 1977). The intrusion of a basaltic magma into a more acidic magma chamber has been cited as a probable trigger on a number of explosive volcanic eruptions, including Pinatubo volcano in 1991 (Pallister *et al.*, 1992, 1996), Krakatau eruption in 1883 (Mandeville *et al.*, 1996), Redoubt Volcano in 1989-1990 (Swanson *et al.*, 1994), and Nevado del Ruiz on 13 November 1985 (Gourgaud and Thouret, 1990).

The general model envisioned for magma mixing is that a magma chamber with a resident, relatively acidic magma is invaded by a hotter and denser basic magma. The basic magma, because of its higher density, temporarily ponds beneath the acidic chamber. For mixing to proceed, the density of the intruding basic magma must be reduced. This may be achieved by heat transfer from the mafic magma to the acidic magma, thus promoting viscosity reduction and convective overturn (*e.g.*, Green, 1988; Blake and Fink, 2000). Alternatively, density reduction is attained by vesiculation through exsolution of dissolved water (Eichelberger, 1990; Huppert *et al.*, 1982; Thomas *et al.*, 1993).

The 1991 eruption of Pinatubo volcano is a well-constrained example of an explosive eruption triggered by mixing of two contrasting magmas: a hotter basalt (~1200°C) and a much colder dacite (~780 °C). The magma mixing produced mingled rocks and a hybrid andesitic lava (Pallister *et al.*, 1996). Disequilibrium features observed in the hybrid rocks include a wide variety and composition of matrix glasses, hornblende rims on olivine and presence of magnetite rims on ilmenite that were preserved. Based on the preservation of these textures, the timing of mixing was determined to be less than 4 days. The timing of mixing was supported by recorded deep (>30 km) long earthquakes during two periods that was related to the ascent of the basaltic magma into the dacitic reservoir (White, 1996).

On the other end of the spectrum, magma mingling between two magmas of little compositional contrast has been suggested as triggering explosive eruptions in Ruapehu (Donoghue *et al.*, 1995, 1999). The eruption that occurred in ~10 ka at Ruapehu was triggered by mingling of two andesitic magmas. The eruptive episode was characterized by closely spaced Plinian eruptions that emplaced the Pourahu ignimbrite and the Okupata tephra fall deposit. A small-volume hot mafic magma heated a lower temperature andesite magma and initiated the eruption. The eruptive products consisted predominantly of the relatively cooler andesitic material.

The 1814 eruption may have been triggered by the intrusion of basaltic andesite magma into a small, shallow reservoir of intermediate andesite beneath Mayon Volcano. This model is consistent with the theory of a periodic injection of basaltic magma at Mayon Volcano by Newhall (1977). The relative abundance of the more basic magma, or, conversely, the smallness of the acidic magma chamber, is indicated by the predominance of basaltic andesite in the 1814 deposits. Partly because of this uneven proportion, magma mixing was not thorough, thus explaining the paucity of a hybrid product. The basic magma was mostly erupted unaltered.

6.7. Comparison of the 1814 event with other eruptions of Mayon

The 1814 eruption is regarded as the most explosive and catastrophic eruption for Mayon Volcano since its first recorded eruption in 1616. Comparison of the 1814

tephra fall deposit with the most recent eruptions show that the 1814 eruption is more explosive. The mapped distribution of the 1814 tephra fall deposit, extending to 15km from the vent, is more extensive than that of any other eruption of Mayon. Historical reports of the wide dispersal of the 1814 tephra further suggest that the eruption was stronger than more recent eruptions. The field data on the 1814 tephra fall, at present, falls short of the requirements to classify the eruption's explosivity using Walker's (1983) criteria.

A rough estimate of the explosivity of the 1814 eruption can be made by comparing the fall distribution of the February 1, 1814 eruption with the February 28, 2000 eruption. The 2000 eruption was characterized by predominantly Strombolian to Vulcanian type eruptions, which generated a 14-km high eruption column (PHIVOLCS, 1990, unpublished report). The eruption deposited 0.02-m thick tephra fall layer at 13 km from the vent. At the same distance, the associated tephra fall from the 1814 deposit was 0.20 m, an order of magnitude thicker.

The magnitude of the eruption can also be estimated by the run-out distance of pyroclastic flows and surges. Run-out distances of pyroclastic flows and surges generated during the 1968, 1984, 1993 and 2000 eruptions never exceeded 6 km. The 1814 lower and upper ignimbrites extend as far away from the vent as 7 km, with the deposits at this distance still 4-5 m thick. The 1814 pyroclastic surge deposit extends up to 8 km in Budiao and 10 km at the Cagsawa Ruins.

6.8. Summary and conclusions

6.8.1. Hazard implications

The positive identification of a wide distribution of pyroclastic surge deposits, extending as far as 10 km from the Mayon crater, requires serious consideration in terms of hazard prevention in the highly populous areas surrounding Mayon. Such far-reaching pyroclastic surges have been underestimated in the assessment of volcanic hazards at Mayon. Historical documents have reported mangled bodies, incineration, damaged houses, and partial burial of infrastructures in the vicinities of Budiao,

Cagsawa and Camalig, Ligao, Sto. Domingo and Legazpi City (formerly Albay) during the 1814 eruption (Espinas, 1978), which was probably caused by the pyroclastic surge. A temperature of not less than 100°C is estimated based on the abundant charred wood in the pyroclastic surge deposit.

Currently, government authorities impose a 6-km radius permanent danger zone, within which no settlement is allowed. An eruption similar in size as the 1814 episode may devastate a much larger area, with pyroclastic surges a particular cause for concern. The sad fact that several villages in the permanent danger zone are inhabited, and that agricultural activities are done at closer distances to the vent, even against government advice, highlight the potential risks that a large eruption at Mayon poses.

6.8.2. Recommendations for future studies

The study of the 1814 eruption can be expanded by further exploring other potential sites for the 1814 tephra fall, which were not covered in this study due to the limited time spent on fieldwork. However, mapping of tephra fall deposits, especially of the fine component far from the vent, is complicated by the presence of other volcanoes present in the vicinity of Mayon, which can make identifying the deposits difficult. Study of glass shards chemistry can aid in determining the provenance of the finer tephra units. Detailed comparative analyses of the 1814 eruptive products with the recent deposits (*e.g.*, from the 2000 and 2001 eruptions) would help to understand better the eruptive processes that operate at Mayon Volcano.

Hazardous pyroclastic surges at Mayon require further studies. It is highly possible that other historical eruptions could have generated similar far-reaching pyroclastic surges as the 1814 event. A comparative study of surge deposits from other historical eruptions shall help to better understand their emplacement patterns and mechanisms. Such study is vital for hazard assessment at Mayon.

This study has recognized proof of magma mixing for the 1814 eruption. Since magma mixing has a direct bearing on the plumbing of a volcano, which is important in hazards evaluation and eruption prediction, further studies of magma mixing – for the 1814 event as well as other eruption episodes of Mayon – are recommended. More samples

of the light brown rock found in the 1814 deposits need to be collected and analyzed for its bulk chemistry. Electron microprobe analyses of matrix glasses, groundmass phenocrysts, and large phenocrysts are needed to better understand the process of magma mixing.

The depth at which magma mixing occurs, which is directly related to the depth of the magma reservoir beneath Mayon, may be investigated by detailed studies of mineral geothermometers and geobarometers. This may be complemented by seismic tomography studies.

It is hypothesized in the study that volatile content could have played a role on the explosivity of the 1814 eruption. Thus, a study on glass inclusions may help to estimate pre-eruption volatile content of the magmas.

References

Abella, E.C., 1883. El Mayon, o Volcan de Albay. Transactions of the Seismological Society of Japan. 5: 405-423.

Aragoneses, F.1814. Suceso espantoso y memorable acaecido en la provincia de Camarines el dia primero de Febrero de este presente ano de 1814, Sampaloc, Manila, 19 pp.

Arcilla, C., 1998. Mantle dynamic implications of Philippine Arc Volcanism. PhD. Thesis, University of Illinois, 246 pp.

Arguden, A.T. and Rodolfo, K.S., 1986. Sedimentology of hot and cold lahar deposits produced during and after the 1984 eruption of Mayon Volcano, Philippines. Philippine Journal of Volcanology. 3(2): 60-78.

Arguden, A.T. and Rodolfo, K.S., 1990. Sedimentologic and dynamic differences between hot and cold laharic debris flows of Mayon Volcano, Philippines. Geological Society of America Bulletin. 102(7): 865-876.

Aurelio, M., Barrier, E., Gaulon, R., and Rangin, C., 1997. Deformation and stress states along the central segment of the Philippine Fault: implications to wrench fault tectonics. Journal of Asian Earth Sciences. 15(2-3): 107-119.

Beavan, J., Silcock, D, Hamburger, M., Ramos, E., Thibault, C., and Feir, R. 2001. Geodetic constraints on postseismic deformation following the 1990 M_s 7.8 Luzon earthquake and implications for tectonics and Philippine Sea plate motion. Geochemistry, Geophysics, Geosystems. 2: Paper No. 2000GC000100, 36 pp.

Besana, G. Negishi, H., and Ando, M., 1997. The three-dimensional attenuation structures beneath the Philippine archipelago based on seismic intensity data inversion. Earth and Planetary Science Letters.151: 1-11.

Blake, S. and Fink, J., 2000. On the deformation and freezing of enclaves during magma mixing. Journal of Volcanology and Geothermal Research. 95: 1-8.

Calleja, A., 1937. Ruta el Mayon, Unpublished manuscript, 50 pp.

Calleja-Reyes, J., 1988. A record of 1814 eruption. Ballad on mighty Mayon. Sunday Inquirer Magazine.

Carey, S., 1991. Transport and deposition of tephra by pyroclastic flows and surges. Sedimentation in Volcanic Settings, SEPM Special Publications 45: 39-56.

Cas, R.A.F. and Wright, J.V., 1988. Volcanic Successions: Modern and Ancient. Chapman and Hall, 528 pp.

Catane, S., Corpuz, E. and Punongbayan, R., 1991. Mayon Volcano's past and possible future eruptive activities.

Catane, S., Mirabueno, M.H.T., Listanco, E.L.L. and Solidum, R., 1995. Characteristics and origin of the pyroclastic flows and surges of the 1993 Mayon volcano eruption, unpublished paper.

Catane, S., Listanco, E.L.L. and Mirabueno, M.H.T., 1995a. Block-and-ash flows: unrecognized hazards at Mayon Volcano, Philippines, International Union of Geodesy and Geophysics XXI General Assembly, p. 420.

Coronas, J. 1898. La erupcion de volcan Mayon en los dias 25 y 26 de Junio de 1897. 55 pp.

Di Vito, M., Lirer, L., Mastrolorenzo, G., and Rolandi, G., 1987. The 1538 Monte Nuovo eruption (Campi Flegrei, Italy). Bulletin of Volcanology, 49: 608-615.

Donoghue, S.L., Gamble, J.A., Palmer, A.S. and Stewart, R.B., 1995. Magma mingling in an andesite pyroclastic flow of the Pourahu Member, Ruapehu volcano, New Zealand. Journal of Volcanology and Geothermal Research, 68: 177-191.

Donoghue, S.L., Palmer, A.S. and McClelland, Hobson, K., Stewart, R.B., Neall, V.E., Lecointre, J. and Price, R., 1999. The Taurewa Eruptive Episode: evidence for climactic eruptions at Ruapehu volcano, New Zealand. Bulletin of Volcanology, 60: 223-240.

Druitt, T.H., 1998. Pyroclastic density currents: In Gilbert, J.S. and Sparks, R.S.J (Eds.) The Physics of explosive volcanic eruptions Geological Society Special Publication, London, pp. 145-182.

Eichelberger, J.C., 1980. Vesiculation of mafic magma during replenishment of silicic magma reservoirs. Nature, 288(5790): 446-450.

Espinas, M., 1978. What you've always wanted to know about Mayon Volcano. Legazpi City Bicol Heritage. 7: 48.

Faustino, L., 1929. Mayon Volcano and its eruptions. The Philippine Journal of Science, 40(1): 1-43.

Fisher, R.V., 1995. Decoupling of pyroclastic currents: hazards assessments. Journal of Volcanology and Geothermal Research, 66: 257-263.

Foreman, J., 1906. The Philippine Islands. Shanghai: Kelley and Walsh Ltd., pp. 16-17.

Gill, J., 1981. Orogenic andesites and plate tectonics. Springer-Verlag, Springer Verlag. Berlin, Federal Republic of Germany, 401 pp.

Green, N., 1988. Basalt-basaltic andesite mixing at Mount Baker Volcano, Washington, I. Estimation of mixing conditions. Journal of Volcanology and Geothermal Research, 34: 251-265.

Gourgaud, A. and Thouret, J.C., 1990. Magma mixing and petrogenesis of the 13 November 1985 eruptive products at Nevado del Ruiz. Journal of Volcanology and Geothermal Research, 41: 79-96.

Hoblitt, R.P. and Kellog, K.S., 1979. Emplacement temperatures of unsorted and unstratified deposits of volcanic rock debris as determined by paleomagnetic techniques. Geological Society of America Bulletin, 90(7): I. 633 - I 642.

Huerta, F, 1865. Estado, geografico, topografico, estadistico, historico-religioso de la Santa y apostolica. 254-258.

Huppert, H.E., Sparks, R.S.J. and Turner, J.S., 1982. Effect of volatiles on mixing in calc-alkaline magma systems. Nature, 297(554-557).

Knittel-Weber, C and Knittel, U., 1990. Petrology and genesis of the volcanic rocks on the eastern flank of Mount Malinao, Bicol arc (southern Luzon, Philippines). Journal of Southeast Asian earth Sciences, 4(No. 4): 267-280.

Lizardo, R., 1986. Statistical analysis of the eruptive events of Mayon Volcano, Philippines. Philippine Journal of Volcanology, 3(2): 1-20.

Loquez, M., unpublished Poem on Budiao during the 1814 eruption. In Diaz, V., The Budiao Church Ruins.

Mandeville, C.W., Carey, S. and Sigurdsson, H., 1996. Magma mixing, fractional crystallization and volatile degassing during the 1883 eruption of Krakatau volcano, Indonesia. Journal of Volcanology and Geothermal Research, 74: 243-274.

Martinez, F., 1859. El volcano de Albay. Illustracion de Filipinas, 1(17): 137-141.

Maso, M.S., 1904. Volcanoes and seismic centers of the Philippine Archipelago, pp. 9-45.

Maso, M.S., 1911. Volcanic eruptions in the Philippines in relation to earthquake, subterranean noises, rainfall and atmospheric pressure. Bulletin of the Weather Bureau, 238-249.

Mata, J., 1814. Erupcion del Volcan de Albay, efemeridas desde el dia 1 de Febrero de 1814 hasta el dia 18 del mismo mes. (with English translation). Unpublished manuscript, Laong Samar.

Moore, J.G. and Melson, W.G., 1969. Nuees ardentes of the 1968 eruption of Mayon Volcano, Philippines. Bulletin of Volcanology 33(2): 600-620.

Newhall, C.G., 1977. Geology and petrology of Mayon volcano, Southeastern Luzon, Philippines. MSc. Thesis, University of California at Davis, California, 292 pp.

Newhall, C.G., 1979. Temporal variations in the lavas of Mayon Volcano, Philippines. Journal of Volcanology and Geothermal Research 6:61-83.

Packard, R.L., 1900. Remarkable volcanic eruptions in the Philippines. Popular Science Monthly, 56: 374-379.

Pallister, J.S., Hoblitt, R.P., and Reyes, A.G., 1992. A basalt trigger for the 1991 eruptions of Pinatubo volcano? Nature, 356: 426-428.

Pallister, J.S., Hoblitt, R.P., Meeker, G., Knight, R. and Siems, D., 1996. Magma mixing at Mount Pinatubo: Petrographic and chemical evidence from the 1991 deposits. In: C.G. Newhall, R.S. Punongbayan (Editors), Fire and Mud: Eruptions and lahars of Mount Pinatubo, Philippines. Philippine Institute of Volcanology and Seismology, University of Washington Press, Quezon City, pp. 687-732.

Panfil, M.S., Gardner, T.W., Hirth, K.G., 1999. Late Holocene stratigraphy of the Tetimpa archaeological sites, northeast flank of Popocatepetl volcano, central Mexico. Geological Society of America Bulletin, 111(No. 2): 204-218.

Peralta, F., 1814. Breve analisis quimica practicada sobre las arenas volcanicas que erupto el de Albay, el dia 1 de Febrero y cayeron en la ciudad de Manila. 22pp

Perry, A., 1860. Documents on Earthquakes and volcano phenomena in the Philippine Archipelago.

PHIVOLCS, (1990). Manual- Operation Mayon.

Ramos, E.G., de Torres, C.B. and Calderon. A.C., 1985. Earth tide influences on the recent activities of Mayon Volcano. Philippine Journal of Volcanology, Vol. 2(Nos. 1 and 2): 172-190.

Ramos-Villarta, S.C., Corpuz, E.G. and Newhall, C.G., 1985. Eruptive history of Mayon Volcano, Philippines. Philippine Journal of Volcanology, Vol. 2(Nos. 1 and 2): 1-35.

Rodolfo, K.S., Solidum, R. U., Ruelo, H.B. and Alonso, R.A, (1989) Reconstruction of the 1814 Mayon eruption from the deposits at Budiao church ruins. Unpublished report.

Rosi, M. and Santacroce, R., 1983. The A.D 472 "Pollena" eruption: Volcanological and petrological data for this poorly-known, Plinian-type event at Vesuvius. Journal of Volcanology and Geothermal Research, 17: 249-271.

Rosi, M., Principe, C., and Vecci, R., 1993. The 1631 Vesuvius eruption. A reconstruction based on historical and stratigraphical data. Journal of Volcanology and Geothermal Research, 58: 151-182.

Saderra, M., 1904. Volcanoes and seismic centers. Bureau of Census, Manila, Philippines.

Sakuyama, M., 1982. Magma mixing and magma plumbing system in Island Arcs. Bulletin of Volcanology, 47(4): 685-702.

Self, S., Rampino, MR, and Carr, MJ, 1989. A reappraisal of the 1835 eruption of Cosiguina and its atmospheric impact. Bulletin of Volcanology, 52: 57-65.

Selga, M., 1914. La erupcion del Mayon en 1814 y el archivo paroquial de Albay.

Selga, M. 1914. La erupcion del Mayon en 1814 y la visita de Daraga. 5 pp.

Shelley, D., 1993. Igneous and Metamorphic Rocks under the Microscope. Chapman and Hall, 445pp.

Sparks, R.S.J., Sigurdsson, H. and Wilson, L., 1977. Magma mixing: a mechanism for triggering acid explosive eruptions. Nature, 267: 315-318.

Sparks, R.S.J., Huppert, H.E. and Turner, J.S., 1984. The fluid dynamics of evolving magma chambers. Philos. Trans. R. Soc. London, Ser. A., 310: 511-534.

Sparks, R., Barclay, J, Jaupart, C., Mader, HM, Phillips JC, 1994. Physical aspects of magmatic degassing I. Experimental and theoretical constraints on vesiculation. In: Mader, HM and. Carroll, J.R (Editor), Volatiles in Magma. Reviews in Mineralogy. Mineralogical Society of America, pp. 413-443.

Sun, S. and McDonnough. W.F. (Editor), 1989. Chemical and isotopic systematics of oceanic basalts: implications for mantle composition and processes. Magmatism in ocean basins, 42. Geological Soc. London. Special Publication, 313-345 pp.

Swanson, S.E., Nye, C., Miller, T. and Avery, V.F., 1994. Geochemistry of the 1989-1990 eruption of Redoubt Volcano: Part II. Evidence from mineral and glass chemistry. Journal of Volcanology and Geothermal Research, 62: 453-468.

Thomas, N., Tait, S. and Koyaguchi, T., 1993. Mixing of stratified liquids by the motion of gas bubbles: application to magma mixing. Earth and Planetary Science Letters, 115: 161-175.

Umbal, J., 1984. Mayon lahars during and after the 1984 eruption. Philippine Journal of Volcanology, 3(2): 38-59.

Valentine, G.A., and Wohletz, K.H., 1989. Numerical models of Plinian eruption columns and pyroclastic flows. Journal of Geophysical Research, 94: 1867-1887.

White, R.A., 1996. Precursory deep long-period earthquakes at Mount Pinatubo; spatio-temporal link to a basalt trigger. In: Newhall, C.G. and Punongbayan R.S. (Editor), Fire and mud: Eruptions and lahars of Mount Pinatubo, Philippines. University of Washington Press United States, Philippine Institute of Volcanology and Seismology, Quezon City, pp. 307-326.

Wilson, M., 1989. Igneous Petrogenesis: A Global Tectonic Approach, 466 pp.

APPENDIX A RESULTS OF XRF ANALYSES (MAJOR ELEMENTS)

Sample	Description	Location	SiO2(%)	TiO2 (%)	Al2O3 (%)	Fe2O3(%)	MnO (%)	MgO (%)	CaO (%)	Na2O(%)	K2O (%)	P2O5 (%)	TOTAL
MAY 24	Scoria clast in surge unit	Anoling gully	54.46	0.82	18.79	8.88	0.17	4.07	8.39	3.70	1.05	0.29	100.62
MAY 25 A-1	Scoria clast in lower ignimbrite unit	Anoling gully	54.45	0.82	18.73	8.86	0.17	4.03	8.32	3.77	1.06	0.29	100.50
May 25 A-2	Dense lithic in surge unit	Anoling gully	54.50	0.82	18.61	8.91	0.17	4.09	8.34	3.73	1.07	0.29	100.53
MAY 25 B	Scoria clast in surge unit	Anoling gully	54.36	0.81	18.62	8.89	0.17	4.12	8.33	3.70	1.06	0.29	100.35
MAY 25 C	Scoria clast in surge unit	Anoling gully	54.43	0.82	18.71	8.88	0.17	4.08	8.35	3.73	1.06	0.29	100.52
MAY25 D	Scoria clast in surge unit	Anoling gully	54.34	0.82	18.64	8.95	0.17	4.13	8.40	3.66	1.06	0.29	100.46
MAY 25 F	Scoria clast in surge unit	Anoling gully	54.35	0.81	18.70	8.89	0.17	4.19	8.39	3.61	1.07	0.28	100.46
MAY 25 G	Scoria clast in surge unit	Anoling gully	54.16	0.82	18.90	8.94	0.17	4.07	8.50	3.68	1.03	0.28	100.55
MAY 26 A	Dense lithic in surge unit	Anoling gully	54.54	0.82	18.68	8.88	0.17	4.14	8.38	3.69	1.06	0.28	100.64
MAY 28C	Dense lithic in surge unit	Anoling gully	52.99	0.77	19.23	8.95	0.17	4.68	9.19	3.35	0.97	0.26	100.56
MAY 29 E	Scoria clast in surge unit	Anoling gully	54.14	0.83	18.88	8.94	0.17	4.07	8.46	3.68	1.01	0.29	100.47
MAY 34	Scoria clast in tephra unit	Bublusan	55.01	0.77	19.50	8.13	0.17	3.42	8.02	3.81	1.02	0.31	100.16
12011-4	Scoria clast in surge unit	Budiao trench	54.09	0.83	18.67	9.06	0.17	4.18	8.46	3.68	1.02	0.28	100.44
MAY 33-A-2	Scoria clast in lower ignimbrite unit	Miisi gully	53.71	0.75	19.29	8.6	0.16	4.46	8.94	3.95	1.05	0.25	100.43
May 2-28P	Scoria clast in surge unit	Mabinit gully	54.57	0.81	18.57	8.73	0.17	4.09	8.31	3.74	1.07	0.29	100.3
May 2-8-C	Scoria clast in upper ignimbrite unit	Mabinit gully	52.5	0.74	19.73	8.71	0.16	4.59	9.53	3.17	0.87	0.24	100.5
May 2-39 D	Scoria clast in surge unit	Budiao gully	54.76	0.79	18.48	8.66	0.16	4.23	8.29	3.59	1.1	0.28	100.23
May 2-12C	Scoria clast in tephra fall unit	Guinobatan	54.56	0.82	18.49	8.69	0.17	4.09	8.32	3.67	1.07	0.28	100.14
May 2-27B	Scoria clast in surge unit	Mabinit gully	52.93	0.77	19.81	8.59	0.16	4.16	9.43	3.39	0.88	0.26	100.1
May 2-24C	Scoria clast in surge unit	Miisi gully	53.94	0.82	18.93	8.83	0.17	4.07	8.72	3.63	0.98	0.28	100.15
May2-24A	Scoria clast in lower ignimbrite unit	Miisi gully	54.59	0.82	18.64	8.73	0.17	4.01	8.3	3.75	1.05	0.29	100.22
May2-GBF	Scoria clast in lower ignimbrite unit	Mabinit gully	54.57	0.77	18.59	8.65	0.17	4.33	8.42	3.5	1.07	0.27	100.19
May2 -24D	Scoria clast in lower ignimbrite unit	Miisi gully	54.4	0.82	18.64	8.8	0.17	4.09	8.32	3.67	1.04	0.29	99.97
May2-6-A	Scoria clast in lower ignimbrite unit	Miisi gully	54.69	0.76	18.71	8.54	0.17	4.3	8.45	3.52	1.1	0.26	100.03
May2-24B	Scoria clast in surge unit	Miisi gully	54.52	0.79	18.59	8.65	0.17	4.16	8.35	3.63	1.07	0.28	100.1
May2-39E	Scoria clast in surge unit	Banadero gully	53.69	0.81	19.07	8.38	0.17	4.1	8.81	3.51	0.96	0.28	100.03

APPENDIX A RESULTS OF XRF ANALYSES (TRACE ELEMENTS in ppm)

Sample	Description	Location	La	Ce	Nd	Ga	Pb	Rb	Sr	Th	Y	V	Cr	Ni	Zn	Zr	Nb	Ba
MAY 24	Scoria clast in surge unit	Anoling gully	10	36	16	18	3	16	682	2	23	249	<3	3	88	95	5	388
MAY 25 A-1	Scoria clast in lower ignimbrite unit	Anoling gully	15	37	20	19	3	16	682	2	24	258	<3	4	88	95	5	402
May 25 A-2	Dense lithic in surge unit	Anoling gully	8	39	17	19	2	16	676	1	23	255	<3	<3	87	94	5	407
MAY 25 B	Scoria clast in surge unit	Anoling gully	7	37	11	18	1	16	672	<1	24	254	3	4	88	95	5	401
MAY 25 C	Scoria clast in surge unit	Anoling gully	8	37	19	19	2	16	676	1	23	252	<3	<3	88	94	5	402
MAY25 D	Scoria clast in surge unit	Anoling gully	7	40	19	19	<1	13	678	1	23	252	3	<3	87	95	5	392
MAY 25 F	Scoria clast in surge unit	Anoling gully	17	42	28	18	5	16	667	1	23	250	<3	3	87	95	5	391
MAY 25 G	Scoria clast in surge unit	Anoling gully	9	40	27	18	3	15	681	2	23	257	<3	4	87	92	5	394
MAY 26 A	Dense lithic in surge unit	Anoling gully	11	44	33	18	3	16	678	3	23	248	<3	<3	87	94	5	393
MAY 28C	Dense lithic in surge unit	Anoling gully	18	60	32	18	4	14	714	4	22	254	5	7	82	88	5	473
MAY 29 E	Scoria clast in surge unit	Anoling gully	12	37	30	19	<1	15	679	<1	23	257	<3	<3	88	94	5	385
MAY 34	Scoria clast in tephra unit	Bublusan	12	30	29	19	3	16	669	<1	24	203	<3	<3	86	102	5	356
12011-4	Scoria clast in surge unit	Budiao trench	10	44	22	19	<1	15	668	1	23	263	<3	<3	88	92	5	374
MAY 33-A-2	Scoria clast in lower ignimbrite unit	Miisi gully	17	26	<10	18	3	14	694	<1	22	203	4	5	76	89	5	357
May 2-28P	Scoria clast in surge unit	Mabinit gully	14	43	29	19	4	12	687	4	24	220	3	5	90	98	5	393
May 2-8-C	Scoria clast in upper ignimbrite unit	Mabinit gully	11	35	11	18	1	9	687	4	24	221	4	6	83	82	4	340
May 2-39 D	Scoria clast in surge unit	Budiao gully	18	40	31	19	3	14	672	4	23	209	5	5	87	100	5	415
May 2-12C	Scoria clast in tephra fall unit	Guinobatan	19	27	18	19	2	13	686	4	25	220	4	3	88	97	4	389
May 2-27B	Scoria clast in surge unit	Mabinit gully	10	35	25	19	<1	10	710	3	22	269	4	<3	81	82	4	319
May 2-24C	Scoria clast in surge unit	Miisi gully	15	40	22	19	2	12	693	3	24	278	4	<3	86	92	4	366
May2-24A	Scoria clast in lower ignimbrite unit	Miisi gully	7	39	29	19	1	13	688	4	25	264	4	<3	88	98	4	375
May2-GBF	Scoria clast in lower ignimbrite unit	Mabinit gully	12	35	35	17	<1	15	674	3	24	241	<3	4	83	99	5	386
May2 -24D	Scoria clast in lower ignimbrite unit	Miisi gully	12	34	27	18	3	14	686	6	25	258	5	<3	88	98	4	382
May2-6-A	Scoria clast in lower ignimbrite unit	Miisi gully	8	25	30	18	<1	15	677	4	23	214	9	<3	79	99	4	385
May2-24B	Scoria clast in surge unit	Miisi gully	12	32	24	17	5	13	680	2	25	254	4	4	86	98	4	386
May2-39E	Scoria clast in surge unit	Banadero gully	10	28	34	19	3	12	691	4	23	276	4	<3	87	90	4	351

APPENDIX B-1 RESULTS OF ELECTRONMICROPROBE ANALYSES OF PLAGIOCLASE

Laboratory No.	1	52	54	57	59	61	62	64	65	69	70	95	96
Location	Anoling gully	Morera	Morera	Morera	Morera	Anoling gully	Anoling gully	Anoling gully	Anoling gully	Anoling gully	Anoling gully	Anoling gully	Anoling gully
Description	Surge	Fall	Fall	Fall	Fall	Surge	Surge	Surge	Surge	Surge	Surge	Surge	Surge
Na2O	1.22	4.39	3.08	4.33	3.79	3.96	4.19	4.56	3.54	4.45	3.08	4.17	3.62
K2O	14.30	0.26	0.26	0.24	0.23	0.21	0.16	0.23	0.12	0.16	0.20	0.20	0.17
Al2O3	18.10	29.45	30.29	27.70	27.52	28.39	28.94	28.48	29.87	28.55	30.11	29.37	30.43
TiO2	0.09	0.00	0.03	0.09	0.00	0.08	0.00	0.06	0.00	0.03	0.09	0.00	0.00
MgO	0.00	0.09	0.09	0.10	0.07	0.08	0.08	0.06	0.07	0.10	0.19	0.11	0.06
CaO	0.00	13.48	15.02	12.34	12.00	12.13	12.47	12.00	13.99	12.06	14.20	13.30	14.10
FeO	0.00	0.80	0.91	0.85	0.95	0.84	0.70	0.71	0.79	0.67	1.19	0.55	0.70
MnO	0.00	0.00	0.02	0.00	0.05	0.06	0.02	0.04	0.00	0.00	0.00	0.00	0.00
Cr2O3	0.00	0.00	0.00	0.02	0.00	0.04	0.00	0.05	0.00	0.06	0.00	0.00	0.00
SiO2	66.16	53.00	49.35	55.13	57.28	54.81	52.52	55.33	51.41	53.20	50.24	52.75	52.27
Total	99.88	101.47	99.05	100.80	101.91	100.59	99.08	101.55	99.78	99.29	99.30	100.45	101.34
Oxygen	32.00	32.00	32.00	32.00	32.00	32.00	32.00	32.00	32.00	32.00	32.00	32.00	32.00
Na	0.43	1.53	1.11	1.51	1.30	1.38	1.49	1.58	1.26	1.58	1.10	1.46	1.26
K	3.34	0.06	0.06	0.06	0.05	0.05	0.04	0.05	0.03	0.04	0.05	0.05	0.04
Al	3.91	6.25	6.62	5.88	5.74	6.02	6.26	5.99	6.44	6.15	6.55	6.28	6.46
Ti	0.01	0.00	0.00	0.01	0.00	0.01	0.00	0.01	0.00	0.00	0.01	0.00	0.00
Mg	0.00	0.02	0.02	0.03	0.02	0.02	0.02	0.02	0.02	0.03	0.05	0.03	0.02
Ca	0.00	2.60	2.99	2.38	2.28	2.34	2.45	2.29	2.74	2.36	2.81	2.58	2.72
Fe	0.00	0.12	0.14	0.13	0.14	0.13	0.11	0.11	0.12	0.10	0.18	0.08	0.10
Mn	0.00	0.00	0.00	0.00	0.01	0.01	0.00	0.01	0.00	0.00	0.00	0.00	0.00
Si	12.11	9.54	9.16	9.92	10.14	9.86	9.63	9.87	9.41	9.73	9.27	9.57	9.41
Total	19.81	20.13	20.11	19.91	19.67	19.83	20.00	19.94	20.01	20.00	20.02	20.05	20.01
Notes	core	rim	rim	clear plag.	clear plag.	skeletal rim	skeletal rim	rim	rim	core	core	clear plag.	core

Appendix B-1 (Continuation) **RESULTS OF ELECTRONMICROPROBE ANALYSES OF PLAGIOCLASE**

Laboratory No.	13	14	18	39	40	97	98	100	101	104	105	109	113
Location	Anoling gully	Anoling gully	Anoling gully	Nasisi	Nasisi	Anoling gully	Anoling gully	Anoling gully	Anoling gully	Anoling gully	Anoling gully	Anoling gully	Anoling gully
Description	Surge	Surge	Surge	Fall	Fall	Surge	Surge	Surge	Surge	Surge	Surge	Surge	Surge
Na2O	2.84	4.53	2.14	4.31	4.55	4.58	4.58	4.16	2.99	4.38	4.54	3.98	4.15
K2O	0.18	0.28	0.08	0.20	0.24	0.23	0.22	0.16	0.12	0.22	0.20	0.19	0.21
Al2O3	30.70	28.47	31.66	28.32	28.12	28.99	27.71	29.26	31.21	29.15	28.21	29.72	29.20
TiO2	0.00	0.00	0.00	0.03	0.04	0.03	0.04	0.08	0.00	0.03	0.00	0.06	0.13
MgO	0.02	0.00	0.02	0.09	0.11	0.11	0.10	0.10	0.08	0.08	0.08	0.07	0.09
CaO	14.81	11.92	16.36	12.30	11.92	12.27	12.05	12.35	15.14	12.30	12.20	12.47	12.35
FeO	0.65	0.81	0.79	0.81	0.77	0.70	0.86	0.90	0.70	0.91	0.77	0.67	0.73
MnO	0.07	0.00	0.00	0.00	0.00	0.00	0.00	0.05	0.00	0.02	0.06	0.00	0.00
Cr2O3	0.00	0.00	0.00	0.00	0.00	0.02	0.00	0.00	0.00	0.03	0.00	0.00	0.00
SiO2	49.79	53.76	48.80	53.56	54.23	54.33	55.19	53.46	50.05	53.23	54.85	53.29	52.39
Total	99.07	99.76	99.85	99.62	99.98	101.27	100.76	100.52	100.30	100.36	100.92	100.46	99.24
Oxygen	32.00	32.00	32.00	32.00	32.00	32.00	32.00	32.00	32.00	32.00	32.00	32.00	32.00
Na	1.02	1.60	0.76	1.52	1.60	1.59	1.60	1.46	1.06	1.54	1.58	1.39	1.47
K	0.04	0.06	0.02	0.05	0.06	0.05	0.05	0.04	0.03	0.05	0.05	0.04	0.05
Al	6.68	6.10	6.86	6.09	6.01	6.13	5.88	6.23	6.72	6.23	5.98	6.32	6.30
Ti	0.00	0.00	0.00	0.00	0.01	0.00	0.01	0.01	0.00	0.00	0.00	0.01	0.02
Mg	0.01	0.00	0.01	0.02	0.03	0.03	0.03	0.03	0.02	0.02	0.02	0.02	0.02
Ca	2.93	2.32	3.22	2.40	2.32	2.36	2.32	2.39	2.96	2.39	2.35	2.41	2.42
Fe	0.10	0.12	0.12	0.12	0.12	0.10	0.13	0.14	0.11	0.14	0.12	0.10	0.11
Mn	0.01	0.00	0.00	0.00	0.00	0.00	0.00	0.01	0.00	0.00	0.01	0.00	0.00
Si	9.20	9.78	8.98	9.76	9.84	9.74	9.93	9.66	9.14	9.65	9.86	9.62	9.60
Total	19.99	20.00	19.98	19.97	19.98	20.01	19.95	19.96	20.04	20.03	19.97	19.93	20.00
Notes	skeletal rim	skeletal rim	skeletal core	rim	skeletal rim	rim	skeletal rim	rim	rim	core	core	rim	core

APPENDIX B-2 RESULTS OF ELECTRONMICROPROBE ANALYSES OF PYROXENE

Laboratory No.		79	80	123	124	141	142
Location	Anoling gully	Anoling gully	Anoling gully	Anoling gully	Anoling gully	Anoling gully
Description	Surge unit	Surge unit	Surge unit	Surge unit	Surge unit	Surge unit
Na2O	0.247	0.299	0.318	0.403	0.348	0.267
K2O	0.016	0.025	0	0	0	0
Al2O3	2.08	2.053	1.747	2.82	2.629	2.176
TiO2	0.572	0.56	0.502	0.705	0.635	0.361
MgO	15.833	15.691	15.893	15.106	14.711	15.429
CaO	19.982	19.857	19.806	19.848	20.093	20.826
FeO	9.811	10.349	9.182	10.245	9.236	8.164
MnO	0.395	0.411	0.341	0.357	0.348	0.354
SiO2	50.336	49.991	52.391	51.848	51.68	52.121
Total	99.2768	99.2411	100.1855	101.3349	99.6825	99.7018
Oxygen	6	6	6	6	6	6
Na	0.0181	0.0219	0.0229	0.0288	0.0251	0.0193
K	0.0008	0.0012	0	0	0	0
Al	0.0925	0.0916	0.0762	0.1225	0.1156	0.0952
Ti	0.0162	0.0159	0.014	0.0195	0.0178	0.0101
Mg	0.8906	0.8858	0.8784	0.83	0.8184	0.8554
Ca	0.8078	0.8057	0.7867	0.7837	0.8034	0.8298
Ni	0	0	0.2847	0.3158	0.2881	0.2539
Fe	0.3096	0.3277	0.0107	0.0111	0.011	0.0111
Si	1.8992	1.8932	1.9425	1.9109	1.9286	1.9383
Total	4.0477	4.0566	4.0167	4.0226	4.0084	4.0135

APPENDIX B-3 RESULTS OF ELECTRONMICROPROBE ANALYSES OF OLIVINE

Laboratory No.	21	22	25	48	49	50	51	82	83	151	153	155	156
Location	Anoling gully	Anoling gully	Anoling gully	Anoling gully	Anoling gully	Morrera	Morrera	Anoling gully	Anoling gully	Anoling gully	Anoling gully	Anoling gully	Anoling gully
Description	Surge unit	Surge unit	Surge unit	Surge unit	Surge unit	Fall unit	Fall unit	Surge unit	Surge unit	Lower ignimbr	Lower ignimbri	Lower ignimbri	Lower ignimbrite
Na2O	0.03	0.03	0.00	0.10	0.02	0.04	0.05	0.04	0.02	0.00	0.00	0.00	0.00
K2O	0.02	0.00	0.00	0.03	0.01	0.04	0.01	0.00	0.02	0.00	0.01	0.00	0.00
Al2O3	0.03	0.00	0.00	0.00	0.00	0.00	0.04	0.00	0.00	0.03	0.00	0.12	0.00
TiO2	0.03	0.00	0.00	0.00	0.03	0.02	0.02	0.00	0.00	0.06	0.00	0.03	0.00
MgO	38.16	38.08	37.01	38.83	39.32	39.13	39.12	39.66	39.87	38.54	38.88	37.51	38.51
CaO	0.14	0.15	0.16	0.14	0.14	0.15	0.16	0.12	0.17	0.14	0.16	0.12	0.14
FeO	24.97	24.27	23.12	22.80	23.72	21.67	23.13	23.53	22.42	23.03	22.24	23.75	23.47
MnO	0.50	0.47	0.48	0.33	0.41	0.41	0.42	0.37	0.50	0.20	0.26	0.41	0.31
SiO2	37.86	38.33	39.58	39.30	37.79	38.36	37.42	36.06	38.42	39.44	39.63	37.26	38.49
Total	101.84	101.31	100.35	101.53	101.45	99.89	100.38	99.81	101.47	101.44	101.19	99.21	100.93
Na	0.00	0.00	0.00	0.00	0.00	0.00	0.00	0.00	0.00	0.00	0.00	0.00	0.00
K	0.00	0.00	0.00	0.00	0.00	0.00	0.00	0.00	0.00	0.00	0.00	0.00	0.00
Al	0.00	0.00	0.00	0.00	0.00	0.00	0.00	0.00	0.00	0.00	0.00	0.00	0.00
Ti	0.00	0.00	0.00	0.00	0.00	0.00	0.00	0.00	0.00	0.00	0.00	0.00	0.00
Mg	1.47	1.47	1.43	1.48	1.52	1.52	1.52	1.56	1.53	1.47	1.48	1.48	1.49
Ca	0.00	0.00	0.00	0.00	0.00	0.00	0.00	0.00	0.00	0.00	0.00	0.00	0.00
Fe	0.54	0.53	0.50	0.49	0.51	0.47	0.51	0.52	0.48	0.00	0.48	0.53	0.51
Mn	0.01	0.01	0.01	0.01	0.01	0.01	0.01	0.01	0.01	1.01	0.01	0.01	0.01
Si	0.98	0.99	1.03	1.01	0.98	1.00	0.98	0.95	0.99	1.01	1.01	0.99	1.00
Total	3.02	3.01	2.97	3.00	3.02	3.00	3.02	3.05	3.01	2.99	2.99	3.01	3.00

APPENDIX B-4 RESULTS OF ELECTRONMICROPROBE ANALYSES OF MATRIX GLASSES

Laboratory No.	71	72	85	88	106	129	134	143	144
Location	Anoling gully	Anoling gully	Anoling gully	Anoling gully	Anoling gully	Anoling gully	Anoling gully	Anoling gully	Anoling gully
Description	Clear glass, surge unit	Dark glass, surge unit	Dark glass, surge unit	Dark glass, surge unit	Dark glass, surge unit	Dark glass, surge unit	Dark glass, surge unit	Clear glass, surg	Clear glass, surge unit
Na2O	3.97	4.21	4.27	4.29	4.21	4.26	4.21	4.36	4.13
K2O	2.03	1.19	0.85	1.27	0.73	0.29	0.87	2.19	2.21
Al2O3	16.47	18.23	15.77	17.26	25.31	22.80	18.92	14.15	14.37
TiO2	1.04	0.65	0.97	1.06	0.31	0.06	0.88	1.15	1.27
MgO	2.43	2.76	2.67	2.98	0.65	0.30	2.27	1.73	1.83
CaO	5.88	7.55	9.44	6.01	10.54	11.47	7.23	4.65	4.85
FeO	7.15	5.87	5.36	8.43	3.24	1.40	7.28	8.75	9.26
MnO	0.14	0.00	0.12	0.15	0.07	0.03	0.15	0.16	0.16
SiO2	57.67	56.13	55.11	54.20	55.94	52.57	53.84	61.88	61.08
Total	96.78	96.64	94.59	95.65	100.99	93.17	95.65	99.04	99.16
Oxygen	10.00	10.00	10.00	10.00	10.00	10.00	10.00	10.00	10.00
Na	0.46	0.49	0.51	0.51	0.46	0.50	0.50	0.49	0.47
K	0.15	0.09	0.07	0.10	0.05	0.02	0.07	0.16	0.17
Al	1.16	1.28	1.14	1.24	1.69	1.64	1.36	0.97	0.99
Ti	0.05	0.03	0.04	0.05	0.01	0.00	0.04	0.05	0.06
Mg	0.22	0.25	0.24	0.27	0.05	0.03	0.21	0.15	0.16
Ca	0.38	0.48	0.62	0.39	0.64	0.75	0.47	0.29	0.30
Fe	0.36	0.29	0.27	0.43	0.15	0.07	0.37	0.43	0.45
Mn	0.01	0.00	0.01	0.01	0.00	0.00	0.01	0.01	0.01
Si	3.45	3.35	3.38	3.31	3.17	3.21	3.27	3.62	3.58
Total	6.23	6.27	6.29	6.32	6.23	6.23	6.29	6.18	6.19

APPENDIX C PETROGRAPHIC DESCRIPTIONS

Sample	Thin section descriptions
May 26 Aw	Anoling pyroclastic surge
Remarks: Probed	Mineral percentage and occurrence: Plagioclase: 14% Orthopyroxene: 2% Clinopyroxene:3% Titanomagnetite:1% Vesicles: 25% Groundmass: 80% Consists of dark glass and microlites of plagioclase and pyroxene *Descriptions*: Plagioclase >1.5mm and <1mm, occur as microphenocryts; larger plagioclase is inclusion rich; small plagioclases are clear; skeletal pronged plagioclase with interstitial glass; dark groundmass and microlites of the main phenocryts assemblage; large vesicles occur in the streaks *Rock textures*: Porphyritic, hypocrystalline
MAY 26 A	Anoling pyroclastic surge
	Mineral percentage and occurrence: Plagioclase: 14% Orthopyroxene: 2% Clinopyroxene:3% Titanomagnetite:1% Vesicles: 30% Groundmass: 80% Consists of dark glass and microlites of plagioclase and pyroxene *Descriptions*: Plagioclase >1.5mm and <1mm, angular to subhedral; some plagioclase are resorbed; occurs as microphenocryts; skeletal pronged plagioclase with interstitial glass; dark groundmass and microlites of the main phenocryts assemblage; some plagioclase are inclusion-rich *Rock textures:* Porphyritic, hypocrytalline
May 24 Remarks: Probed	Anoling pyroclastic surge Mineral percentage and occurrence: Plagioclase: 17% Orthopyroxene: 3% Clinopyroxene:4% Titanomagnetite:1% Olivine: 1% Vesicles: 25% Groundmass: 75% Consists of dark glass and microlites of plagioclase and pyroxene; groundmass plagioclase are swallow-tailed Descriptions: Plagioclase size range is >2.0mm and <1mm, occur as microphenocryts; exhibits oscillatory zoningskeletal pronged plagioclase with interstitial glass occurs; euhedral to subhedral; streaks of brown glass with large plagioclase and clinopyroxene; glomeroporphyritic clots of plagioclase and augite, presence of microphenocrysts of euhedra and anhedral, mosaic olivine

MAY 31	Anoling pyroclastic surge
Remarks: Probed	A) Mineral percentage and occurrence in dark rock: Plagioclase: 14% Orthopyroxene: 3% Clinopyroxene:2% Titanomagnetite:1% Vesicles: 30% Groundmass: 80% Consists of dark glass and microlites of plagioclase and pyroxene *Descriptions*: Consists of light and dark rocks, sharp boundary; streaks of light rock present Plagioclase >2mm and <1mm, angular to subhedral; some plagioclase are resorbed occurs as microphenocryts; skeletal pronged plagioclase with interstitial glass B) Mineral percentage and occurrence in dark rock: Plagioclase: 20% Orthopyroxene: 5% Clinopyroxene:3% Titanomagnetite:3% Vesicles: 15% Groundmass: Most groundmass was removed; clear glass present, *Descriptions:*Plagioclase mostly >1.8mm and are inclusion-rich; anhedral to subhedral, plagioclase exhibits oscillatory zoning; clear, small plagioclase also occurs
May 39D	Budiao pyroclastic surge
	Mineral percentage and occurrence: Plagioclase: 13% Orthopyroxene: 3% Clinopyroxene:4% Titanomagnetite:1% Olivine: 4% Vesicles: 25% Groundmass: 75% Consists of dark glass and microlites of plagioclase and pyroxene; swallow-tailed microphenocryst plagioclase *Descriptions*: Plagioclase 2mm and <1mm, microphenocryts plagioclase; exhibits oscillatory zoning, abundant sieved and oscillatory zoned plagioclase; abundant sieved plagiocalse; euhedral to subhedral and broken; streaks of brown glass with large plagioclase and clinopyroxene; glomeroporphyritic clots of plagioclase and augite and clots of augite; abundant euhedral to anhedral olivine; glomeroporphyritic clots of olivine and pyroxene *Rock textures*: Porphyritic and hypocrytalline

May 39F	Budiao pyroclastic surge
	Mineral percentage and occurrence: Plagioclase: 15% Orthopyroxene: 3% Clinopyroxene:4% Titanomagnetite:<1% Olivine: 3% Vesicles: 25% Groundmass: 75% Consists of dark glass and microlites of plagioclase; micrometer vesicles *Descriptions*: Plagioclase 3.5mm and <1mm, to microphenocryts; exhibits oscillatory zoning, abundant sieved and oscillatory zoned plagioclase; corroded plagioclase; euhedral to subhedral and broken; swallow-tailed plagioclase streaks of brown glass with large plagioclase and clinopyroxene; glomeroporphyritic clots of plagioclase and augite and clots of augite *Rock textures*: Porphyritic and hypocrytalline
May 39D2	Mabinit gully
	Mineral percentage and occurrence: Plagioclase: 13% Orthopyroxene: 3% Clinopyroxene:4% Titanomagnetite:1% Olivine: 4% Vesicles: 25% Groundmass: 75% Consists of dark glass and microlites of plagioclase and pyroxene; swallow-tailed microphenocryst plagioclase; abundant small vesicles in dark rock *Descriptions*: Plagioclase 3.0mm and <1mm, to microphenocryts; exhibits oscillatory zoning, abundant sieved and oscillatory zoned plagioclase; euhedral to subhedral and broken plagioclase; streaks of light rock with large plagioclase and clinopyroxene; glomeroporphyritic clots of plagioclase and augite and clots of augite; abundant euhedral to anhedral olivine; glomeroporphyritic clots of olivine and pyroxene *Rock textures*: Porphyritic and hypocrytalline
May2-28	Mabinit lower ignimbrite
	Mineral percentage and occurrence: Plagioclase: 15% Orthopyroxene: 4% Clinopyroxene:7% Titanomagnetite:1% Olivine: 3 Vesicles: 25% Groundmass: 70% Consists of dark glass and microlites of plagioclase; *Descriptions*: Plagioclase 2.0mm and <1mm, to microphenocryts; exhibits oscillatory zoningeuhedral to subhedral and broken; swallow-tailed plagioclase glomeroporphyritic clots of plagioclase and augite and clots of augite; abundant euhedral to anhedral *Rock textures*: Porphyritic and hypocrytalline

May 2-29E	Anoling pyroclastic surge
Remarks: Probed	Mineral percentage and occurrence in light component: Plagioclase: 13% Orthopyroxene: 3% Clinopyroxene:4% Titanomagnetite:1% Vesicles: 10% Groundmass: , clear glass Mineral occurrence of *Descriptions*: Plagioclase 3.0mm and <1mm, to microphenocryts; exhibits oscillatory zoning, abundant sieved; euhedral to subhedral and broken; streaks of brown glass with large plagioclase and clinopyroxene; glomeroporphyritic clots of plagioclase and augite and clots of augite;large vesicles *Rock texture*: Porphyritic
May 2-6 B	Mabinit surge deposit
	Mineral percentage and occurrence of light component: Plagioclase: 10% Orthopyroxene: 2% Clinopyroxene:4% Titanomagnetite:<1% Vesicles: 15% Groundmass: 85%, Groundmass not observed; clear glass present clear glass occurs in the light rock, with large vesicles. Dark rock: Large and small plagioclase phenocryts, plagioclase occurring as microphenocysts; consists of euhedral to subhedral olivine, some have mosaic extinction.